INFORMATION TO USERS

This reproduction was made from a copy of a document sent to us for microfilming. While the most advanced technology has been used to photograph and reproduce this document, the quality of the reproduction is heavily dependent upon the quality of the material submitted.

The following explanation of techniques is provided to help clarify markings or notations which may appear on this reproduction.

1. The sign or "target" for pages apparently lacking from the document photographed is "Missing Page(s)". If it was possible to obtain the missing page(s) or section, they are spliced into the film along with adjacent pages. This may have necessitated cutting through an image and duplicating adjacent pages to assure complete continuity.

2. When an image on the film is obliterated with a round black mark, it is an indication of either blurred copy because of movement during exposure, duplicate copy, or copyrighted materials that should not have been filmed. For blurred pages, a good image of the page can be found in the adjacent frame. If copyrighted materials were deleted, a target note will appear listing the pages in the adjacent frame.

3. When a map, drawing or chart, etc., is part of the material being photographed, a definite method of "sectioning" the material has been followed. It is customary to begin filming at the upper left hand corner of a large sheet and to continue from left to right in equal sections with small overlaps. If necessary, sectioning is continued again—beginning below the first row and continuing on until complete.

4. For illustrations that cannot be satisfactorily reproduced by xerographic means, photographic prints can be purchased at additional cost and inserted into your xerographic copy. These prints are available upon request from the Dissertations Customer Services Department.

5. Some pages in any document may have indistinct print. In all cases the best available copy has been filmed.

University Microfilms International
300 N. Zeeb Road
Ann Arbor, MI 48106

Marshall, Hal George

A NUMERICAL STUDY OF NONLINEAR CASCADING OF ATMOSPHERIC BAROCLINIC AND BAROTROPIC FLOW WITH A TWO-LAYER QUASI-GEOSTROPHIC MODEL

Iowa State University PH.D. 1983

A numerical study of nonlinear cascading of atmospheric baroclinic and barotropic flow with a two-layer quasi-geostrophic model

by

Hal George Marshall

A Dissertation Submitted to the
Graduate Faculty in Partial Fulfillment of the
Requirements for the Degree of
DOCTOR OF PHILOSOPHY

Department: Earth Sciences
Major: Meteorology

Approved:

Signature was redacted for privacy.

In Charge of Major Work

Signature was redacted for privacy.

For the Major Department

Signature was redacted for privacy.

For the Graduate College

Iowa State University
Ames, Iowa

1983

TABLE OF CONTENTS

I. INTRODUCTION

A. General

Conservation theorems and the resulting quantities (and related budgets) play an important role in many of the physical sciences. Atmospheric dynamics is no exception. Energy, potential vorticity, etc., and their budgets have been calculated in numerous studies. Fjortoft's (1953) pioneering study which examined the upscale and downscale cascading of kinetic energy and enstrophy showed the importance of the constraints of energy and enstrophy.

Many studies have been made of energy balance in the atmosphere with different subdivisions (Lorenz, 1967). The subdivision of energy and enstrophy by longitudinal scale (respectively, Saltzman, 1957; Steinberg, 1971) enables one to access the relative roles of different scales and the exchanges of energy between scales (the cascades). The subdivision of energy into vertical mean and shear has been proposed and calculated by Wiin-Nielsen (1962) and Smagorinsky (1963). The vertical dependence of the atmosphere in processes such as baroclinic instability makes a vertical subdivision of energy attractive.

This study combines these latter two types of subdivisions (Chen and Tribbia, 1981) to study the cascading in the simplest, fully nonlinear, baroclinic model. Through experimentation, theories of cascades such as Rhines (1977) can be evaluated. Also, the observational results of Chen and Tribbia's present observational study can be investigated further.

B. Previous Studies and Background

This review begins by discussing the basic parts of the method of analysis to be used and then progresses to piece together some theoretical results for latter consumption. The vertical shear (baroclinic) and mean (barotropic) kinetic energetics are reviewed first. Second, the spectral energetics and spectral enstrophy equations are discussed. The recent observational calculation of the spectral energetics and spectral enstrophy equations with the vertical shear and mean by Chen and Tribbia (1983) is then noted. Theory for the cascading is examined last. A comprehensive theory does not exist for the atmospheric cascades; however, an interesting picture can be pieced together by using the two-level model results and theory of Wiin-Nielsen (1962), Rhines (1977) and Salmon (1978).

The vertical shear and mean energies were first set forth by Wiin-Nielsen (1962) and Smagorinsky (1963). To introduce these energies we begin by defining the vertical mean

$$( )_M = \frac{1}{P_o}\int_o^{P_o} ( )dp \tag{1.1}$$

and the vertical shear

$$( )_S = ( ) - ( )_M \tag{1.2}$$

of a quantity. This division is simply a vertical extension of the zonal and eddy departure idea. Applying (1.1) and (1.2) to the velocities and performing the vertical integration, the vertical shear (baroclinic)

and mean (barotropic) kinetic energies are defined. Wiin-Nielsen (1962) and Smagorinsky (1963) derived the vertical shear and mean energetics. Wiin-Nielsen took the vertical shear and mean of the primitive momentum equations and assumed ($\omega = \frac{dP}{dt} = 0$) at the top and bottom of the atmosphere. His results are shown symbolically in the following equations and Figure 1.1.

$$\frac{dA}{dt} = C(K_S,A) + G(A), \tag{1.3}$$

$$\frac{dK_S}{dt} = C(A,K_S) + C(K_M,K_S) + D(K_S), \tag{1.4}$$

$$\frac{dK_M}{dt} = C(K_S,K_M) + D(K_M). \tag{1.5}$$

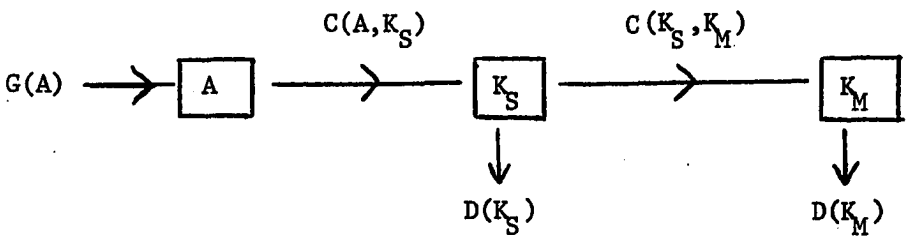

Figure 1.1. Vertical shear and mean energy diagram

A is the available potential energy (Lorenz, 1955), D(B) and G(B) are the dissipation and generation, respectively, of an energy form B. The conversion $C(A,K_S)$ is of the same form as C(A,K), where K is the total kinetic energy, in Lorenz (1955). Note the available potential energy is only converted directly into K_S according to the above equations.

The available potential energy and the shear kinetic energy are not independent. These two forms of energy are partially related by

the thermal wind relation in the actual atmosphere. In the two-layer quasi-geostrophic model, the hydrostatic and geostrophic relations demand the thermal field completely define the amount of available potential and shear kinetic energy (see Chapters II and III).

The form of the conversion $C(K_S,K_M)$ in equation (1.5) is

$$C(K_S,K_M) = \frac{-P_o}{g}\int_s [\vec{V}_M \cdot (\vec{V}_S \frac{\partial \omega}{\partial p}) + (\vec{V}_M \times \hat{k}) \cdot (\xi_S \vec{V}_S)_M]ds, \quad (1.6)$$

(e.g., Wiin-Nielsen and Drake, 1965). The first term of this integral is smaller than the second as one would expect from a comparison of divergence and vorticity. The second term can be shown to be the only one appearing in the quasi-geostrophic system. To illustrate the physical processes of this second conversion term, examine the simpler form of this conversion in the two-layer quasi geostrophic model after Wiin-Nielsen (1962). In doing this, note the Laplacian of temperature is proportional to shear vorticity (see Chapter II). Instead of using the vertical shear vorticity, a quantity most meteorologists would not be familiar with, the thermal field is used

$$C(K_S,K_M) = \frac{\Delta P^2 \, R_*^2}{f^2 \, 4Pg}\int \nabla^2 T \vec{V}_M \cdot \nabla T ds, \quad (1.7)$$

where R_* is the ideal gas constant, ΔP = 500 mb, P = 1000 mb, g is gravity, and f is the Coriolis parameter (see Chapter III). Thus, we see that warm advection in a region of temperature maximum produces the conversion of baroclinic kinetic energy into barotropic kinetic energy and vice versa if cold advection or a region of temperature minimum occurs.

There are several approaches to the subdivision of vertical structure. Unlike the zonal and eddy subdivision around a latitude circle of finite length, the top of the atmosphere for the vertical averaging must be made. This is usually done with the top boundary condition of $\omega\left(\frac{dP}{dt}\right) = 0$ at the top. Different heights of the set "top" will give different divisions of vertical shear and mean energy.

One approach is the vertical empirical orthogonal function method (Holmström, 1963; Baer, 1981). In this method, the vertical subdivision is made into orthogonal functions that match the vertical variation with the least number of basis functions. This method is just as arbitrary if not more so than the vertical shear and mean. These basic functions change with time so a cascading calculation with them would be difficult, if not impossible.

The vertical normal modes of a linearized set of atmospheric equations seems an obvious choice; however, a complete set of orthogonal functions does not exist to the so-called vertical structure equation for a "realistic" (radiation condition) top boundary condition (Pedlosky, 1979).

The use of top boundary conditions, such as rigid lids, does give complete sets of orthognal functions. Wiin-Nielsen's study (1974) is one such example. He assumed a basic state of rest, a constant lapse and $\omega = 0$ at $p = 0$. He found a complete set of orthogonal functions (Bessel functions). Using these orthogonal functions one could, in principle, calculate the cascades; however, the practical difficulties would be immense.

The vertical normal modes without a constant lapse rate assumption but with a rigid lid have been computed by Kasahara and Puri (1981) with the level approximations of a general evaluation model (GCM). The first and strongest mode of their study has correspondence with the vertical mean in that a vertical mean picks up most of the variation of this mode. The other modes with greater order than the first may be grouped together as baroclinic but contain some vertical mean when vertically averaged. This shows that the vertical shear and mean have some physical basis, but also have a serious drawback in that these modes are mixed with vertical mean despite different dynamics. The simple structure of the two-layer model used in this study has only two vertical modes that are orthogonal and naturally can be distinguished by the vertical mean and shear. In oceanography these modes, along with their horizontal structure, are referred to as barotropic and baroclinic Rossby waves (e.g., Rhines, (1977).

Equations (1.3) through (1.7) can be further subdivided into zonal and eddy (zonal departures) parts. These subdivisions can be seen in Figure 3.2 for the nondivergent primitive equations. The integral form of these equations can be found in Smagorinsky (1963), Wiin-Nielsen and Drake (1966) and Chen and Tribbia (1981). The details are long and tedious and are not presented here except to make note that the results of the quasi-geostrophic derivation of these equations are very different. The difference can explain physically the more complicated primitive equation results (see Chapter III).

A further subdivision is to decompose the eddies by Fourier decomposition around a latitude circle. This gives a one dimensional scale decomposition. The zonal flow becomes wave number zero. The

resulting equations (without the barotropic-baroclinic subdivision) are known as the spectral energetics (Saltzman, 1957). Saltzman's equations are schematically shown in Figure 1.2, in analogy with the Lorenz energy diagram (after Tomatsu, 1979). A(0) and K(0) are the zonal available potential energy and zonal kinetic energy, respectively. A(k) and K(k) are any of the Fourier components of these types of energies. Wave numbers (k) higher than 18 are not accurate in observation studies because of data gaps over the oceans and data resolution.

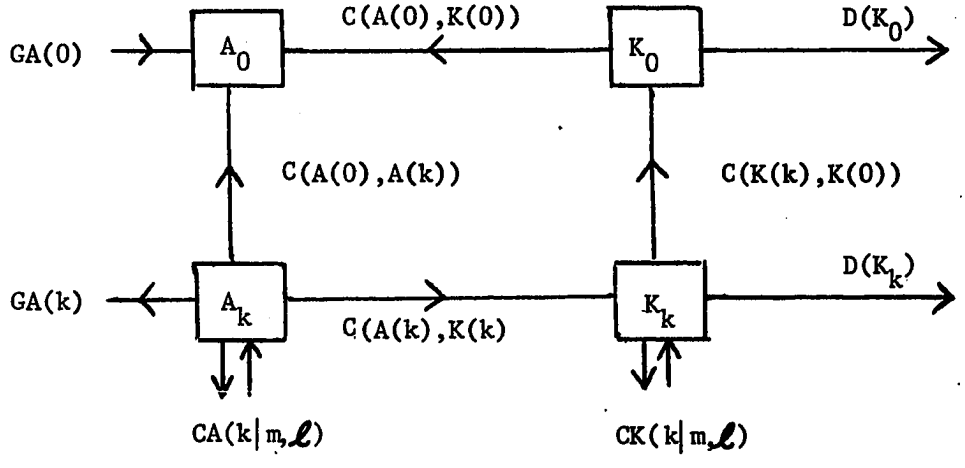

Figure 1.2. Schematic of the spectral energetics (after Tomatsu, 1979)

The generation GA(k), the dissipation DK(k) and the conversions C(A(k),K(k)), C(A(0),A(k)) and C(K(0), K(k)) have only k as the wave number argument because they only directly effect one Fourier component. In other words, they do not transfer energy between components. These terms come from linear terms in the momentum and thermodynamic equations.

$CA(k|m,\ell)$ and $CK(k|m,\ell)$ are nonlinear exchange terms and represent changes of energy scale (wave number) but not changes in energy form. ℓ and m are wave numbers such that the triad relation $m \pm \ell = k$ is met. The trial relation requires the participation of three wave numbers. The nonlinear terms involve only a redistribution of energy among wave number components.

The spectral energetics scheme of Saltzman (1957) is based on the primitive equation model. Tomatsu (1979) has rederived these equations with the quasi-geostrophic theory; however, his nonlinear terms do not satisfy the aforementioned redistribution of energy. When barotropic and baroclinic components are summed up, the linear terms of Chapter III give the same results as Tomatsu.

A number of calculations have been done with the spectral energetics (e.g., Yang, 1967; Chen, 1982; Chen and Marshall, 1983). The results discussed here are based on Yang (1967), Tomatsu (1979), Saltzman (1970), and Chen (1982) which are calculations for various winters of the northern hemisphere. There exist differences in the results of these studies. A subjective average of these results will be made to define the observed spectral energetics; however, significant differences do exist between studies.

To review these results, begin by starting in the left-hand corner of Figure 1.2 and proceed counterclockwise around the diagram. Energy flows into the zonal available potential energy (A) mainly by the generation (diabatic) term. All wave numbers of A are supported by conversion from zonal A. Two maximums in this conversion are found at wave numbers

2 and 6 (e.g., Chen, 1982). Most wave numbers lose energy to diabatic processes GA(k); however, this term is usually poorly known and difficult to calculate. The A_0 has the largest energy in the zonal flow. Next, but much less, is the A of wave number 1. A steadily decreases with wave number with a -3 power law in the regime of wave numbers 8-18, though the nonlinear term A is lost from wave numbers 2-6 to be gained mainly by lower wave numbers. All wave numbers convert A into kinetic energy with a maximum conversion at wave number 6 and a secondary maximum at wave number 2. Except for a weak peak at wave number 3 (or 2) kinetic energy declines with wave number by a -3 power law in wave numbers 7-18. The nonlinear term shows energy is transferred from wave numbers 2 and 5-10 and gained by other wave numbers (Yang, 1967); however, results vary greatly for this quantity but contain this general trend. Most, but not all, wave numbers lose energy to what is denoted as the dissipative term. This term is not well-known. Most wave numbers are found to convert energy into zonal kinetic energy (e.g., Chen, 1982) but some very different results are sometimes found (Yang, 1967; Chen and Marshall, 1983).

Some of these results, especially those of synoptic scales, can be expected from linear baroclinic instability and some finite amplitude modification (Gall et al., 1979). The behavior of wave numbers 2 and 3 are probably in part a result of land-sea contrast and the orography of the northern hemisphere (e.g., Charney and Eliassen, 1949; Smagorinsky, 1953). These latter two effects are not investigated in this study.

The cascading of kinetic energy to larger scales can be explained or at least motivated in the context of two-dimensional turbulence, which will be addressed later. The downscale cascading of A has been motivated by Fjortoft (1959). The behavior of other terms can be explained in the usual context of the Lorenz energy cycle (e.g., Lorenz, 1967).

The spectral enstrophy and potential enstrophy equation have not often been used in atmospheric calculations. Steinberg (1971) formulated and computed them, in spectral form, for the northern hemisphere. We follow Steinberg's (1971) results since this quasi-geostrophic study is not valid in lower latitudes. Figure 1.3 has a schematic of the potential enstrophy equation. The generation and dissipation terms for the atmosphere were not calculated by Steinberg. His results show the zonal potential enstrophy (E(0)) is supported by conversion of potential enstrophy from wave numbers 1-4 but a loss from the zonal to the other wave numbers combined. In the nonlinear terms, wave numbers 1-8 lose potential enstrophy mainly to wave numbers 12-18 with a little loss to 9-12. The magnitude of the nonlinear exchange for wave number 15 of Steinberg indicates that the truncation of this wave number (mandated by the data) is severe.

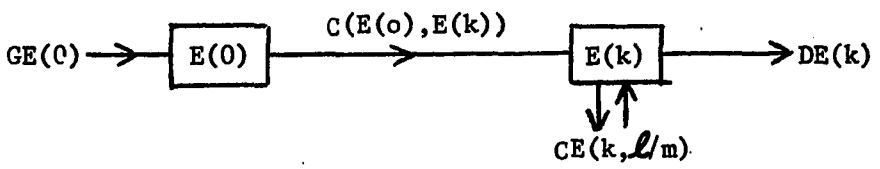

Figure 1.3. Schematic of enstrophy conversion and cascading (after Steinberg, 1971)

Recently, Chen and Tribbia (1981) have formulated the vertical shear and mean energetics combined with the spectral energetics and spectral enstrophy equations. Their energetics formulation is based on the nondivergent primitive equations. Their spectral potential enstrophy equations are quasi-geostrophic and multi-level. The form of Chen and Tribbia's (1981) equations is not presented here because of its great length. The interested reader is directed to their technical report.

Two-dimensional turbulence has been investigated for many years now (Rhines, 1979). Even though this research may not be directly applicable, we can point out that the two-dimensional turbulence has several conceptual advantages. The constraints of two-dimensional turbulence, namely the conservation of kinetic energy and enstrophy, are of the same form as those of a quasi-geostrophic atmosphere. The constraints of a quasi-geostrophic flow are conservation of energy and potential enstrophy. As a result of this similarity of conservation laws, Charney (1971) found,

> . . . theorems pertaining to energy exchange components in two-dimensional flow may be shown to apply to three-dimensional quasi-geostrophic flow as well, but now it is the geostrophic constraint, not the two-dimensionality that prevents the cascade.

The cascade that Charney refers to is the downscale cascade of energy. Fjortoft (1953) and Onsager (1949) found this result for two-dimensional nondivergent flow. (Note that in order to be strictly correct, Fjortoft's results must be modified according to Merilees and Warn (1972)). An interesting way this cascade may be inhibited by Rossby waves has been discussed by Rhines (1975).

Another, possibly more direct, similarity is that between two-dimensional turbulence and the barotropic or vertical mean flow. The vertically averaged quasi-geostrophic potential vorticity equation has no vortex stretching term when a rigid lid is the top boundary condition. The resulting barotropic potential enstrophy is the same as two-dimensional enstrophy. There is an extra advective term in which the baroclinic components have a role; however, in some regions of the flow or under certain circumstances, this term is small (see Chapter II).

One major difference between the two-dimensional flow and the barotropic flow of a two-layer model (other than the forcing) is the nature of the triads. Nonlinear wave-wave interactions must involve three waves (Fourier components); hence, the name triad. Fjortoft (1953) showed that energy must flow to or away from the middle wave number of the triad in two-dimensional flow. In the simplest model that contains A and potential enstrophy, the two-layer quasi-geostrophic model, the triads of Fjortoft are found plus mixed barotropic-baroclinic triads (Salmon, 1978). These barotropic-baroclinic triads consist of a barotropic component and two baroclinic components. Energy does not have to flow to or away from the middle wave number in all triads of the barotropic-baroclinic triads (Marshall and Chen, 1982). The directions of energy flow and the triads allowed are shown schematically in Figure 1.4. An inertial subrange theory such as that of Kraichnan (1967) which is based on the nature of the two-dimensional triads would have to be generalized for these different triads for application to the two-layer model.

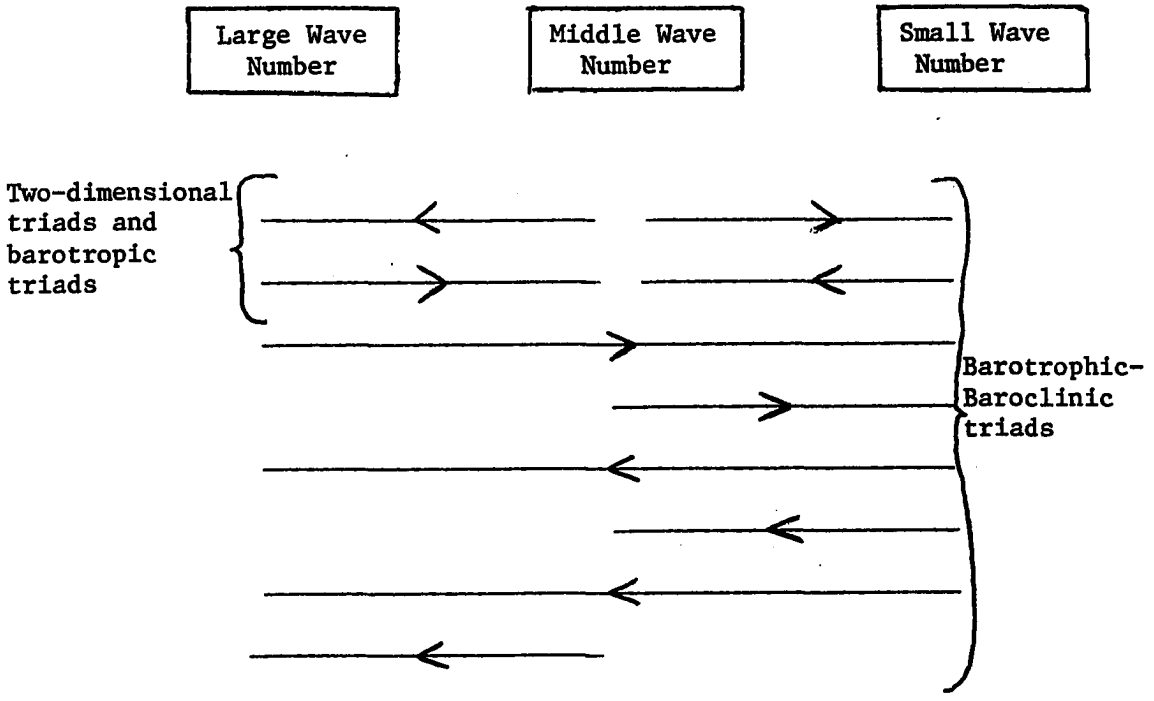

Figure 1.4. The directions of energy exchanges possible for different types of triads

Many studies of two-dimensional turbulence and geostrophic turbulence have been concerned with the spectral power laws of kinetic energy, available potential energy and enstrophy in the high wave number regime. Kraichnan (1967) and Leith (1968) have postulated inertial subrange theories appropriate to two-dimensional turbulence far from the scales of forcing and dissipation. These scales are theorized to have an enstrophy flux toward high wave number that is independent of wave number, zero kinetic energy flux and have a -3 power law for the kinetic energy and -1 for enstrophy wave numbers. The -3 power law has been confirmed in numerical simulations of two-dimensional turbulence (Lilly, 1969). Charney (1971) predicts a -3 power law for geostrophic kinetic energy and

available potential energy. The -3 power law had been observed in the kinetic energy spectrum of the atmosphere before any of these theories (Horn and Bryson, 1963; Wiin-Nielsen, 1967).

A major part of this study is concerned with spectral nonlinear transfer and conversion. The theory of geostrophic turbulence before Rhines (1977) said little about the details of the spectral dynamics of the flow. Rhines (1977, 1979) developed a theory of nonlinear cascading for the ocean which is sometimes referred to as barotropization. Salmon (1978, 1980) has elaborated Rhines' theory further for the atmosphere. Both Rhines' and Salmon's theories are based heavily on the behavior of the quasi-geostrophic two-layer model. The Barros and Wiin-Nielsen (1974) study shows the usefulness of this model in investigating the cascades diagnostically. (Chapter II, Section B discusses this model's usefulness and drawbacks.)

Salmon defines "baroclinic energy" as the sum of shear kinetic energy and the available potential energy while Wiin-Nielsen (1962) has defined it as the former. The barotropic energy definition is the same for both authors. Figure 1.5 is based on Salmon (1978).

As shown in Figure 1.5 there is a net downscale cascade of baroclinic energy. This energy is also converted to barotropic energy. This conversion occurs mainly at scales close to the Rossby deformation radius. The barotropic energy cascades upscale in midscales and downscale in smaller scales and dissipates by friction. Both Rhines (1977, 1979) and Salmon (1978, 1980) did not calculate the actual energy cascades.

Rhines inferred his results from the flow fields and Salmon inferred his results from flow fields plus closure modeling.

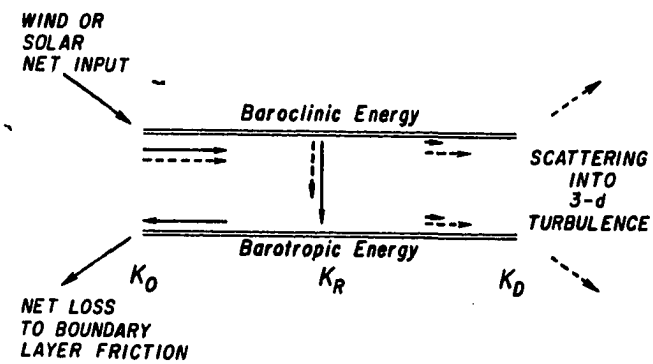

Figure 1.5. Schematic of energy flow in wave number space (from Salmon, 1978)

A conversion of energy between barotropic and baroclinic modes is possible away from the scales close to the internal Rossby radius of deformation (Marshall and Chen, 1982); however, they are expected to be small. Rhines explains the inferred conversion between baroclinic and barotropic energy as a result of the top and bottom layers locking at the radius of deformation. Indeed, his experiments with a two-layer model show that small scale energy will cascade upscale independently in the two layers until the Rossby deformation scale is reached.

An alternative but related explanation can be found in the earlier work of Wiin-Nielsen (1962). He substituted a single wave and zonal flow into an equation similar to (1.7), which is appropriate for the two-layer

model. His barotropic (vertical mean) stream function and temperature field are

$$\psi = -V_T y + A \sin(kx) \cos(my) \tag{1.8}$$

$$T = -V_T y + A_T \sin(kx + \alpha_T) \cos(my) \tag{1.9}$$

Note α_T is the phase between ψ and T where $k = \frac{2\pi}{L}$ and $m = \frac{\pi}{L_y}$, L_x is the length of the channel and L_y is the width. Substituting (1.8) into (1.7) results in

$$C(K_M) \propto \tfrac{1}{2} k(k^2 + m^2) A A_T U_T \sin \alpha_T \tag{1.10}$$

Thus, the conversion from shear kinetic energy to vertical mean (barotropic) energy depends, in this simple case, on the strength of the zonal vertical shear, wave number, amplitude and phase of the fields. The phase determines the sign of the conversion. Just as in baroclinic instability theory of the two-layer model, a phase lag of 90° between the thermal and dynamical field is optimal for conversion. Noting this, Wiin-Nielsen also compared the conversion of A.P.E. (A) to shear kinetic energy to the barotropic-baroclinic conversion. The ratio of the two is

$$\frac{C(K_S, K_M)}{C(A, k_S)} = \frac{1}{2} + \frac{k^2 + m^2}{4R^2} \tag{1.11}$$

Note the ratio is small for wave numbers small compared to the Rossby deformation wave number. However, large wave numbers have little energy to give away in the atmosphere since they are stabilized by the static

stability (e.g., Pedlosky, 1979). The conversion C(A,K) for the two-layer model can be seen in Barros and Wiin-Nielsen (1974). Their conversion is peaked at wave number 4 with a strong wave number 5 conversion also. Based on this simple theory, one would expect from relation (1.11) that the conversion $C(K_S,K_M)$ would be similar with the maximum shifted slightly to higher wave numbers.

The foregoing theory only assumed a single wave component and a zonal flow. Wave-wave interactions were ruled out a priori. This study includes the many-wave field. This makes numerical solution a must. The cascades and conversions of barotropic and baroclinic energy are calculated directly. The parts of Figure 1.5 can be stated in numerical values, thus attaining knowledge as Lord Rayleigh would have it.

C. Outline

In this section, a brief outline for the rest of this study is discussed and important points, especially those for use in later chapters, are noted.

Section A.1 of Chapter II discusses the basic physics of the model. Relevant points are: the conditions for which the model equations are valid, the Jacobians present in the model, the conditions when the barotropic vorticity equation reduces to the two-dimensional vorticity equation, and the relation between τ and the thermal wind. Section A.2 evaluates the physics of the two-layer quasi-geostrophic model. Some relevant points are: the problems of such models with small wave number standing waves, the power law for high wave numbers of available potential energy and the vertical structure of this model's two normal modes. The

three-dimensional index for the model is also discussed. Section B of Chapter II discusses the numerics of the spectral transform model. Section C of Chapter II displays the general circulation of the model and compares the results to observed mid-latitude flow. Also, the "quasi-equilibrium" regime of the flow used for later analysis is shown.

The first three sections of Chapter III discuss and derive the barotropic and baroclinic energetics without further subdivision, with the zonal and eddy subdivision and with the subdivision by zonal wave number. The vertical shear and mean of quantities is never used in this chapter; however, the baroclinic and barotropic distinction is equivalent. The quasi-geostrophic form of these equations, especially in regard to zonal and eddy decomposition, are different in form than previous studies. Indeed, the zonal and eddy forms of the quasi-geostrophic equations are used to explain some primitive equation calculations of Wiin-Nielsen and Drake (1965) in section III.B. The differences found in the zonal and eddy decomposition carries over to the wave number decomposition. The last three sections of Chapter V discuss and derive the barotropic and baroclinic potential enstrophy. Wiin-Nielsen's (1962) wave and zonal flow example is extended for the barotropic-baroclinic potential enstrophy equation. The general picture resulting from the derivation of these potential enstrophy equations is similar to Chen and Tribbia (1981) even though the details are not.

Section A of Chapter IV discusses the experiments performed. Linear baroclinic instability theory is used as a reference for many of the experiments. The study of Marshall and Chen (1982) suggests changes in

the flow, due to a change of the Rossby deformation, beyond those changes expected from linear theory. Section B of Chapter IV discusses the zonal and eddy conversions and reservoirs of barotropic and baroclinic energy and potential enstrophy. Some conversions are calculated for the first time. The spectral distributions of the various energy quantities are shown in different wave number indices. Friction has the most dramatic effects on the spectra. The barotropic and baroclinic kinetic energies in a two-dimensional index are shown and are argued to be easily related to the spectra of all quantities. Section C displays and discusses the conversion and cascading in the zonal wave number. First, the conversion and cascading of barotropic and baroclinic energy comprises the first part of this section. Potential enstrophy comprises the second part. Conversion and cascading are not seen to be independent. The spectra for most conversion and cascading are more similar than dissimilar for most of the experiments. Some results are found to contradict those expected from Salmon (1978) and Rhines (1977). Chapter V highlights some of the results found in this study and uses them to redraw the schematic diagram for cascading and conversion proposed by Salmon (1978). These modifications follow from the derivations of Chapter III and the calculated results of Chapter IV.

II. THE MODEL

A. Model Theory

1. Description

For the purposes of this study, the quasi-geostrophic two-layer beta plane channel model is used. This is the simplest fully nonlinear model that includes the basic mechanisms of baroclinic instability.[1] All the energy forms for a baroclinic and barotropic analysis are present.

The quasi-geostrophic vorticity equation and the thermodynamic equations are the foundation of the two-layer model. The quasi-geostrophic vorticity equation can be derived by expanding the Navier-Stokes equations, for a rotating fluid, in small Rossby number and aspect ratio (Merilees, 1976). This procedure results in ignoring vertical motion except when multiplied by the ambient vorticity and ignoring relative vorticity compared to ambient vorticity. This latter assumption is the least acceptable by an order-of-magnitude consideration in the primitive vorticity equation, but is strictly required by the integral constraints of the flow (Wiin-Nielsen, 1959b).

The quasi-geostrophic vorticity equation with pressure as the vertical coordinate is (Charney, 1948)

$$\frac{\partial \xi}{\partial t} + \vec{V} \cdot \nabla(\xi * + f) = f_o \frac{\partial \omega}{\partial p} + \text{dissipation} \qquad (2.1)$$

---

[1] Another possible model is the one-layer barotropic model coupled with the thermal cycle (e.g., Nielsen et al., 1981).

The thermodynamic equation in pressure coordinates is

$$\frac{\partial T}{\partial t} + \vec{V} \cdot \nabla T = \frac{P\sigma}{R^*}\omega + \frac{R^*}{Cp} H \qquad (2.2)$$

The notation is standard (except ξ^* which is the vorticity at a level and R* is the ideal gas constant) and is listed in the Appendix.

Consider a region in (x,y,p) such that: x is periodic with $f(x + L_x)$ where L_x is the length of the channel (length of the Earth's 45° latitude line), and impermeable boundaries at y = 0 and y = L_y (corresponding to 10° and 80° latitude, respectively). A north-south cross section of this region is shown in Figure 2.1.

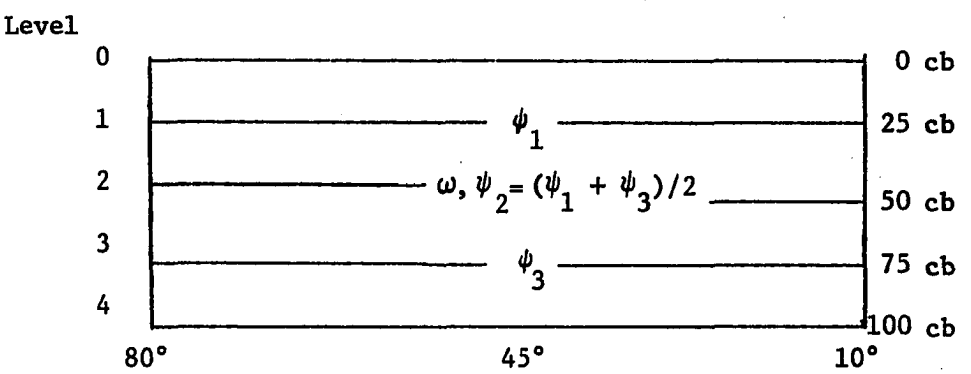

Figure 2.1. A north-south cross section of the channel

Following Phillips (1951, 1956), the quasi-geostrophic vorticity equation is specified at 25cb with $\xi_1 = \nabla^2 \psi_1$ ($V_1 = \hat{k} \times \nabla\psi_1$) and at 75cb with $\xi_3 = \nabla^2\psi_3$ ($V_3 = \hat{k} \times \nabla\psi_3$). Since only two levels are present, the relation between thickness and temperature requires that the thermodynamic equation be specified at 50cb and the static stability to be

defined externally. The static stability (σ) is a specified constant in this study.

Using the thickness relation, three equations with ψ_1, ψ_3 and ω as unknowns can be found.

$$\frac{\partial}{\partial t}\nabla^2\psi_1 + J(\psi_1, \nabla^2\psi_1 + f) = \frac{f_o\omega}{\Delta P} + \text{dissipation} \tag{2.3}$$

$$\frac{\partial}{\partial t}\nabla^2\psi_3 + J(\psi_3, \nabla^2\psi_3 + f) = \frac{f_o\omega}{\Delta P} + \text{dissipation} \tag{2.4}$$

$$\frac{\partial}{\partial t}(\psi_1 - \psi_3) + J(\psi, \psi_1 - \psi_3) = \frac{\sigma\Delta P}{f_o}\omega + \frac{R^*}{C_p}H \tag{2.5}$$

The potential vorticity equations of 25cb and 75cb can be found by eliminating ω in equations (2.3) and (2.4) by using the thermodynamical equation (2.5). Define the model stream function as $\psi = (\psi_1 + \psi_2)/2$ and $\tau = (\psi_1 - \psi_3)/2$. The resulting equations for the model are:[2]

$$\frac{\partial\xi}{\partial t} + J(\psi, \xi + f) + J(\tau, n) = \text{dissipation} \tag{2.6}$$

$$\frac{\partial q_s}{\partial t} + J(\psi, q_s) + J(\tau, \xi + f) = \frac{R^*}{C_p}H + \text{dissipation} \tag{2.7}$$

where $\xi = \nabla^2\psi$, $\eta = \nabla^2\tau$, $R^2 = \dfrac{2f_o^2}{\sigma(\Delta P)^2}$ and $q_s = n - R^2\tau$. Equation (2.6) will be denoted as the barotropic (potential) vorticity equation and (2.7) will be denoted as the baroclinic potential vorticity equation.

---

[2]These equations are usually attributed to Lorenz (1960); however, this author finds a set of equations of very similar form but of different notation in Wiin-Nielsen (1959a).

Note that in a barotropic atmosphere (pressure is a function of density only) the second Jacobian of equation (2.6) is zero and both Jacobians of equation (2.7) are zero. What is left is the equation of two-dimensional nondivergent flow, the basic equation of two-dimensional turbulence. Thus, it will not be surprising in the next chapter when the barotropic energetics contains the terms of two-dimensional turbulence and the baroclinic energetics have all different Jacobians. Note the barotropic vorticity is redistributed in the model domain by the barotropic advection of the barotropic potential vorticity and the baroclinic (thermally controlled) advection of the baroclinic vorticity. The baroclinic potential vorticity is redistributed in the model domain by the barotropic advection of baroclinic potential vorticity and vice versa. Also, note there is no baroclinic advection of any baroclinic vorticity in equation (2.7) or vice versa. Equation (2.7) includes the thermodynamic equation (2.5) and (2.6) does not. This latter fact results in (ξ) the barotropic vorticity not being stretched by thermal processes. As a direct result of this, the barotropic potential vorticity is $\xi+f$ and the baroclinic potential vorticity is $q_s = n - R^2\tau$.

Denoting the stream function (τ) and related parameters as "baroclinic" is no accident. The thermal wind relation and thickness relation makes τ proportional to temperature as well as the stream function of the vertically sheared wind. τ could just as well be denoted as the thermal stream function.

The boundary conditions of the model are simply: No flow through any boundary ($\frac{\partial \psi}{\partial x}, \frac{\partial \tau}{\partial x} = 0$, at y = 0 and L_y). No slip of the zonal departures of the zonal velocity at the side walls is allowed: ($\psi' = \psi - \overline{\psi}, \overline{\psi} = \frac{1}{L_y}\int \psi dx, \frac{\partial \psi'}{\partial y} = 0$, at y = 0 and L_y). A constant in time slip of the zonal mean velocity at the latitude boundaries ($\frac{\partial}{\partial t}$ ($\frac{\partial \overline{\psi}}{\partial y}$) = 0 at y = 0 and L_y). This latter assumption of inviscid walls at the north and south side walls are chosen so as to avoid a side wall layer which would have no analogy with the atmosphere.

Diabatic heating of the model was simulated by simple Newtonian heating. The form of the heating term is $\gamma C_p (\tau - \tau_E)$. The equilibrium temperature profile (proportional to τ_E) was extracted from the 50cb zonally averaged temperature profile of January 1963 northern hemisphere (Wiin-Nielsen, 1970). (The equilibrium temperature profile is shown in Figure 2.6.) γ is the inverse of the Newtonian relaxation time.

Dissipation is accomplished by a linear drag law, to parameterize surface effects, and by diffusion. The form of the dissipation terms in equations (2.6) and (2.7), respectively, become $k(1.6\xi - .8\eta) + \gamma\nabla^2\xi$ and $k(1.6\xi - .8\eta) + \gamma\nabla^2 q$. The drag laws are the same as those of Barros and Wiin-Nielsen (1974) only rearranged for the form of these equations. The inclusion of diffusion is to avoid energy buildup in the near truncation wave numbers where downscale cascading is forbidden.

2. Evaluation

The limitations of the model must be considered in order for latter comparisons with the real atmosphere. The relative simplicity of the

model compared to the atmosphere is a definite conceptual advantage in studying such processes as the cascades of energy. Other advantages follow.

Stone (1978) has shown remarkable agreement between the linear instability of the two-layer quasi-geostrophic model and the mid-latitude zonal vertical wind shears of the earth's troposphere. Barros and Wiin-Nielsen (1974) have shown the ability of the two-layer model in simulating the spectral energies of the atmosphere. The statements of Colucci et al. (1981) are particularly encouraging for the model and the solution method (see next section).

> . . . . The two-dimensional Fourier analysis yields a quantitatively similar result as the spherical harmonic analysis. This lends confidence in some situations to the qualitative application of channel model results to the study of real atmospheric phenomena.

The model's simplicity is not without adverse effects. Any model based on the quasi-geostrophic approximation suffers from inaccuracy in the largest planetary (especially the standing ones) scales. This can be deduced from Burger's (1958) scale analysis. The Newtonian diabatic heating and surface friction are certainly oversimplifications but give conceptual advantage. The diffusion may be the most objectionable parameterization. Some consolation can be taken in that the diffusion coefficient used in most of the experiments is very low compared to similar models.

The reduction of the troposphere to two-layers is also not without adverse effects. Those scales that have vertical dimensions less than the troposphere cannot be simulated correctly by such a model. The geostrophic turbulence of the model may differ from the atmosphere as

a result (Herring, 1980). The power law of available potential energy is changed from (-3) to (-5) (Merilees and Warn, 1972). Also, as a result of the two-level approximation and the top B.C., the model equations when linearized have two sets of normal modes with the two vertical structures presented in Figure 2.2.

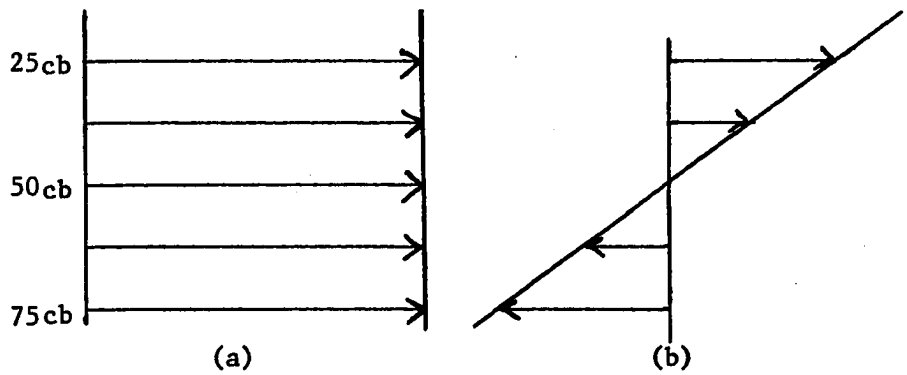

Figure 2.2. A schematic of the vertical structure of the (a) barotropic and (b) baroclinic sets of normal modes

The earth's atmosphere does not have a vertical mode analogous to the "baroclinic" vertical normal mode (Pedlosky, 1979, p. 362). Resonance involving these baroclinic modes may artificially affect the baroclinic kinetic energy cascade in the way Rhines (1975) discussed for "barotropic" cascade termination.

Note one advantage of these two vertical modes and the two-dimensional index of the next section, the model quantities are in a three-dimensional index. Thus, the stream functions ψ and τ can be thought of as the first and second vertical modes, respectively. The x and y coordinate Fourier transforms of ψ and τ complete the three-dimensional index.

B. Numerical Structure

Equations (2.6) and (2.7) are solved by a spectral method. The basis functions employed are the solutions to Laplace's equations subject to the boundary conditions of the model; $\psi(x,y) = \psi(x + L_x)$, $\frac{\partial \psi'}{\partial x} = 0$ at $y = 0$ and L_y, and $\frac{\partial}{\partial y}\int \psi dx = 0$ at $y = 0$ and L_y. Note the zonally averaged flow has a different boundary condition than does the zonal departure at the north and south channel walls. The resulting expansion of the stream function (ψ or τ) is

$$\psi(x,y) = \sum_{m=1}^{\infty} \sum_{k=-\infty}^{\infty} \psi(k,m) \exp(ik \frac{\pi}{L_x}) \sin (\frac{m\pi y}{L_y}) + \sum_{m=1}^{\infty} \psi(0,m) \cos (\frac{m\pi}{L_y} y). \quad (2.8)$$

This same expansion was used by Boville (1980) with a similar two-layer model. Using the orthogonality of these functions, one finds

$$\psi(k,m) = \frac{2\pi^2}{L_x L_y} \int^{L_x} \int^{L_y} \psi(x,y) \exp(ik\frac{2\pi x}{L_x}) \sin (\frac{m\pi y}{L_y}) \, dxdy \quad (2.9)$$

except when $k \neq 0$. For $k = 0$, then

$$\psi(0,m) = \frac{\pi}{L_y} \int^{L_y} \frac{1}{L_x} \left| \int^{L_x} \psi(x,y)dx \right| \cos (\frac{m\pi}{L_y} y)dy \quad (2.10)$$

where k is the wave number in the x-direction (zonal) and m is the wave number in the y-direction.

The x-axis Fourier analysis in equation (2.9) and synthesis in equation (2.8) is performed numerically with a fast Fourier transform (Peterson, 1978). The y-axis Fourier sine and cosine analysis was performed by actually integrating the y integrals of (2.9) and (2.10). The stream function and sine or cosine were multiplied at 35 grid points then integrated by Simpson's rule. A fast Fourier analysis technique was also tested by using odd y-axis extensions of the channel for equation (2.9) and even y-axis extentions if the channel for equation (2.10); however, no increase in computation time or accuracy was found.

The infinite truncations in (2.8) are not possible numerically. The x transform was truncated to 39 components plus the zonal component. The y transform was truncated to 11 components. The latter is the most expensive transform; hence, this truncation was the most compromising of the model as measured by the magnitude of the highest wave numbers energy.

The linear terms of equations (2.6) and (2.7) are easily calculated in "Fourier space" because differentiation becomes an algebraic operation. For example, Laplace's operator (∇^2) becomes a constant for a spectral component; therefore, a component of vorticity can be found by multiplying the same component of the stream function by a constant ($-(k^2 + m^2)$). These constants can be stored preceding the model run. Note from equation (2.9) and (2.10) that $\frac{\partial \psi(0,m)}{\partial y}$ and $\frac{\partial \psi(k\neq 0,m)}{\partial y}$ have opposite signs for stream function Fourier coefficients of similar sign.

The nonlinear terms in equations (2.6) and (2.7) are not directly expanded with (2.8). If this procedure was followed, one would be

multiplying two series together (interaction coefficient method) which is time and/or storage consuming for all but the lowest truncations (Robert, 1966). Basically, the method used consists of four steps. The derivatives needed for the Jacobians are calculated in "Fourier Space." These derivatives are transformed to "physical space." The Jacobians are multiplied out on a grid. Finally, the Jacobians are transformed back into "Fourier Space." After these four steps, the coefficients of the Jacobians can be handled like any linear term.

The grid used in this model has 35 points in the y-direction and 128 points in the x-direction. These points are marked on the left and bottom of Figure 2.5. The number of grid points is chosen by exceeding the revised estimate suggested by Orzag (1971). This keeps the model transforms reasonably alias-free. He suggested the grid points along an axis should be three times greater than the highest wave number plus one. The highest wave number in the x-direction has 3.2 grid points per wave length and over 3.1 grid points per highest wave length in the y-direction. The distance between grid points is 2.0 degrees latitude (222 km) in the y-direction and 2.8 degrees longitude (221 km) in the x-direction. (The value of beta and the length of the channel corresponds to 45 degrees latitude on the earth.)

The time integration is accomplished by using the first N-cycle scheme in fourth order as proposed by Lorenz (1971). This scheme consists of four substeps of time interval δt in which each substep, completed of the four, is used to find the next substep tendency until four subsets are completed (one time step of $\Delta t = 4\delta t$). The

process is then repeated. The substep (N) calculation can be stated as

$$\Delta Y_N = \sum_{i=1,N} \Delta Y_{i-1} + Z_i$$

where $Z_i = (A_i Z_{i-1} + F_i(Y))/B_i$, $A_i = \frac{(1 - i)}{\Delta t}$, $B_i = A_i + \frac{1}{\delta t}$, and $\Delta Y_o = 0$. $F_i(Y)$ is the forcing and ΔY the tendency, which can be stated as $\frac{\partial Y}{\partial t} = F$. The major time step Δt was 1800 seconds which gave no computational instabilities in the final form of the model. Eight seconds Cray-1 time was needed for one day simmulation time.

The sequence of calculations in the model are shown in the following simple flow chart for substep (N) in the N-cycle scheme.

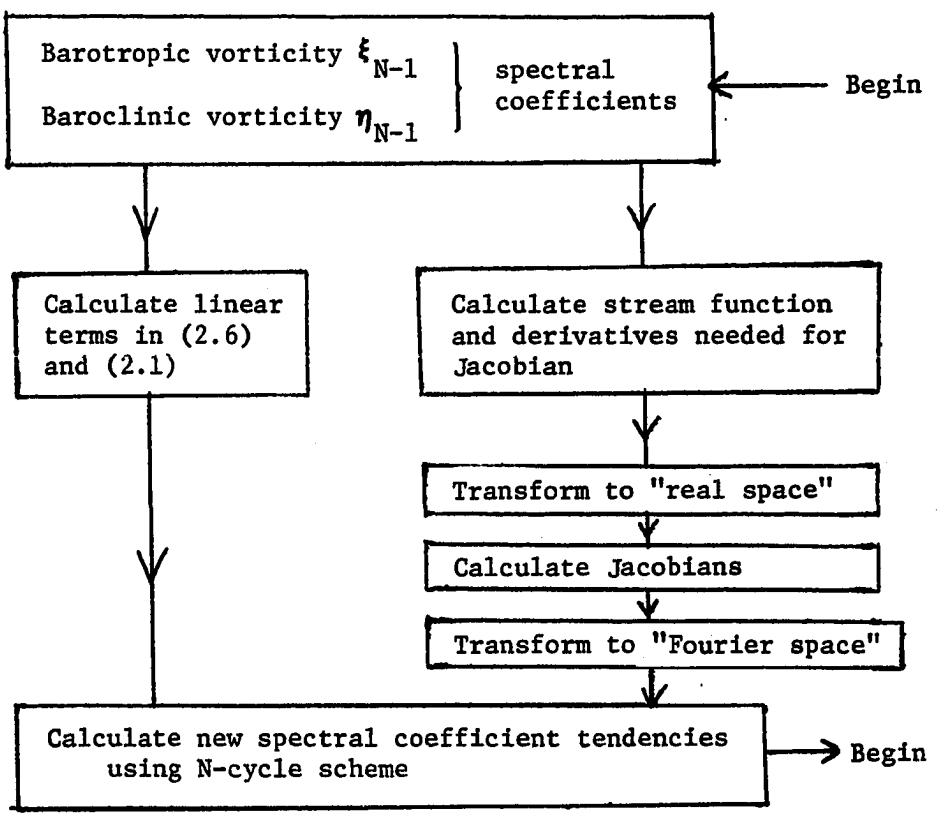

The equations (2.6) and (2.7) and the boundary conditions constitute a well-posed initial value problem (Pedlosky, 1970). The initial field for τ is 0.8 of the equilibrium temperature field of the Newtonian heating in Figure 2.6. The initial field for ψ is infinitesimal pertubations.

C. General Circulation of the Control Experiment

Simple diagnostics of the model's general ciculation statistics and energy cycle are presented. The purpose of this section is to display the model's performance. A detailed discussion of the model runs will be made in Chapter IV, following the derivation of the quasi-geostrophic barotropic and baroclinic energetics. Only the control run is discussed here. The parameters of the control run are in Table 4.1.

The evolution of zonal and eddy available potential energy and kinetic energy is shown in Figures 2.3 and 2.4. The detailed analysis of the spin up process with the formulation of Chapter III will form a separate later study. The main concern of this study is the "quasi-equilibrium regime." The barotropic kinetic energy peaks at day 39. This peak represents an overshoot of the equilibrium. At the time of this peak, most energy of the eddies is contained in wave numbers four and five. After the 39 day peaks, the energy gained by the baroclinically unstable modes redistributes by nonlinear cascading to smaller and larger scales. By day 50, this process is reasonably completed. Note also that the zonal avalable potential energy of the model's specified Newtonian temperature profile is 36% greater than the actual available potential energy of the model during the quasi-equilibrium regime.

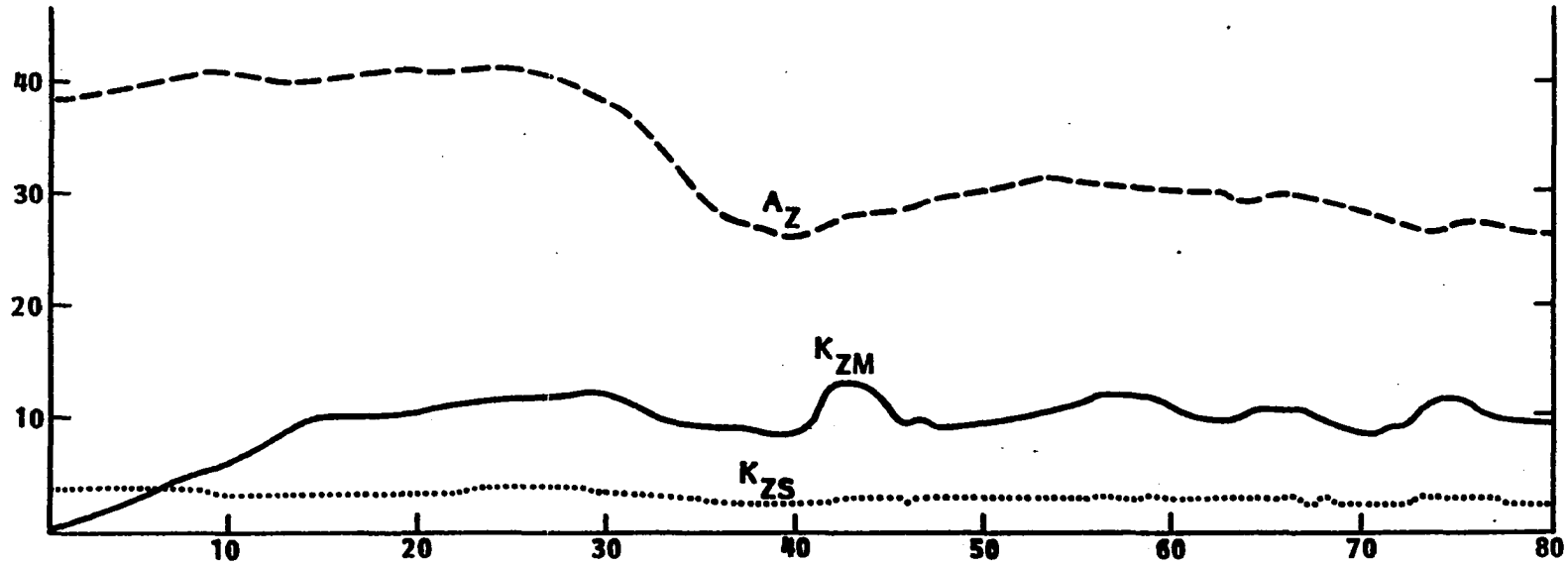

Figure 2.3. Evolution of the zonal energies in days past the start of the model, Units $10^5 Jm^{-2}$

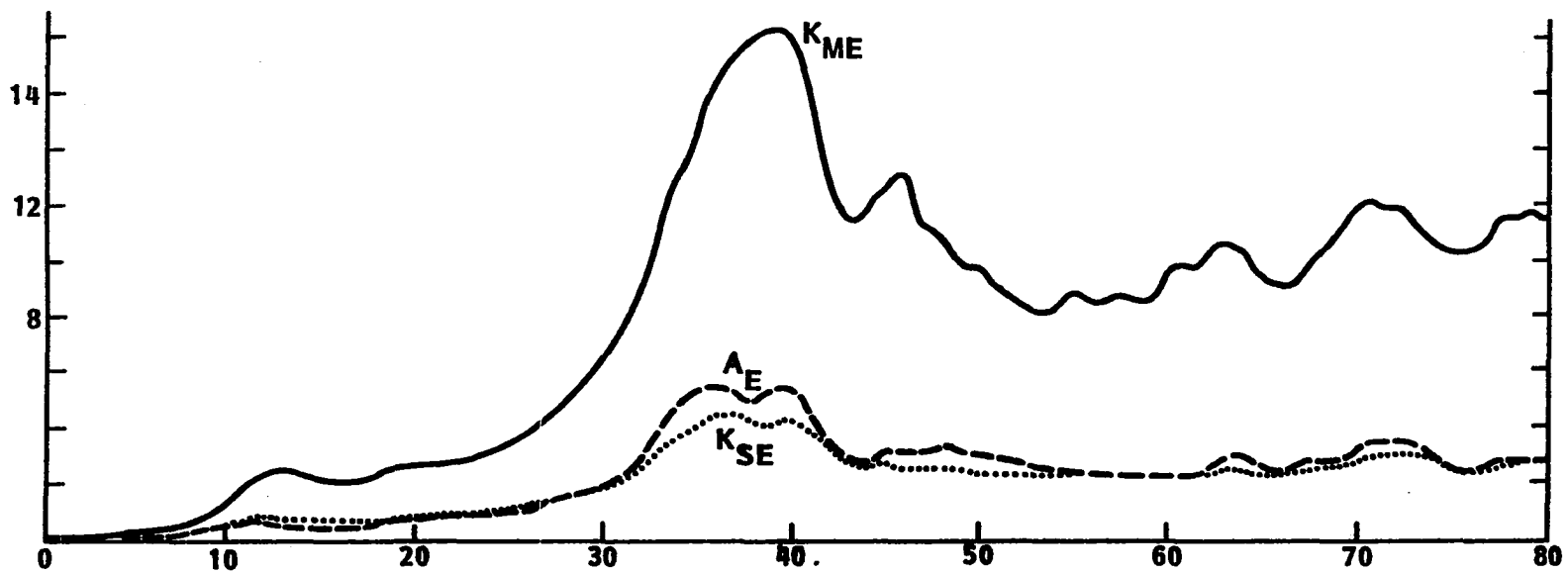

Figure 2.4. Evolution of the zonal energies in days past the start of the model, Units $10^5 Jm^{-2}$

The 30-day average of barotropic and baroclinic stream function beginning on day 50 is shown in Figure 2.5. Note that the barotropic stream function (in this model) is equivalent to the 50cb stream function and the baroclinic stream function is proportional to temperature. The general pattern is reminiscent of a similar field found in the primitive equation channel model of Smagorinsky (1963). The equilibrium temperature from Wiin-Nielsen (1970) is shown in Figure 2.6. The 30-day average zonal winds at 75cb and 25cb are shown in Figure 2.7. The average January and February zonal winds in the FGGE northern hemisphere show a maximum wind of 38.4 meters per second at 20cb (Chen and Buja, personal communication) which is comparable to the wind maximum of 39.5 meters per second at 25cb in this model. This maximum occurs at 34° N which is the same as in the FGGE year. At 85cb, the FGGE data show maximum westerly zonal winds at 42° with a speed of 12 meters per second. The model westerly zonal wind maximum is at 38° and speed 15.4 meters per second (m/sec). The easterlies in the model are too far south and too strong compared to the feeble polar easterlies of the northern hemisphere FGGE that are below 75cb. This polar easterly problem is not surprising considering the geometrical difference between the Earth's sphere and the channel.

The momentum transport is shown in Figure 2.8 for 25cb and 75cb. Compared with the December through February results of Chen and Marshall (1983) for the FGGE year, the 75cb momentum transport is too far south by 9° and the maximums are about 7 m^2/sec^2 too strong. The 25cb momentum transport shows a divergence of momentum at around 55° and a convergence

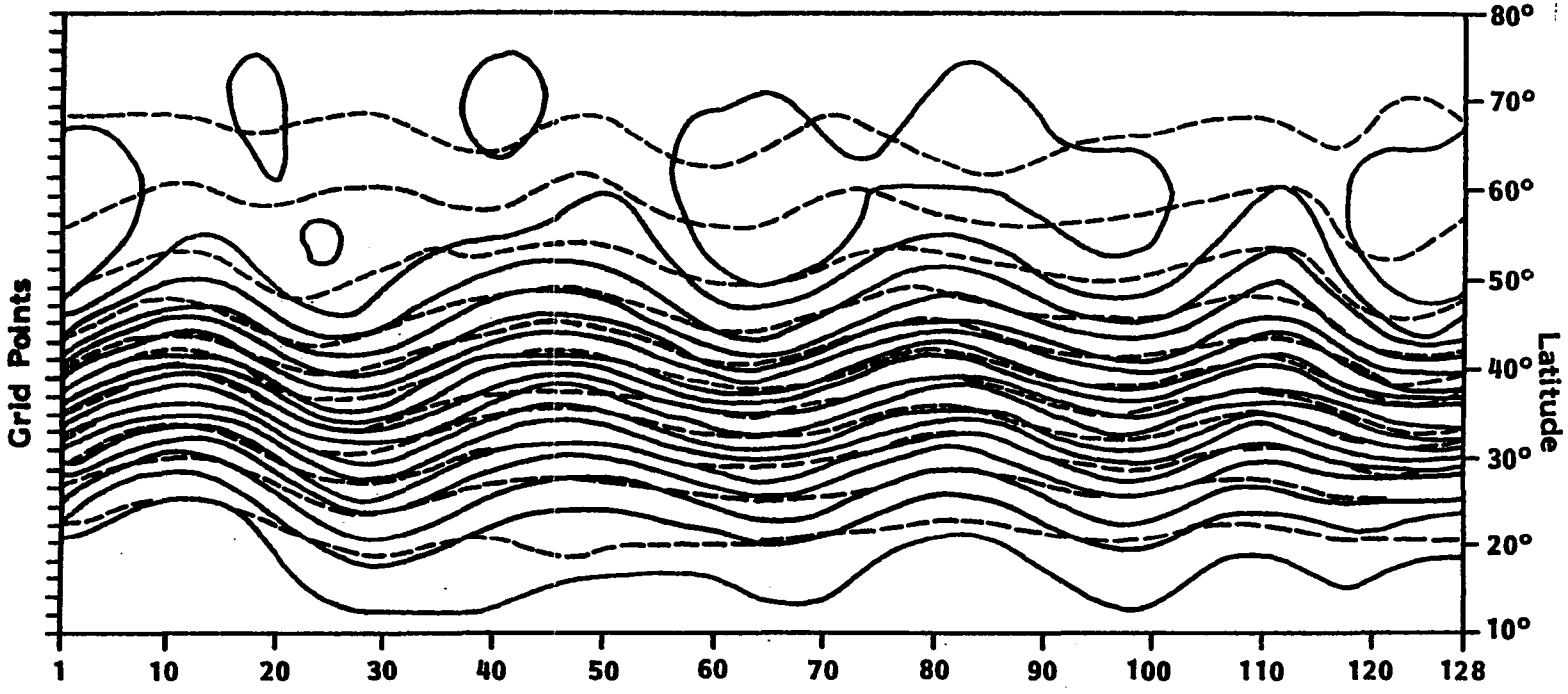

Figure 2.5. The barotropic (solid line) and baroclinic (dashed line) stream functions. Note the contours of baroclinic stream function are also contours of temperature. The left-hand side of the graph displays the spacing of the y-grid. The bottom of the graph displays every tenth point. The position of the 360 degrees of longitude is arbitrary along the x-axis

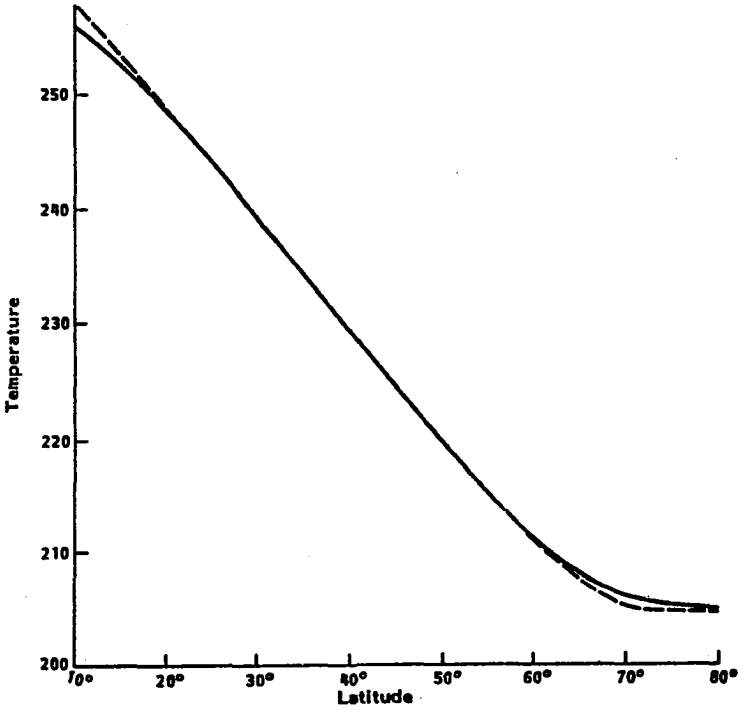

Figure 2.6. The zonal equilibrium Newtonian temperature profile (extracted from Wiin-Nielsen, 1970) (solid line). The profile after truncation to 8 y-direction spectral components is a dashed line, Units °k

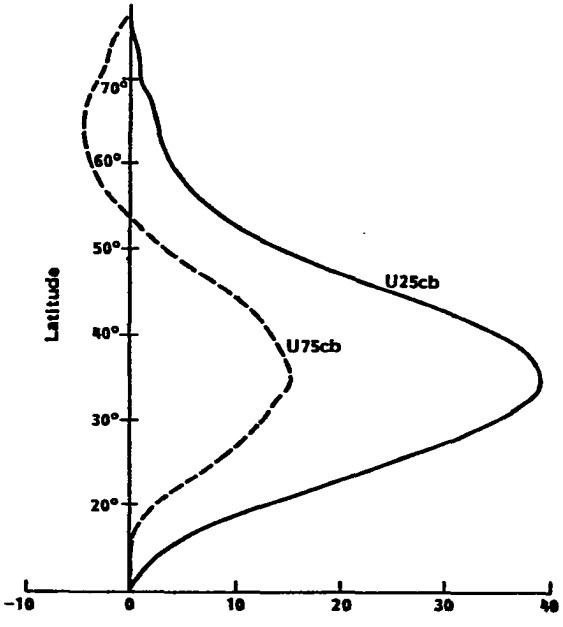

Figure 2.7. Thirty-day average zonal winds, Units ms^{-1}

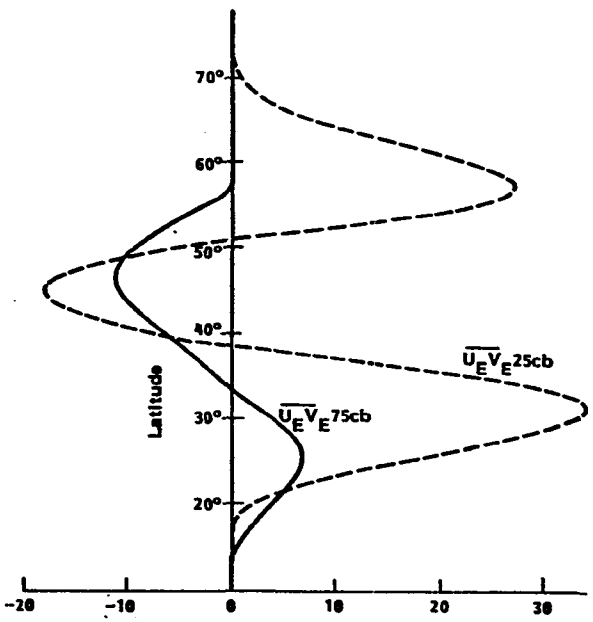

Figure 2.8. Momentum transport in the model, Units 2 $m^2 s^{-2}$

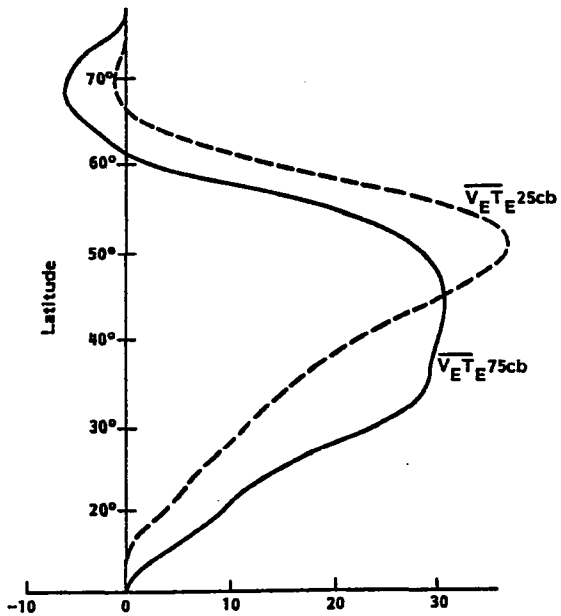

Figure 2.9. Sensible heat transport in the model, Units mks^{-1}

of momentum around 38° latitude. The peak at 33° with a magnitude of 69.8 m^2/sec^2 compares well with the observed peak 34° N with a magnitude of 71 m^2/sec^2. The minimum at 47° of -37.4 m^2/sec^2 in the model compares with -46 m^2/sec^2 at 60° N in the FGGE winter. The second maximum at 59° N has no correspondence with observation (northern hemisphere).

The heat transport is shown in Figure 2.9. The latitude and magnitude of the model maximum heat transport value at 75cb of 28.8 m deg/sec and 54° compare to the observed values of 26 m deg/sec and 51° N of Chen and Marshall (1983). The latitude of maximum model heat transport at 25cb is 48° with a magnitude of 25 m deg/sec which is too strong and a little north compared to observation of 45° and magnitude of 19 m deg/sec.

Figure 2.10 shows the classical Lorenz energy cycle for the model. The numbers in brackets are the observed FGGE winter estimates in the latitude band between 20° N and 65° N. The overall energy cycle is good considering the simplicity of the model. One would expect the eddy kinetic energy and eddy available potential energy to be less than observed because of the lack of mountains and a longitudinal dependence of diabatic heating. This is not found for eddy kinetic energy because the baroclinically unstable waves four and five are much stronger than observed (see Chapter IV). The conversion of energy between A_z and K_z is small compared to this observation. The observational value of $C(A_z,K_z)$ is very dependent on latitude integration due to the cancellation between the Ferrel and Hadley cell. An integration including lower latitudes

gives a smaller observed value (e.g., Wiin-Nielsen, 1967). The conversion $C(K_E,K_Z)$ is anomalous in 78-79 observation. The value found in Chen (1982) for 1976-77 observation of .31 w m^{-2} is more representative of most winters.

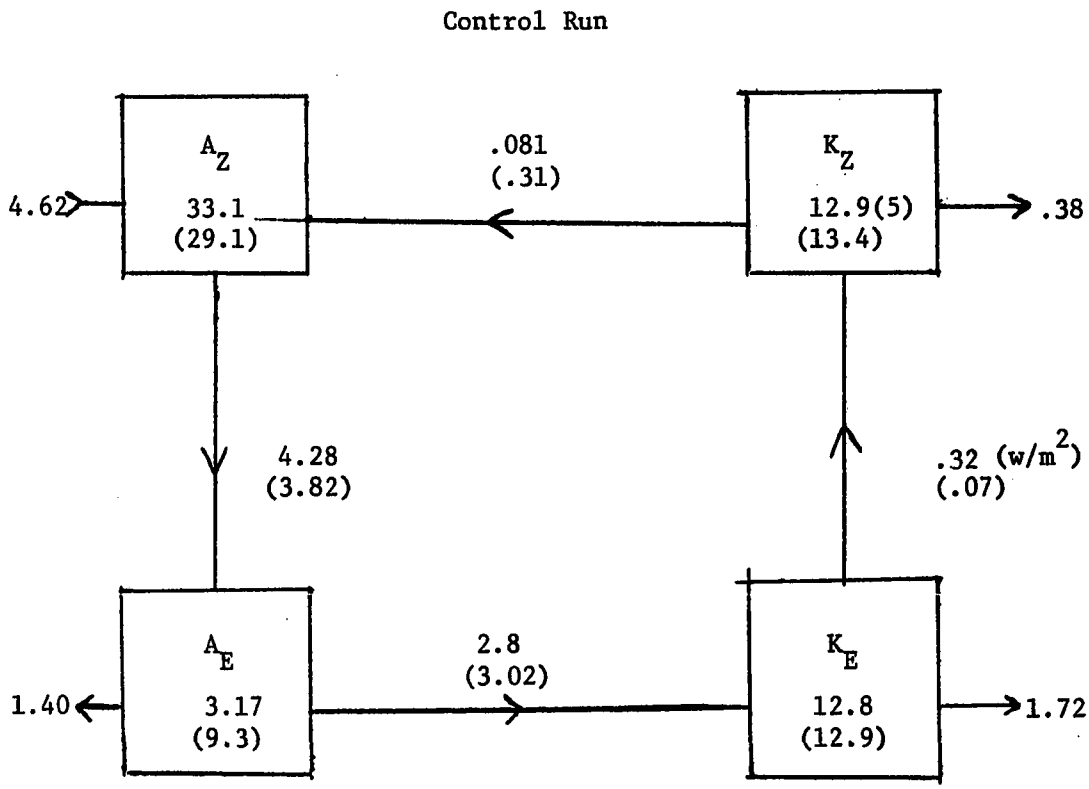

Figure 2.10. The classical Lorenz energy cycle for the model (quantities in parentheses are observations from Chen and Marshall, 1983)

III. FORMULATION AND DERIVATION

The purpose of this chapter is similar to the technical report of Chen and Tribbia (1981). Their equations for kinetic energy are based on the nondivergent primitive momentum equations. The kinetic energy equations of this thesis are based on the quasi-geostrophic equations. This results in considerable differences. The potential enstrophy equations found by Chen and Tribbia (1981) are derived from quasi-geostrophic theory as the ones derived here, but the simpler form of potential vorticity and the baroclinic vorticity equation of the two-layer model makes changes in form. The equations found, though somewhat lengthy, are simpler in form than those of Chen and Tribbia (1981). The most important physical processes are retained. This suits the conceptual aim of this thesis.

The Appendix has a list of symbols used.

A. The Barotropic and Baroclinic Energy Equations

The kinetic energy equations of barotropic and baroclinic flows has been discussed by Wiin-Nielsen (1962) and Wiin-Nielsen and Drake (1965, 1966). In this section, the kinetic energy equations of barotropic and baroclinic flows are derived with no other divisions of the kinetic energy. The equation for available potential energy is mentioned only briefly because its form appears in many other studies (e.g., Lorenz, 1955).

The barotropic kinetic energy for the two-layer model is

$$K_M = \frac{P_o}{2sg} \int \frac{\nabla\psi \cdot \nabla\psi}{2} \, ds. \tag{3.1}$$

The time rate of change of kinetic energy in a closed domain is

$$\frac{d K_M}{dt} = \frac{-P_o}{2sg} \int_s \psi \frac{\partial \nabla^2 \psi}{\partial t} \, ds. \tag{3.2}$$

Equation (2.6), the barotropic vorticity equation, and the continuity equation can be combined to arrive at the flux form of the barotropic vorticity equation,

$$\frac{\partial}{\partial t} \nabla^2 \psi = - \nabla \cdot (\vec{V}_\psi (\nabla^2 \psi + \beta_y)) - \nabla \cdot (\vec{V}_\tau \nabla^2 \tau) + F_M. \tag{3.3}$$

Multiply by $-\psi$,

$$-\psi \frac{\partial \nabla^2 \psi}{\partial t} = \psi \nabla \cdot (\vec{V}_\psi (\nabla^2 \psi + \beta_y)) + \psi \nabla \cdot (\vec{V}_\tau \nabla^2 \tau) - \psi F_M. \tag{3.4}$$

Consider the second term of equation (3.4)

$$\psi \nabla \cdot (\vec{V}_\psi (\nabla^2 \psi + \beta_y) = \nabla \cdot (\psi \vec{V}_\psi (\nabla^2 \psi + \beta_y) - \nabla\psi \cdot \vec{V}_\psi (\nabla^2 \psi + \beta_y).$$

Note $\nabla\psi \cdot \vec{V}_\psi = 0$.

Consider the third term of (3.4),

$$\psi \nabla \cdot (\vec{V}_\tau \nabla^2 \tau) = \nabla \cdot (\psi \vec{V}_\tau \nabla^2 \tau) - \nabla\psi \cdot \vec{V}_\tau \nabla^2 \tau.$$

Integrating over the area of the channel and multiplying by a constant (3.4) with the above terms becomes[1]

$$\frac{d}{dt}K_S = \frac{P_o}{sg}\int_s \nabla\psi \cdot \vec{V}_\tau \nabla^2\tau ds - \frac{P_o}{sg}\int_s F_M\psi ds, \qquad (3.5)$$

(a) (b)

which is the barotropic kinetic energy equation.

The baroclinic kinetic energy and the rate of change of baroclinic energy are, respectively:

$$K_S = \frac{P_o}{sg}\int_s \frac{\nabla\tau\cdot\nabla\tau}{2} ds, \quad \frac{dK_g}{dt} = \frac{-P_o}{2sg}\int_s \tau\frac{\partial\nabla^2\tau}{\partial t} ds.$$

Note the thermal field completely specifies K_S and $\frac{dK_S}{dt}$. Shear kinetic energy is zero for a barotropic atmosphere ($\zeta = \zeta(P)$). This is demanded by the hydrostatic equation and the thermal wind equation of the two-layer mdoel. Note, as mentioned in Chapter II, the vertical shear stream function (τ) and the temperature field are proportional to each other for the two-layer model. The baroclinic potential vorticity equation (2.7), and the continuity equation are combined into

$$\frac{\partial\nabla^2\tau}{\partial t} + \nabla\cdot(\vec{V}_\psi\nabla^2\tau) + \nabla\cdot(\vec{V}_\tau(\nabla^2\psi + \beta_y)) = \frac{-f_o\omega}{\Delta P} + F . \qquad (3.6)$$

Multiply by $\frac{-P_o}{sg}\tau$, and integrate (3.6) over the area of the channel model to find the baroclinic kinetic energy equation of the model,

$$\frac{dK_S}{dt} = \frac{P_o}{sg}\int_s \nabla\tau\cdot\vec{V}_\psi\nabla^2\tau ds - \frac{P_o f_o}{\Delta P s}\int_s \omega\tau ds - \frac{P_o}{s}\int_s F_S\tau ds. \qquad (3.7)$$

(a) (b) (c)

The available potential energy for the model can be shown to be

$$A = \frac{P_o}{sg} k^2 \int_s \tau^2 ds. \tag{3.8}$$

Remember τ is proportional to temperature. The available potential energy equation can be put in the form,

$$\frac{dA}{dt} = \underbrace{\frac{2f_o P_o}{\Delta P sg} \int_s \omega \tau ds}_{(a)} - \underbrace{\frac{P_o f_o^2}{sg\sigma\Delta P} \int_s H\tau ds}_{(b)}. \tag{3.9}$$

Term (a) of (3.5) and term (a) of (3.7) represent the conversion between barotropic and baroclinic kinetic energy. In a region with a negative Laplacian of temperature (i.e., region of temperature maximum), positive thermal advection results in a conversion of baroclinic kinetic energy into barotropic kinetic energy. The form of this integral motivates one to use the thermal field rather than the vertical shear vorticity in interpreting some of the results of Wiin-Nielsen. Note that such an interpretation is strictly valid only in hydrostatic and quasi-geostrophic two-layer flow. Note that the available potential energy is converted into baroclinic kinetic energy only in terms (a) of (3.9) and (b) of (3.7). Terms (b) of (3.5), (c) of (3.7), and (b) of (3.9) are the dissipation of barotropic kinetic energy, baroclinic kinetic energy, and the generation of available potential energy, respectively. Note that these equations can be written symbolically as equations (1.3)- (1.5).

Care should be taken in describing term (c) of (3.7) and term (b) of (3.5). Their sum should give a net outflow of energy from the model.

However, term (c) of (3.7) can be positive at times. This can be understood by considering the hypothetical situation of an initially barotropic flow and the effect of surface friction on the flow. Baroclinic kinetic energy, originally zero, would be produced.

B. Zonal and Eddy Barotropic and Baroclinic Energy Equations

The division of energies into the zonal average $\left(\overline{(\ )} = \frac{1}{L_x}\int_0^{L_x}(\ )dx\right)$ and the zonal departure or "eddy" $\left((\ )' = (\ ) - \overline{(\ )}\right)$ has two purposes. One, the interaction of the eddy field with the zonal flow can be studied. Two, the spectral formulation of the next section can be checked by summing up the nonzonal Fourier components (or wave numbers) to obtain the zonal and eddy components to compare with the formulation here.

The zonal mean of (3.3) is

$$\frac{\partial \nabla^2\overline{\psi}}{\partial t} = -\frac{\partial}{\partial y}\overline{(V_\psi(\nabla^2\psi + \beta_y))} - \frac{\partial}{\partial y}\overline{(V_\tau \nabla^2\tau)} + \overline{F_M}. \tag{3.10}$$

Note $\overline{V_\psi} = \overline{V_\tau} = 0$. Expand the variables of the nonlinear terms in zonal and eddy components.

$$\frac{\partial \nabla^2\overline{\psi}}{\partial t} = -\frac{\partial}{\partial y}\overline{(V'_\psi\, \nabla^2\psi')} - \frac{\partial}{\partial y}\overline{(\tau'\, \nabla^2\tau')} + \overline{F_M}. \tag{3.11}$$

Multiply by $-\psi\frac{P_o}{gs}$ and integrate (3.11) over the area of the channel model. The resulting zonal <u>barotropic kinetic energy</u> equation is

$$\begin{aligned}\frac{dK_{MZ}}{dt} &= \frac{P_o}{gs}\int \underset{(a)}{-\overline{\psi}\frac{\partial \nabla^2\overline{\psi}}{\partial t}}\, ds \\ &= \underset{(b)}{\frac{P_o}{gs}\int\overline{\psi}\frac{\partial}{\partial y}\overline{(V_\psi'\, \nabla^2\psi')}} + \underset{(c)}{\frac{P_o}{gs}\int_s\overline{\psi}\frac{\partial}{\partial y}\overline{(V_\tau'\nabla^2\tau')}ds} - \frac{P_o}{gs}\int\overline{\psi}\,\overline{F_M}ds.\end{aligned} \tag{3.12}$$

Another form of this equation can be obtained by integrating (b) and (d) of the above equation by parts,

$$\frac{dK_{MZ}}{dt} = \frac{-P_o}{gs}\int_s \frac{\partial \bar{U}_\psi}{\partial y}\,\overline{(V_\psi' U_\psi')}\,ds - \frac{P_o}{gs}\int_s \frac{\partial \bar{U}_\psi}{\partial y}\,(V_\tau' U_\tau')\,ds$$

(a) (b)

$$- \frac{P_o}{gs}\int \overline{\psi F_M}\,ds. \qquad (3.13)$$

(c)

The eddy barotropic kinetic energy is derived from the barotropic eddy vorticity equation which can be found by subtracting equation (3.10) from (3.3).

$$\frac{\partial \nabla^2\psi'}{\partial t} = \nabla\cdot(\vec{V}_\psi\,(\nabla^2\psi + \beta_y)) + \frac{\partial}{\partial y}\,\overline{(V_\psi'\,\nabla^2\psi')} - \nabla\cdot(\vec{V}_\tau\,\nabla^2\tau)$$

$$+ \frac{\partial}{\partial y}\,\overline{(V_\tau'\,\nabla^2\tau')} + F'_M. \qquad (3.14)$$

Multiply (3.14) by $-\frac{P_o}{gs}\psi'$ and integrate over the area of the channel model to find

$$\frac{dK_{ME}}{dt} = \frac{P_o}{gs}\int_s \Big\{ \psi'\nabla\cdot(\vec{V}_\psi(\nabla^2\psi + \beta_y) - \psi'\,\frac{\partial}{\partial y}\,\overline{(V_\psi'\,\nabla^2\psi')}$$

$$+ \psi'\nabla\cdot(\vec{V}_\tau\nabla^2\tau) - \psi'\,\frac{\partial}{\partial y}\,\overline{(V_\tau'\,\nabla^2\tau')} - \psi' F_M' \Big\}\,ds. \qquad (3.15)$$

The following identity is helpful in simplifying the above equation.

$$\nabla\cdot(\psi\vec{V}_\tau\nabla^2\tau) = \nabla\psi\cdot\vec{V}_\tau(\nabla^2\tau) + (\bar{\psi} + \psi')\,\nabla\cdot(\vec{V}_\tau\nabla^2\tau).$$

The resulting equation for the eddy barotropic kinetic energy equation is

$$\frac{dK_{ME}}{dt} = \frac{P_o}{sg}\int_s \Big\{ \underbrace{-\psi' \frac{\partial}{\partial y}\overline{(V_\psi' \nabla^2\psi')}}_{(a)} - \underbrace{\bar{\psi}\frac{\partial}{\partial y}\overline{(V_\psi' \nabla^2\tau')}}_{(b)} \underbrace{-\nabla\psi\cdot V_\tau(\nabla^2\tau)}_{(c)}$$

$$\underbrace{-\overline{\psi' F_M'}}_{(d)} \Big\} ds. \qquad (3.16)$$

Terms (a) and (b) can be put into the form of (3.13(a)) and (3.13(b)) by twice integrating by parts and by using the channel boundary conditions.

The zonal average of the baroclinic vorticity equation (3.6) gives

$$\frac{\partial}{\partial t}\nabla^2\bar{\tau} = -\frac{\partial}{\partial y}\overline{(V_\psi' \nabla^2\tau')} - \frac{\partial}{\partial y}\overline{(V_\tau' \nabla^2\psi')} - \frac{f_o}{\Delta P}\bar{\omega} + \bar{F}_S. \qquad (3.17)$$

Multiply (3.17) by $-\frac{P_o}{s}$ and integrate the area of the channel model to receive

$$\frac{dK_{SZ}}{dt} = \frac{P_o}{sg}\int_s \Big\{ \underbrace{\bar{\tau}\frac{\partial}{\partial y}\overline{(V_\psi'\nabla^2\tau')}}_{(a)} + \underbrace{\bar{\tau}\frac{\partial}{\partial y}\overline{(V_\tau'\nabla^2\psi')}}_{(b)} + \underbrace{\bar{\tau}\frac{f_o\bar{\omega}}{\Delta P}}_{(c)} - \underbrace{\bar{F}_S\bar{\tau}}_{(d)} \Big\} ds. \qquad (3.18)$$

The zonal baroclinic kinetic energy equation can be cast in the following form by integrating terms (a) and (b) of (3.18) by parts,

$$\frac{dK_{SZ}}{dt} = \frac{P_o}{sg}\int_s \Big\{ \underbrace{-\frac{\partial\bar{U}_\tau}{\partial y}\overline{(V_\psi' U_\tau')}}_{(a)} \underbrace{-\frac{\partial U_\tau}{\partial y}\overline{(V_\tau' U_\psi')}}_{(b)} + \bar{\tau}\bar{\omega}\frac{f_o}{\Delta P}$$

$$\underbrace{-\bar{F}\bar{\tau}}_{(d)} \Big\} ds. \qquad (3.19)$$

By subtracting (3.17) from (3.6), multiplying by $-\frac{P_o \tau}{gs}$, integrating over the area of the channel model and using the following identities:

$$\tau\nabla\cdot(\vec{V}_\psi \nabla^2\tau) = \nabla\cdot(\tau\vec{V}_\psi\nabla^2\tau) - \nabla\tau\cdot\vec{V}_\psi\nabla^2\tau$$

$$\nabla\cdot(\tau\vec{V}_\tau(\nabla^2\psi + \beta_y)) = \tau\nabla\cdot(\vec{V}_\tau(\nabla^2\psi + \beta_y)) + \nabla\tau\cdot\vec{V}_\tau(\nabla^2\psi + \beta_y)$$

$$\text{and } \nabla\tau\cdot\vec{V}_\tau = 0,$$

one can arrive at

$$\frac{dK_{SE}}{dt} = \frac{P_o}{sg}\int_s \Big\{ \underbrace{-\overline{\tau}\frac{\partial}{\partial y}\overline{(V_\psi'\nabla^2\tau')}}_{(a)} \underbrace{-\overline{\tau}\frac{\partial}{\partial y}\overline{(V_\tau'\nabla^2\psi')}}_{(b)} \underbrace{-\nabla\tau\cdot\vec{V}_\psi\nabla^2\tau}_{(c)} + \underbrace{\frac{f_o}{\Delta P}\overline{\omega'\tau'}}_{(d)} + \underbrace{\overline{F_S'\tau'}}_{(e)} \Big\} ds. \qquad (3.20)$$

Terms (a) and (b) of (3.20) can be put in classical momentum transport form by twice integrating by parts and by using some algebra.

$$(a) \sim -\frac{\partial U_\tau}{\partial y}\overline{(V_\psi' U_\tau')} \quad \text{and} \quad (b) \sim \frac{\partial U_\tau}{\partial y}\overline{(V_\tau' U_\tau')}.$$

Terms (a) and (b) of (3.13) and (3.16) are the conversion of energy between zonal and eddy barotropic kinetic energy. Term (c) of (3.16) and (3.20) is the conversion between barotropic and baroclinic energy. Note, this conversion is between the eddies. This point shall be discussed again. Terms (c) of (3.13), (d) of (3.16), (c) of (3.18), and (d) of (3.20) are the dissipation of zonal and eddy barotropic kinetic energy, and zonal and eddy baroclinic kinetic energy, respectively. Terms (c) of (3.18) and (d) of (3.20) represent conversions between the shear kinetic energy and the available potential energy.

The zonal and eddy available potential energy equations are

$$\frac{dA_Z}{dt} = -\frac{P}{sg}\,2R^2\int\bar{\tau}\frac{\partial}{\partial y}\overline{(V_\psi'\tau')}ds - \frac{f_o^2 P_o}{\Delta pgs}\int_s\bar{\omega}\bar{\tau}\,ds$$

$$-\frac{f_o^2 P}{\Delta P\sigma S_g}\int\bar{\tau}\,\bar{H}\,ds, \qquad (3.21)$$

$$\frac{dA_E}{dt} = \frac{P}{sg}\,2R^2\int_s\bar{\tau}\frac{\partial}{\partial y}\overline{(V_\psi'\tau')}\,ds - \frac{f_o^2 P_o}{\Delta Pgs}\int_s\overline{\omega'\tau'}\,ds$$

$$-\frac{f_o^2 P}{\Delta P\,\sigma\,S_g}\,\overline{\tau'H'}ds. \qquad (3.22)$$

Explanations of these available potential energy (A) terms and their derivation can be found elsewhere (e.g., Lorenz, 1955).

Figure 3.1 is a schematic of these energy exchanges. The conversion from baroclinic to barotropic kinetic energy is expanded, in Figure 3.1, to show the zonal and eddy variables involved. The dotted lines show which types of energy are catalytic and what processes are involved. The term "catalytic" is used to denote an energy that is involved in a conversion but is not directly affected. The arrows in the diagram are a result of the sign of the conversion term only.

The form of this diagram differs significantly from the diagrams of Smagorinsky (1963), Wiin-Nielsen and Drake (1965) and Chen and Tribbia (1981). These differences will obviously be reflected in the spectral form of these equations. Figure 3.2 is the diagram from Chen and Tribbia's energy equations of a nondivergent primitive equation calculation. For purposes

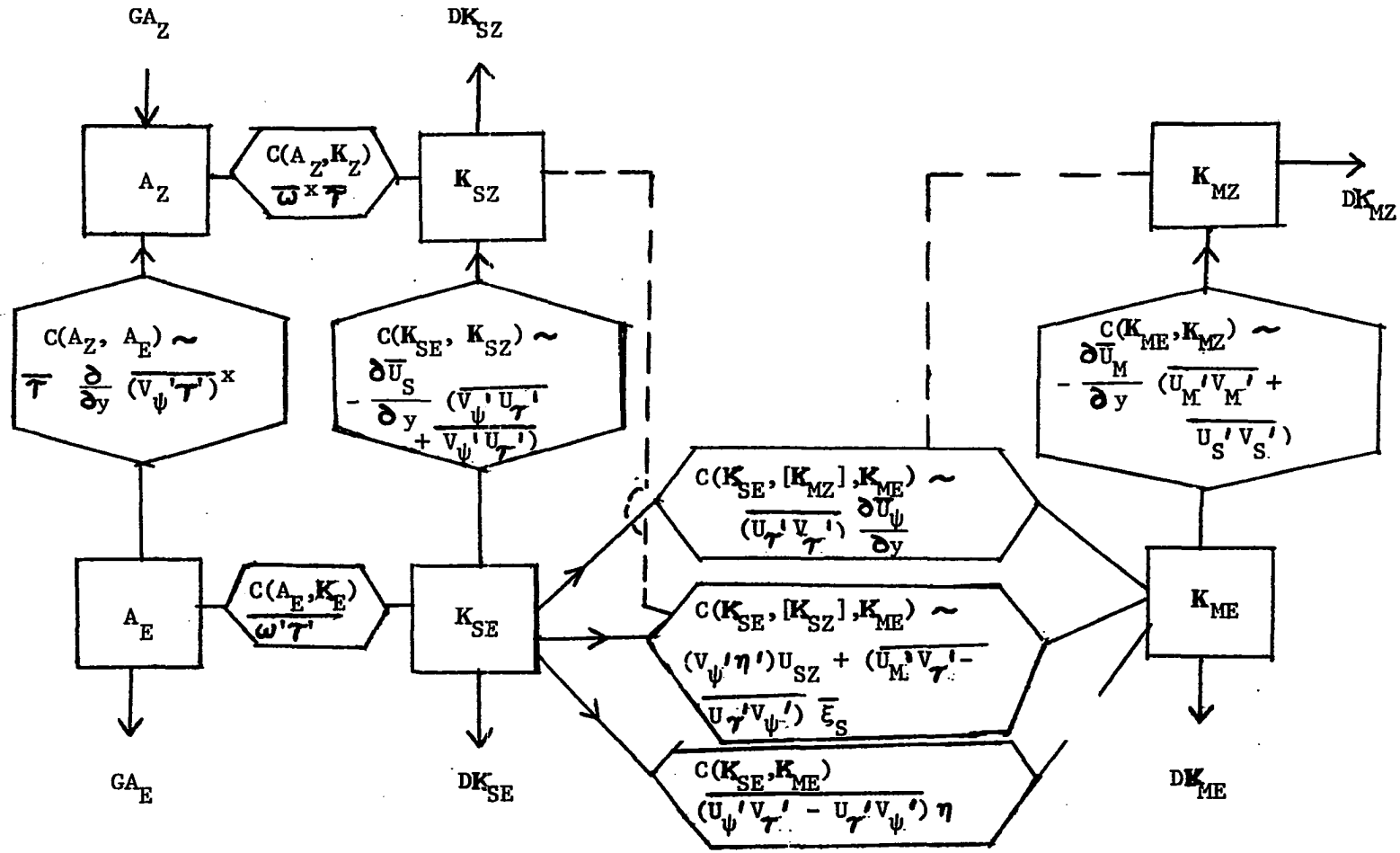

Figure 3.1. The two-level quasi-geostrpophic barotropic and baroclinic energy cycle. Only the integrands are displayed

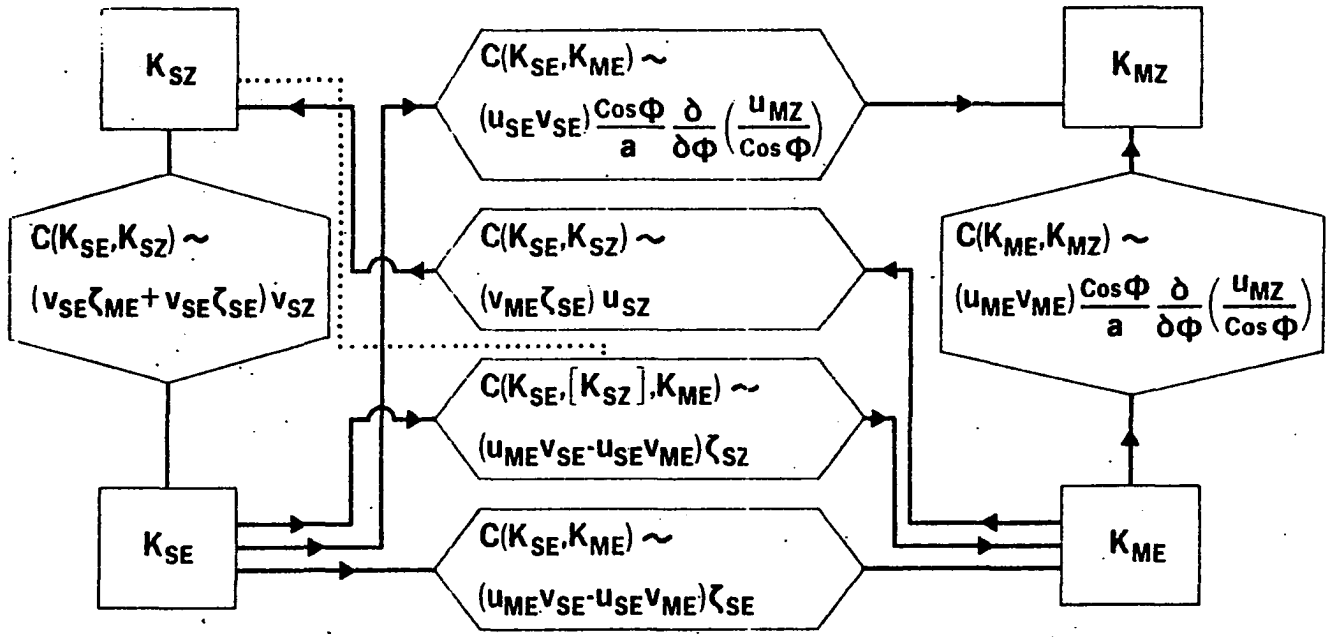

Figure 3.2. Schematic vertical shear and mean energy diagram (after Wiin-Nielsen and Drake, 1966; Chen and Tribbia, 1981)

of comparison, note the subscripts ψ and M, and τ and S have the same definition in Figure 3.1. Note the conversions $C(K_{SE}, K_{ME})$ in the two-layer quasi-geostrophic derivation (Figure 3.1) found here. Also, the eddy to zonal conversions in Figure 3.1 and Figure 3.2 are not equivalent.

Wiin-Nielsen and Drake's calculation (1965) shows the conversion $C(K_{SE}, K_{ME})$ to be one of the larger conversions. This is surprising because the formulation here does not even have a conversion of energy between these reservoirs as seen in Figure 3.2. Inspection of Wiin-Nielsen's results shows the conversion $C(K_{SE},K_{SZ})$ and $C(K_{SZ},K_{ME})$ are of similar magnitude with the former being slightly larger. Over the different periods he computed, these two conversions are usually within 10% or less of each other. Thus, energy just flows through K_{SZ} with a small amount left to maintain K_{SZ}. The quasi-geostrophic formulation inherently contains this catalytic role of K_{SZ}. In other words, the relationship between $C(K_{SE},K_{ME})$ and $C(K_{SZ},K_{ME})$ found in Wiin-Nielson and Drake (1965) is due primarily to the nature of quasi-geostrophic flow.

The conversion $C(K_{SE}, K_{MZ})$ displayed in Figure 3.1 has a similar term in Figure 3.2 only as part of the conversion $C(K_{SE},K_{ME})$ similar to the term discussed in the previous paragraph. Note Figure 3.2 is for the spherical geometry and Figure 3.1 is for the channel model geometry. The conversions (Figure 3.2) $C(K_{SZ},K_{SE})$ and $C(K_{MZ},K_{ME})$ have a different role than those shown in Figure 3.1. In the quasi-geostrophic formulation, their sole purpose is to "maintain" K_{SZ} and K_{MZ}. The form of this conversion is analogous to the classical momentum transport form (Starr, 1965).

Remembering that γ is proportional to temperature, the conversions involving A are in a conventional form (e.g., Lorenz, 1955).

The differences between quasi-geostrophic and the nondivergent primitive energetics seen in Figure 3.1 and 3.2 carry over, as one would expect, into the spectral energetics of the next section.

C. Barotropic and Baroclinic Spectral Energetics

The symmetry of the rotating Earth suggests the decomposition of a variable along a constant in latitude circle, into Fourier components. Other reasons for decomposing the variables only in this manner are: Rossby waves on the ambient planetary vorticity gradient only propagate along lines of constant latitude, the role of the zonal wave number in baroclinic instability, the waves can be damped or propagated in the y direction (north-south) (e.g., Derome, 1979) but only propagated in the x direction (east-west). Because of the spherical geometry of the Earth, spherical harmonics are an obvious choice but are not appropriate to the geometry of the channel model. We can be somewhat consoled by noting that the zeros of a particular Legendre function are not equally spaced so different scales are picked up in the y direction with the same wave number. Figure 4.5 in Chapter IV, reveals some of the relation between a two-dimensional and a one-dimensional index.

An atmospheric variable can be decomposed into the zonal wave numbers (zonal components) by applying the Fourier series (e.g., Saltzman, 1957)

$$f(x) = \sum_{n=-\infty}^{\infty} f(k)e^{ikx},$$

where f(k) is defined by

$$f(k) = \frac{1}{L_x} \int_0^{L_x} f(x)e^{ikx}dx,$$

and L_x is the length of a latitude circle.

Some useful identities for this section are:

Parseval's theorem

$$\frac{1}{L_x} \int_0^{L_x} g(x)f(x)dx = \sum_{m=-\infty}^{\infty} (g(m)f(-m) + f(m)\, g(-m)) \frac{1}{1 + \delta(k,0)}, \tag{3.23}$$

where f(-m) = f*(m) (* symbolizes the complex conjugate). $\delta(k,0)$ is the Dirac delta function.

Convolution theorem (or Faltung integral or folding theorem)

$$\frac{1}{L_x} \int_0^{L_x} f(x)g(x)e^{-ikx}dx = \sum_{m=-\infty}^{\infty} f(m)g(k-m)$$

$$= \sum_{m=-\infty}^{\infty} f(k-m)g(m). \tag{3.24}$$

With these ideas in mind, the spectral energetics of baroclinic and barotropic flow can be derived. The method used is, in principle, that of Chen and Tribbia (1981), but because quasi-geostrophic theory requires the use of the vorticity equation rather than the momentum equation, the details of the derivation are different from their derivation.

The rate of change of a spectral component (or wave number) of barotropic kinetic energy is from (3.23) and (3.2)

$$\frac{dK_M(k)}{dt} = \frac{P_o}{gs} \int_s \left(\psi(-k) \frac{\partial \xi(k)}{\partial t} + \psi(k) \frac{\partial \xi(-k)}{\partial t}\right)\left(\frac{1}{1 + \delta(k,0)} ds\right), \quad (3.25)$$

where $\delta(k,0)$ is the Dirac delta function.[2] The Fourier transform of the barotropic vorticity equation (3.3) is (using 3.24).

$$\frac{\partial \xi(k)}{\partial t} = - \sum_{m=-k}^{k} \left\{ imU_\psi(k-m)\, \xi(m) + V_\psi(k-m) \frac{\partial \xi(m)}{\partial y} - imU_\tau(k-m)\eta(m) - V_\tau(k-m) \frac{\partial \eta(m)}{\partial y} \right\} - \beta V_\psi(k) + F_S(k) \quad (3.26)$$

The above equation and its conjugate are used to form

$$\frac{dK_M(k)(1 + \delta(k,0))}{dt} = \frac{P_o}{gs} \int_s \left\{ -im\xi(m) \underbrace{[U_\psi(k-m)\, \psi(-k) + U_\psi(-k-m)\, \psi(k)]}_{(a)} \right.$$

$$\underbrace{- \frac{\partial \xi(m)}{\partial y} [V_\psi(k-m)\psi(-k) + V_\tau(-k-m)\psi(k)]}_{(b)}$$

$$\underbrace{- im\eta(m) [U_\tau(k-m)\psi(k) + U_\tau(-k-m)\psi(k)]}_{(c)} \quad (3.27)$$

$$\left. \underbrace{- \frac{\partial \eta(m)}{\partial y} [V_\tau(k-m)\psi(-k) + V_\tau(-k-m)\psi(k)]}_{(d)} \right.$$

---

[2] The above equation defines the barotropic kinetic energy by dropping the time derivatives. The barotropic kinetic energy in a two-dimensional index, for this equation, is found by letting (k) become (k,ℓ), except in the delta function. ℓ is the meridional wave number.

$$-\beta\,[V_\psi(k)\,\psi(-k) + V_\psi(-k)\,\psi(k)] + [F_M(k)\,\psi(-k) + F_M(-k)\,\psi(k)]\Big\}\,ds.$$

(e) (f)

Terms (b) and (d) are integrated by parts to give (showing the integrand only)

$$\xi(m)\,\left[\frac{\partial V_\psi(k-m)}{\partial y}\,\psi(-k) + \frac{\partial V_\psi(-k-m)}{\partial y}\,\psi(k)\right]$$

$$+\xi(m)\,\left[V_\psi(k-m)\,\frac{\partial \psi(-k)}{\partial y} + V_\psi(-k-m)\,\frac{\partial \psi(k)}{\partial y}\right]$$

$$+\,\eta(m)\,\left[V_\tau(k-m)\,\frac{\partial \psi(-k)}{\partial y} + V_\tau(-k-m)\,\frac{\partial \psi}{\partial y}(k)\right]$$

$$+\,\eta(m)\,\left[\frac{\partial}{\partial y}\,V_\tau(k-m)\psi(-k) + \frac{\partial}{\partial y}\,V_\tau(-k-m)\,\psi(k)\right].$$

The transformed continuity equation and the above can be combined to form

$$\xi(m)\,[-i\,(k-m)\,U_\psi(k-m)\psi(-k) - i\,(-k-m)\,U_\psi(k-m)\psi(k)]$$

$$\xi(m)\,[-V_\psi(k-m)\,U_\psi(-k) - V_\psi(k-m)\,U_\psi(k)]$$

$$+\,\eta(m)[-i(k-m)\,U_\tau(k-m)\,\psi(-k) - i(-k-m)\,U_\tau(k-m)\,\psi(k)]$$

$$+\,\eta(m)[-V_\tau(k-m)\,U(-k) - V_\tau(-k-m)\,U(k)]. \qquad (3.28)$$

Noting m is a "dummy" variable and putting (3.28) into (3.27), one arrives at the barotropic spectral kinetic energy equation.[3]

---

[3]All of the negative wave numbers can be easily eliminated. Break the summation into two parts, one with positive wave number and the other with negative wave numbers. In the summation over negative wave numbers, let (-k) go to (k). For all variables with the negative wave number change, (-k) go to (+k) and take the complex conjugate such as V(-k) = V*(k). This is not done here because it would double the size of these equations with no advantage in physical interpretation.

$$\frac{d K_M(k)}{dt}(1+\delta(k,0)) = \frac{P_o}{gs}\int \Bigg\{ \underbrace{\frac{\partial U(0)}{\partial y}\,[V_\psi(-k)\,U_\psi(k) + V_\psi(k)\,U_\psi(-k)]}_{(a)}$$

$$+ \tfrac{1}{2}\sum_{\substack{m=-\infty \\ m\neq 0}}^{\infty} \xi(m)[V_\psi(-k)\,U_\psi(k-m) - V_\psi(k-m)\,U_\psi(-k)]$$

$$+ \xi(k)[V_\psi(-m)\,U_\psi(m-k) - V_\psi(m-k)\,U_\psi(-m)] \Bigg\}$$

$$\underbrace{\qquad\qquad\qquad\qquad\qquad\qquad\qquad\qquad}_{(b)}$$

$$+ \tfrac{1}{2}\sum_{\substack{m=-\infty \\ m\neq 0}}^{\infty} \Big\{ \xi(m)[V_\psi(k)\,U_\psi(-k-m) - V_\psi(-k-m)\,U_\psi(k)$$

$$+ \xi(k)[V_\psi(m)\,U_\psi(-k-m) - V_\psi(-k-m)\,U_\psi(m)] \Big\}$$

$$\underbrace{\qquad\qquad\qquad\qquad\qquad\qquad\qquad\qquad}_{(c)}$$

$$+ \sum_{m=-\infty}^{\infty} \Big\{ \eta(m)[V_\psi(-k)\,U_\tau(k-m) + V_\tau(k)\,U_\tau(-k-m)]$$

$$\underbrace{\qquad\qquad\qquad\qquad\qquad\qquad\qquad\qquad}_{(d)}$$

$$- \eta(m)[V_\tau(k-m)\,U_\psi(-k) + V_\tau(-k-m)\,U_\psi(k)]$$

$$\underbrace{\qquad\qquad\qquad\qquad\qquad\qquad\qquad\qquad}_{(e)}$$

$$+ [F_M(k)\,\psi(-k) + F_M(-k)\psi(k)] \Big\}\, ds. \qquad (3.29)$$

Term (b) is the conversion of energy between the Fourier component of wave number k and the zonal barotropic flow. Terms (b) and (c) are the nonlinear triad interaction terms in which barotropic kinetic energy is redistributed among the different wave numbers. Examination of a particular term of the summations in (b) and (c) denoted as $L_1(k,m)$ shows there always exists another term such that $L_1(k,m) = L_2(k,m)$ when summed over all k. Thus, if terms (b) and (c) are summed over all wave numbers (k) they sum to zero. This could be anticipated from Section B. Just as the

advection of kinetic energy in Section B only redistributes the energy in physical space, the terms (b) and (c) redistribute energy among the wave numbers. Terms (a) and (e) are the conversions between barotropic and baroclinic wave numbers of kinetic energy. Note the triad nature of these terms. These terms will be discussed further following the derivation of the spectral baroclinic kinetic energy equation. Term (f) is the dissipation.

Next, the baroclinic spectral kinetic energy equations will be derived. The spectral form of the rate of change of the baroclinic kinetic enery is (using (3.1):

$$\frac{dK_S(k)}{dt} = \frac{P_o}{gs}\int_s \left(\left(\tau(-k)\,\frac{\partial \eta(k)}{\partial t} + \psi(k)\,\frac{\partial \eta(-k)}{\partial t} \right) ds \left(\frac{1}{1+\delta(k,0)} \right) \right) \tag{3.30}$$

By repeating the procedure used to arrive at (3.29), one can find

$$\begin{aligned}
\frac{dK_S(k)}{dt}\,(1+\delta(k,0)) = \frac{P_o}{gs}\int_s \Bigg\{ & \underbrace{\frac{\partial U_\tau(0)}{\partial y}\,[\,U_\psi(k)\,V_\tau(-k) + U_\psi(-k)\,V_\tau(k)\,]}_{(a)} \\
& + \sum_{\substack{m=-k \\ k\neq m}}^{k} \eta(m)\,\underbrace{[U_\psi(k-m)\,V_\tau(-k) - V_\psi(k-m)\,U_\tau(k)]}_{(b)} \\
& + \sum_{m=-k}^{k} \eta(m)\,\underbrace{[U_\psi(-k-m)\,V_\tau(-k) - V_\psi(-k-m)\,U_\tau(k)]}_{(c)} \\
& + \sum_{m=-k}^{k} \Bigg\{ \xi(m)\,\underbrace{[V_\tau(-k)\,U_\tau(k-m) + V_\tau(k)\,U_\tau(-k-m)]}_{(d)} \\
& + \xi(m)\,[V_\tau(k-m)\,U_\tau(-k) + V_\tau(-k-m)\,U_\tau(k)] \Bigg\} \Bigg\}
\end{aligned} \tag{3.31}$$

$$-\xi(k)\ [V_\tau(-m)\ U_\tau(m-k) - V_\tau(m-k)\ U_\tau(-m)]$$

$$-\xi(k)\ [V_\tau(m)\ U_\tau(-k-m) - V_\tau(-k-m)\ U\ (m)]$$

(e)

$$+\ [F_S(k)\ \tau(-k) + F_S(-k)\ \tau(k)]$$

(f)

$$-\frac{f_o}{\Delta P}\ [\omega(k)\ \tau(-k) + \omega(-k)\ \tau(k)]\Big\}ds. \qquad (3.31)$$

(g)

Term (a) of (3.31) is the conversion of baroclinic kinetic energy between the wave number k and the zonal flow. Terms (d) and (e) are the nonlinear triad exchange terms. Terms (d) and (c) redistribute the baroclinic energy among wave numbers just like terms (b) and (e) of (3.29) do for barotropic kinetic energy. However, note that the triads in these equations of (3.31) involve a barotropic component and two baroclinic components (Marshall and Chen, 1982). Term (g) is the conversion between available potential energy and baroclinic kinetic energy of wave number k. Term (f) is the dissipation. Terms (b) and (c) are the conversion between barotropic and baroclinic kinetic energy. This conversion between two types of energy is different from the other conversions. This conversion is best described as a <u>triad conversion</u>. The total loss of baroclinic kinetic energy of, say, wave number 8, will not generally be the amount gained by the barotropic kinetic energy of wave number 8. This conversion also redistributes the energy among wave number, besides conversion in type of energy. Thus, as a result of the triad nature of this conversion, barotropic kinetic energy wave numbers can gain energy from barotropic kinetic energy of different wave numbers and vice versa. However,

the sum over all wave numbers (k) of the terms (d) and (e) of (3.29) must be equal to those of terms (b) and (c) of (3.29) so that energy is conserved. The proof of this follows.

First, consider terms (b) and (c) of (3.31). In term (b), let $\eta = k-m$ and in term (c) let $p = -k-m$. The result is

$$\sum_{n=-k}^{k} \eta(n-k)\,[U_\psi(n)\,V_\tau(-k) - U_\tau(-k)\,V_\psi(n)] + \sum_{p=-k}^{k} \eta(-p-k)\,[U_\psi(p)\,V_\tau(-k) - V_\psi(p)\,U_\tau(-k) \tag{3.32}$$

The same can be done with terms (d) and (e) of (3.29).

$$\sum_{n=-k}^{k} \eta(k-n)\,[V_\psi(-k)\,U_\tau(n) - V_\tau(n)\,U_\psi(-k)] + \sum_{n=-k}^{k} \eta(-k-p)\,[U_\tau(p)\,V_\psi(-k) - V_\tau(p)\,U_\psi(-k)] \tag{3.33}$$

Note for every term in the sum of (3.32) there is a term in (3.33) with k and n (or k and p) switched and with the opposite sign.[4] Thus, if one sums the terms of (3.31) and (3.32), over all k and adds (3.32) and (3.33) the result will be zero.

The spectral available potential energy (A) equation can be formulated by similar methods (e.g., Yang, 1967):

---

[4] $V(-k) = V^*(k)$ and $V^*(k)U(p) = U^*(p)V(k)$.

$$\frac{dA(k)}{dt}(1+\delta(,0)) = \frac{2R^2P}{sg}\int_s \Bigg\{ \underbrace{\frac{\partial \tau_{(o)}}{\partial y}\left[V_\psi(k)\tau(-k) + V_\psi(-k)\tau(k)\right]}_{(a)}$$

$$+ \sum_{m=-k}^{k} \Bigg\{ \underbrace{-im\tau(m)\left[U_\psi(k-m)\tau(-k) + U_\psi(-k-m)\tau(k)\right]}_{(b)}$$

$$- \underbrace{\tau(m)\frac{\partial}{\partial y}\left[V_\psi(k-m)\tau(-k) + V_\psi(-k-m)\tau(k)\right]}_{(c)} \Bigg\}$$

$$+ \underbrace{\frac{\Delta P\sigma}{2f_o}\left[\tau(-k)\omega(k) + \tau(k)\omega(-k)\right]}_{(d)}$$

$$+ \underbrace{\left[H_o(k)\tau(-k) + H_o(-k)\tau(k)\right]}_{(e)} \Bigg\}\, ds. \qquad (3.34)$$

Note that temperature is advected only by the barotropic velocity (vertical mean) in the two-layer quasi-geostrophic model (see equation (2.5)). Also remember, τ is proportional to temperature. Term (a) is the conversion A of wave number k and the zonal A. Term (d) is the conversion with baroclinic kinetic energy of the A. Term (e) is the "generation" of A. Terms (b) and (c) are the nonlinear terms, which are not in a form such that one can easily see for every term of the sums there exists another term, when summed over k, that is the same but of opposite sign. Terms (b) and (c) can be put in such a form by using the continuity equation. The result is

$$\tfrac{1}{2}\sum_{m=-k}^{k}\Big\{ - V_\tau(m)\,[U_\psi(k-m)\tau(-k) + U_\psi(-k-m)\tau(k)]$$

$$- V_\tau(m)\,[V_\psi(k-m)\tau(-k) + V_\psi(-k-m)\tau(k)]$$

$$+ \tau(m)\,[V_\tau(-k)\,U_\psi(k-m) + V_\tau(k)\,U_\psi(-k-m)]$$

$$+ \tau(m)\,[V_\psi(k-m)\,U_\tau(-k) + V_\tau(-k-m)\,U_\tau(k)]\Big\}.$$

Note that for every term of the summation there is a term with k and m switched and the opposite sign (also, note the negative wave numbers in the summation). Thus, this term represents the redistribution of A among the spectrum of wave numbers.

The results of this section can be checked against the results of the previous section, when these equations are summed over all wave numbers. The nonlinear terms sum to zero. The barotropic to baroclinic conversion of kinetic energy are the same. This can be seen by extracting the zonal quantities (wave number zero) from (b) + (c) from (3.31) or (d) and (e) of (3.29).

The classical spectral energetics can be found by adding (3.30) and (3.31). Then the baroclinic-barotropic kinetic energy exchanges add to zero when summed over all wave numbers but are involved in a redistribution of the kinetic energy spectrum.

D. Barotropic and Baroclinic Potential Enstrophy Equations

The potential vorticity for the quasi-geostrophic system of equations is:

$$q = \xi + f + \frac{\partial}{\partial P}\frac{f_o^2}{\sigma}\frac{\partial \psi}{\partial P} \qquad (3.35)$$

for an arbitrary level. The potential vorticity in the upper layer of the two-layer model is

$$q_1 = \xi_1 - 2R^2\tau + f \tag{3.36}$$

where $R^2 = \frac{f_o^2}{2\sigma(\Delta P)^2} = \frac{1}{(L_R)^2}$. In the lower layer, the potential vorticity is $q_3 = \xi_3 + 2R^2 + f$. The model vertical shear and mean potential vorticities are defined, and referred to as baroclinic potential vorticity

$$q_S = \frac{q_1 - q_3}{2} = \eta - R^2\tau \tag{3.37}$$

and barotropic potential vorticity

$$q_M = \frac{q_1 + q_3}{2} = \xi + f.$$

From these, we define the barotropic and baroclinic potential enstrophy as

$$E_M = \frac{1}{s}\int \frac{\xi^2}{2}\, ds, \text{ and } E_S = \frac{1}{s}\int \frac{q_S^2}{2}\, ds \tag{3.38}$$

respectively. Note f has been excluded from E_M because it is not a function of time. By multiplying equation (3.3) by ξ, using the two-dimensional divergence theorem and the boundary conditions one finds

$$\frac{dE_M}{dt} = \underbrace{\frac{1}{s}\int \nabla\xi \cdot \tilde{V}_\tau\, \eta\, ds}_{(a)} + \underbrace{\frac{1}{s}\int F_M\, \xi\, ds}_{(b)} - \underbrace{\frac{1}{s}\int \xi\beta V ds}_{(c)} \tag{3.39}$$

for the barotropic enstrophy equation. To find the baroclinic potential enstrophy equation begin with (2.7). This equation can be cast in the form

$$\frac{\partial q_S}{\partial t} + \vec{V}_\psi \cdot \nabla q_S + \vec{V}_\tau \cdot \nabla \xi + \beta V_\tau = F + H = F_o \tag{3.40}$$

where F is the dissipation term, H is the diabatic term and F_o is their sum. Multiply by q_S and use the continuity equation to find

$$\frac{\partial q_S^2}{\partial t} + \nabla \cdot (\vec{V}_\psi \frac{q_S^2}{2}) + q_S \vec{V}_\tau \cdot \nabla \xi + \beta q_S V_\tau = F_o \tag{3.41}$$

The following identities are helpful.

$$\tau \vec{V}_\tau \cdot \nabla \xi = \nabla \cdot (\vec{V}_\tau \tau \xi) - (\nabla \cdot \vec{V}_\tau) \tau \xi - \nabla \tau \cdot \vec{V}_\tau \xi$$

$$\nabla \tau \cdot \vec{V}_\tau = 0 = \nabla \cdot \vec{V}_\tau$$

These identities, the two-dimensional divergence theorem and the model boundary conditions can be used to arrive at the baroclinic potential enstrophy equation.

$$\frac{dE_S}{dt} = -\frac{1}{s}\int \eta \vec{V}_\tau \cdot \nabla \xi \, ds - \frac{1}{s}\int \beta q_S V_\tau \, ds + \frac{1}{s}\int F_o q_S \, ds \tag{3.42}$$
$$\text{(a)} \qquad \text{(b)} \qquad \text{(c)}$$

Note the baroclinic potential energy is trivially constant for a barotropic atmosphere ($\zeta = \zeta(P)$).

Term (a) of (3.39) and (3.42) is the conversion between baroclinic potential enstrophy and barotropic enstrophy. From the form of this integral, one finds that there is a conversion from baroclinic potential enstrophy to barotropic enstrophy when the vertical mean vorticity is advected by the vertical shear velocity in a region of relative temperature maximum. For an alternative interpretation, rewrite the integrand as $(\nabla^2 \tau) J(\xi, \tau)$ where J is the Jacobian. Terms (c) of (3.39) and

(b) of (3.42) are due to the change in enstrophy from the advection of the ambient planetary vorticity gradient which is zero for our closed domain. Term (b) of (3.39) and (c) of (3.42) are the dissipation of the respective enstrophies.

To gain further insight into term (3.42(a)), consider the highly truncated stream function

$$\psi = -\overline{V}_y + A\sin(kx)\cos(my)$$
$$\tau = \overline{V}_{\tau y} + A_\tau \sin(kx + \alpha_\tau)\cos(my).$$

Note wave-wave interactions are excluded a priori with these simplified stream functions. (3.42(a)) becomes

$$\frac{A_\tau A}{4}(k^2 + m^2)^2 k\ \overline{U_\tau}\sin\alpha_\tau.$$

This result is of a similar form (phase relationship, etc.) to that found for the conversion barotropic to baroclinic kinetic energy (Wiin-Nielsen, 1962). The only difference is the conversion from barotropic to baroclinic potential enstrophy has a higher wave number dependence.

E. Zonal and Eddy Barotropic and Baroclinic Potential Enstrophy Equations

The zonal and eddy barotropic and baroclinic potential enstrophy quations are formulated as a check on the spectral formulation of the next section and to gain insight with less complexity of the next section's equations. First, zonally average (2.7) and multiply by $\overline{\xi}$ to find

$$\frac{\partial \overline{\xi}^2}{\partial t} = -\frac{\partial}{\partial y}\left(\overline{\xi}\ \overline{(V_\psi'\ \xi')}\right) + \frac{\partial \overline{\xi}}{\partial y}\ \overline{(V_\psi \xi)} - \frac{\partial}{\partial y}\left(\overline{\xi}\ \overline{(V_\tau'\ \eta')}\right)$$

$$+ \frac{\partial \overline{\xi}}{\partial y}\ \overline{(V_\tau'\eta')} + \overline{F}\ \overline{\xi} \qquad (3.43)$$

Integrating over area and using the model boundary conditions, one finds

$$\frac{dE_{MZ}}{dt} = \frac{1}{s}\int \left\{ \underbrace{\frac{\partial \overline{\xi}}{\partial y}\ \overline{(V_\psi'\ \xi')}}_{(a)} + \underbrace{\frac{\partial \overline{\xi}}{\partial y}\ (V_\tau'\eta')}_{(b)} + \underbrace{\overline{F}_M \overline{\xi}}_{(c)} \right\} ds, \qquad (3.44)$$

for the zonal barotropic potential enstrophy equation. Subtract (3.43) from (2.6) multiplied by ξ and expand in zonal and eddy quantities to find

$$\frac{\partial \overline{\xi'^2}}{\partial t} = \frac{\partial}{\partial y}\left(\overline{V_\psi'\ \frac{\xi'^2}{2}}\right) - \frac{\partial}{\partial y}\left(\overline{V_\tau'\xi'\eta'} + \overline{V_\tau'\xi'\eta'}\right) + \overline{\nabla\xi \cdot V_\tau \eta} - \overline{\beta \xi' V_\psi'}$$

$$+ \overline{F_M'\xi'} - \frac{\partial \overline{\xi}}{\partial x}\left(\overline{V_\psi'\xi'} + \overline{V_\tau'\eta'}\right). \qquad (3.45)$$

Integrate over y and use the boundary conditions to find

$$\frac{dE_{ME}}{dt} = \underbrace{\frac{1}{s}\int \nabla\xi \cdot \vec{V}_\tau ds}_{(a)} - \underbrace{\frac{1}{s}\int \overline{\beta \xi' V_\psi' ds}}_{(b)} + \underbrace{\frac{1}{s}\int \overline{F'\xi' ds}}_{(c)} - \underbrace{\frac{1}{s}\int \frac{\partial \xi}{\partial y}\ (V_\psi'\xi')ds}_{(d)}$$

$$- \frac{1}{s}\int \frac{\partial \xi}{\partial y}\ \overline{(V_\tau'\eta')}ds. \qquad (3.46)$$

Expand term (a) in zonal and eddy parts

$$\frac{\partial \xi}{\partial x} U_\tau \eta + \frac{\partial \xi}{\partial y} V_\tau \eta = \overline{\frac{\partial \xi'}{\partial x}\eta'}\overline{U}_\tau + \overline{\frac{\partial \xi'}{\partial x} U_\tau'}\overline{\eta} + \frac{\partial \xi'}{\partial x} U_\tau'\eta'$$

$$+ \frac{\partial \overline{\xi}}{\partial y}\overline{V_\tau'\eta'} + \overline{\frac{\partial \xi'}{\partial y} V_\tau'}\overline{\eta} + \overline{\frac{\partial \xi'}{\partial y} V_\tau'\eta'}.$$

Examine the terms $\overline{\eta}\,\overline{U_T'\frac{\partial \xi'}{\partial x}}$ and $\overline{V_T'\frac{\partial \xi'}{\partial x}\eta}$

$$\overline{\eta\left(U_T'\frac{\partial \xi'}{\partial y}+V_T'\frac{\partial \xi'}{\partial x}\right)}=\overline{\eta\left(U_T\frac{\partial \xi}{\partial x}+V_T\frac{\partial \xi}{\partial y}\right)}$$

$$=\overline{\eta}\,\frac{\partial}{\partial y}\left(V_T\xi\right)$$

$$=\frac{\partial}{\partial y}\left(\overline{\eta}\,V_T\xi\right)-\frac{\partial\overline{\eta}}{\partial y}\overline{V_T'\xi'}.$$

The eddy barotropic potential enstrophy becomes

$$\frac{\partial E_{ME}}{\partial t}=\frac{1}{s}\int\Bigg\{\underbrace{\overline{\frac{\partial \xi'\eta'}{\partial x}U_T}}_{(a)}+\underbrace{\overline{\frac{\partial \xi'}{\partial x}U_T'\eta'}}_{(b)}+\underbrace{\overline{\frac{\partial \xi'}{\partial y}V_T'\eta'}}_{(c)}-\underbrace{\overline{\frac{\partial \eta}{\partial y}V_\psi'\xi'}}_{(d)}$$

$$\underbrace{-\overline{\beta\,\xi'V_\psi'}}_{(e)}+\underbrace{\overline{F_M'\xi'}}_{(f)}-\underbrace{\overline{\frac{\partial \xi}{\partial y}V_\psi'\xi'}}_{(g)}\Bigg\}. \tag{3.47}$$

These terms will be classified after derivation of the zonal and eddy baroclinic potential enstrophy equations.

Next, the zonal baroclinic potential enstrophy equations are derived. Begin by zonally averaging (2.7) and then multiplying by q_s to find

$$\underbrace{\frac{d}{dt}\left(\frac{q_S^2}{2}\right)}_{(a)}+\overline{q_S}\,\frac{\partial}{\partial y}\underbrace{\left(\overline{V_\psi'\,q_S'}\right)}_{(b)}+\overline{q_S}\,\frac{\partial}{\partial y}\underbrace{\left(\overline{V_T'\xi'}\right)}_{(c)}=\overline{F_o}\,\overline{q_S} \tag{3.48}$$

Note $$\overline{q_S}\,\frac{\partial}{\partial y}\left(\overline{V_\psi'\,q_S'}\right)=\frac{\partial}{\partial y}\left(\overline{q_S}\,\overline{V_\psi'\,q_S'}\right)-\frac{\partial \overline{q_S}}{\partial y}\left(\overline{V_\psi'q_S'}\right) \tag{3.49}$$

Using (3.49) in (3.48) and a similar expression for term (c) in (3.48), and integrating, the zonal baroclinic potential enstrophy equation is found.

$$\frac{dE_{SM}}{dt} = \frac{1}{s}\int\left\{\underbrace{\frac{\partial \bar{q}_S}{\partial y}\overline{(V_\psi' q_S')}}_{(a)} + \underbrace{\frac{\partial \bar{\eta}}{\partial y}\overline{(V_\tau' \xi')}}_{(b)} - \underbrace{R^2 \bar{U}_\tau \overline{(V_\tau' \xi')}}_{(c)} + \underbrace{\overline{F_o' \xi'}}_{(d)}\right\} ds. \tag{3.50}$$

Next, the eddy baroclinic potential enstrophy equation is formed. Subtract (3.48) from (3.41) and integrate over area to form

$$\frac{dE_{SE}}{dt} = \frac{1}{s}\int\left\{\underbrace{-\eta \vec{V}_\tau \cdot \nabla \xi}_{(a)} \underbrace{-\beta q_S V_\tau}_{(b)} + \underbrace{\overline{F_S' q_S'}}_{(c)} \underbrace{- \frac{\partial \bar{q}_S}{\partial y}\overline{(V_\psi' q_S')}}_{(d)} - \underbrace{\frac{\partial \bar{q}_S}{\partial y}\overline{(V_\tau' \xi')}}_{(e)}\right\} ds. \tag{3.51}$$

Term (a) can be expanded as was done in arriving at (3.47). Term (e) can be expanded using (3.37). The eddy baroclinic potential enstrophy equation is:

$$\frac{dE_{SE}}{dt} = -\frac{1}{s}\int\left\{\underbrace{\overline{\frac{\partial \xi'}{\partial y}\eta' U_\tau}}_{(a)} + \underbrace{\overline{\frac{\partial \xi'}{\partial x} U_\tau' \eta'}}_{(b)} + \underbrace{\frac{\partial \bar{\xi}}{\partial y}\overline{V_\tau' \eta'}}_{(c)} + \underbrace{\overline{\frac{\partial \xi'}{\partial y} V_\tau' \eta'}}_{(d)}\right.$$

$$\left.\underbrace{-\beta \overline{q_S' V_\tau'}}_{(e)} + \underbrace{\overline{F_S' q_S'}}_{(f)} \underbrace{- \frac{\partial \bar{q}_S}{\partial y}\overline{(V_\psi' q_S')}}_{(g)} + \underbrace{R^2 \frac{\partial \bar{\tau}}{\partial y}\overline{(V_\tau' \xi')}}_{(h)}\right\} ds. \tag{3.52}$$

Terms (a), (b) and (c) of (3.52) and of (3.47) represent direct conversions of eddy enstrophy between barotropic and baroclinic forms. Term (d) in (3.52) and (term (b) in (3.44) are the conversion between zonal barotropic enstrophy and eddy baroclinic potential enstrophy. Term (e) of (3.52) and term (f) of (3.47) are the changes of baroclinic and barotropic enstrophy due to advection of the planetary ambient vorticity. Terms (g) and (h) of (3.52) and the terms (a) and (c) of equation (3.50) are the conversions between eddy and zonal baroclinic potential enstrophy.

The remaining terms are the dissipation of the various forms of the potential enstrophy.

These equations can be compared to the equation of Chen and Tribbia (1981). Their results are for the vertical shear and mean of a multi-layer atmosphere. The difference in these equations can be traced to the absence of shear transport of shear quantities in the baroclinic vorticity equation,[5] as well as the simple form of the potential vorticity appropriate to the two-layer quasi-geostrophic approximations.

F. Barotropic and Baroclinic Spectral Potential Enstrophy Equations

The rate of change of the barotropic enstrophy for a wave number is, using Parceval's identity,

$$\frac{dE_M(k)}{dt} = \frac{1}{s}\int_s \left(\xi(k)\frac{\partial \xi(-k)}{\partial t} + \xi(-k)\frac{\partial \xi(k)}{\partial t}\right)\left(\frac{1}{1+\delta(k,0)}\right) ds \qquad (3.53)$$

Multiply (3.26) by $\xi(k)$ and integrate are to form

$$\frac{dE_M(k)}{dt} = \frac{1}{s}\int_s \Bigg\{ \underbrace{-im\xi(m)\left[U_\psi(k-m)\xi(-k) + U_\psi(-k-m)\xi(k)\right]}_{(a)}$$

$$\underbrace{-\frac{\partial \xi(m)}{\partial y}\left[V_\psi(k-m)\,\xi(-k) + V_\psi(-k-m)\,\xi(k)\right]}_{(b)}$$

$$\underbrace{-im\eta(m)\left[U_\tau(k-m)\,\xi(-k) + U_\tau(-k-m)\,\xi(k)\right]}_{(c)}$$

---

[5] In the equation of the baroclinic potential vorticity (Equation 2.6) for the two-layer model, the three advection terms involve advection of certain quantities of the barotropic flow by the baroclinic flow and vice versa. However, the baroclinic flow does not advect baroclinic quantities

(Footnote 5 continued)

$$-\frac{\partial \eta(m)}{\partial y}\,[V_T(k-m)\,\xi(-k) + V_T(-k-m)\,\xi(k)]$$

(d)

$$-\beta\,[V_\psi(k)\,\xi(-k) + V_T(-k-m)\,\xi(k)]$$

(e)

$$+\,[F_M(k)\,\xi(-k) + F_M(-k)\,\xi(k)]\Big\}\,ds. \qquad (3.54)$$

(f)

Next, take m = 0 out of the summations and integrate one-half of the terms (b) and (d) by parts. The change in form of the nonlinear term or "redistribution" term is preferable in that it will make it easier to see that this term will sum to zero when summed over all wave numbers.

$$\frac{dE_M(k)}{dt} = \frac{1}{s}\int_s \Bigg\{ -\frac{\partial \xi(0)}{\partial y}\,[V_\psi(k)\,\xi(-k) + V_\psi(-k)\,\xi(k)]$$

(a)

$$-\frac{\partial \eta(0)}{\partial y}\,[V_T(k)\,\xi(-k) + V_T(-k)\,\xi(k)]$$

(b)

$$+\,U_T(0)\,[-ik\eta(k)\,\xi(-k) + ik\eta(-k)\,\xi(k)]$$

(c)

$$+\sum_{\substack{m=-k\\ m\neq 0}}^{k} \tfrac{1}{2}\,[\xi(m)\,[-ikU_\psi(k-m)\,\xi(-k) + ikU_\psi(-k-m)\,\xi(k)]$$

(d)

$$+\,\xi(m)\,\left[V_\psi(k-m)\,\frac{\partial \xi(-k)}{\partial y} + V_\psi(-k-m)\,\frac{\partial \xi(k)}{\partial y}\right]$$

(e)

$$-\,im\xi(m)\,[U_\psi(k-m)\,\xi(-k) + U_\psi(-k-m)\,\xi(k)]$$

(f)

(Footnote 5 continued) in this equation. The vertical shear potential vorticity equation for a multi-level atmosphere does have this term and results in some of the differences in the results of this section and those of Chen and Tribbia (1981).

$$- \frac{\partial \xi(m)}{\partial y} [V_\psi(k-m)\, \xi(-k) + V_\psi(-k-m)\, \xi(k)]$$

(g)

$$+ \eta(m) [V_T(k-m) \frac{\partial \xi(-k)}{\partial y} + V_T(-k-m) \frac{\partial \xi(k)}{\partial y}$$

(h)

$$+ \sum_{\substack{m=-k \\ m\neq 0 \\ m\neq k}}^{k} - ik\eta(m)\, U_T(k-m)\, \xi(-k)$$

(i)

$$+ \sum_{\substack{m=-k \\ m\neq 0 \\ m\neq k}}^{k} ik\eta(m)\, U_T(-k-m)\, \xi(k)$$

(j)

$$- \beta [V_T(k)\, \xi(-k) + V_\psi(-k)\, \xi(k)]$$

(k)

$$- [F_m(k)\, \xi(-k) + F_m(-k)\, \xi(-k)] \Big\} \, ds. \qquad (3.55)$$

(l)

Term (a) of (3.55) is the conversion between the barotropic enstrophy of wave number k and the zonal barotropic enstrophy. Term (b) is the conversion between the barotropic enstrophy of wave number k and the zonal (k=0) baroclinic potential enstrophy. Terms (c), (h), (i), and (j) comprise the conversion of enstrophy between barotropic enstrophy of wave number k and all the wave numbers of the baroclinic potential enstrophy. Terms (d), (e), (f), and (g) are the nonlinear exchange between the barotropic enstrophy of wave number k and all other wave numbers of this same enstrophy. The form of these latter terms are such that, for any term in the summation, a term can be found such that when k and m are switched then two terms can be found that are the negatives of each other.

Term (k) results from the advection of the ambient planetary vorticity and is zero over a closed domain. Term (l) is the dissipation of barotropic enstrophy.

In a similar manner, the baroclinic potential enstrophy equation can be found. The only added detail is to expand the baroclinic potential vorticity variable into baroclinic vorticity (η) and the "thermal" baroclinic vorticity ($R^2\tau/2$). The resulting equation is

$$\frac{dE_S}{dt} = \frac{1}{s}\int_s \Bigg\{ -\frac{\partial q_S(0)}{\partial y}\,[q_S(-k)\ V_\psi(k) + q_S(k)\ V_\psi(-k)] \qquad \text{(a)}$$

$$-\frac{\partial \xi(0)}{\partial y}\,[\eta(-k)\ V_\tau(k) + \eta(k)\ V_\tau(-k)] \qquad \text{(b)}$$

$$- U_\tau(0)\,[i\eta(-k)\,\xi(k) - ik\eta(k)\ \xi(-k)] \qquad \text{(c)}$$

$$-\sum_{\substack{m=-k\\ m=o}}^{k} \tfrac{1}{2} \Bigg\{ imq_S(m)\ [q_S(-k)\ U_\psi(k-m) + q_S(k)\ U_\psi(-k-m)] \qquad \text{(d)}$$

$$- q_S(m)\ [-ikU(k-m)\ q_S(-k) + ikU_\psi(-k-m)\ q_S(k)] \qquad \text{(e)}$$

$$+\frac{\partial q_S(m)}{\partial y}\,[q_S(-k)\ V_\psi(k-m) + q_S(K)\ V_\psi(-k-m)] \qquad \text{(f)}$$

$$- q_S(m)\ \left[V_\psi(k-m)\ \frac{\partial q_S(-k)}{\partial y} + V_\psi(-k-m)\ \frac{\partial q_S(k)}{\partial y}\right] \Bigg\} \qquad \text{(g)}$$

$$\sum_{m=-k}^{k} \Bigg\{ R^2\ \xi(m)\ [U_\tau(-k)\ V_\tau(k-m) + U_\tau(k)\ V_\tau(-k-m)] \qquad \text{(h)}$$

$$
\begin{aligned}
&- R^2\ \xi(m)\ [V_T(-k)\ U_T(k-m) + V_T(k)\ U_T(k-m)] \\
&\qquad\qquad (i) \\
&+\frac{\partial\ \xi(m)}{\partial y}\ [\eta(-k)\ U_T(k-m) + \eta(k)\ V_T(-k-m)] \Bigg\} \\
&\qquad\qquad (j) \\
&+ \sum_{\substack{m=-k \\ m=k}}^{k} - im\ \xi(m)\ \eta(-k)\ U_T(k-m) + \sum_{m=-k}^{k} - im\ \xi(m)\ \eta(k)\ U_T(-k-m) \\
&\qquad\qquad (k) \qquad\qquad\qquad\qquad (l) \\
&- \beta\ [V_T(k)\ q_S(-k) + V_T(-k)\ q_S(k)] \\
&\qquad\qquad (m) \\
&+ [F_o(k)\ q_S(-k) + F_o(-k)\ q_S(k)] \Bigg\}\ ds. \qquad\qquad (3.56)
\end{aligned}
$$

Term (a) is the conversion between the baroclinic potential enstrophy of wave number k and the zonal baroclinic potential enstrophy. Term (b) is the conversion between the baroclinic potential enstrophy of wave number k and the zonal barotropic enstrophy. Terms (c), (j), (k), and (l) are the conversions between a wave number k of baroclinic potential enstrophy and all baroclinic potential enstrophy wave numbers. Terms (d), (e), (f), (g), (h), and (i) are the nonlinear exchanges of the baroclinic potential enstrophy of wave number k with other wave numbers. In order to see that these latter terms sum to zero, as we have seen for other triad nonlinear exchanges, group together terms (d) and (e), (f) and (g), and (h) and (i). Note that each of these pairs of terms separately will sum to zero when summed over k (they are already summed over m). Term (m) results from the advection of planetary ambient vorticity and is zero when integrated

over the closed domain of the model. Term (n) results from the dissipation of the baroclinic potential vorticity due to surface friction, diffusion and generation due to diabatic heating.

The final form of all the spectral equations derived in this section are such that when they are summed over all nonzonal wave numbers (k), every term matches with a term in the previous section on the zonal and eddy subdivision. This provides a check for these equations.

G. A Classification and Summary of the Spectral Exchanges Examined

The spectral equations derived in this chapter for the two-layer, quasi-geostrophic two-layer channel system can be written symbolicly as

$$\frac{dK_M(k)}{dt} = CT(K_S, K_M(k)) + C(K_S(k), K_M(k)) + CT(K_M, K_M(k)) + C(K_M(0), K_M(k)) + DK_M(k), \tag{3.57}$$

$$\frac{dK_S(k)}{dt} = CT(K_M, K_S(k)) - C(K_M(k), K_S(k)) + CT(K_S, K_S(k)) + C(K_S(0), K_S(k)) + C(A(k), K_S(k)) + DK_S(k), \tag{3.58}$$

$$\frac{dA(k)}{dt} = CT(A, A(k)) - C(A(k), {}_S(k)) + C(A(0), A(k)) + GA(k), \tag{3.59}$$

$$\frac{dE_m(k)}{dt} = C(E_M, E_M(k) + C(E_S E_M(k)) + C(E_M(0), E_M(k)) + C(E_S(0), E_M(k)) + DE_S(k), \tag{3.60}$$

$$\frac{dE_S(k)}{dt} = C(E_S, E_S(k)) + C(E_M, E_S(k)) + C(E_M(0), E_S(k))$$

$$+ C(E_S(0), E_S(k)) + DE_S(k) + GE_S(k). \qquad (3.61)$$

Note the fundamental differences between these equations and Chen and Tribbia (1981). The definition of all these quantities follows.

The nonlinear kinetic energy of wave number k change rate is

$$\frac{dK_M(k)}{dt} = -\frac{P_o}{gs}\int_s (\psi((k)\ \frac{\partial \xi(k)}{\partial t} + \psi(k)\ \frac{\partial \xi(-k)}{\partial t})(\frac{1}{1+\delta(k,0)})ds.$$

The rate of change of baroclinic kinetic energy of wave number k is

$$\frac{dK_S(k)}{dt} = -\frac{P_o}{gs}\int_s (\tau(-k)\ \frac{\partial \eta(k)}{\partial t} + \tau(k)\ \frac{\partial \eta(-k)}{\partial t}\ (\frac{1}{1+\delta(k,0)})ds.$$

The conversion of energy between barotropic (vertical mean) and baroclinic (vertical shear) kinetic energy is broken into triad and wave-mean flow terms. This latter term corresponds to the conversion of baroclinic kinetic energy into barotropic kinetic energy discussed by the simple one wave and zonal flow example of Wiin-Nielsen (1962) in Section B of the Introduction. This term is

$$C(K_S(k), K_M(k)) = \frac{-P_o}{gs}\int \Big\{ U_\tau(0)\ (V_\psi(-k)\,\eta_\tau(k) + V_\psi(k)\,\eta\tau(-k))$$
$$+ \eta(0)\ (V_\tau(-k)\ U_\tau(k) - U_\tau(k)\ V_\psi(-k)$$
$$+ \eta(0)\ (V_\tau(k)\ U_\tau(-k) - U_\tau(-k)\ V_\psi(k) \Big\} ds.$$

This term involves only exchanges between the same wave numbers. The nonlinear triad exchanges of the barotropic kinetic energy wave

number (k) and all the wave numbers of baroclinic kinetic energy is

$$CT(K_S, K_M(k)) = \frac{-P_o}{gs} \int \sum_{\substack{m=-k \\ m\neq 0 \\ m\neq k}}^{k} \eta(k-m)\ [V_\psi(-k)\ U_\tau(m) - V_\tau(m)\ U_\psi(-k)]$$

$$+ \sum_{\substack{m=-k \\ m\neq 0 \\ m\neq k}}^{k} \eta(-k-m)\ [U_\tau(m)\ V_\psi(-k) - V_\tau(m)\ U_\psi(-k)].$$

Note this triad conversion has not only kinetic energy exchanges between type, but between scale as well. The nonlinear exchange between the baroclinic kinetic energy of wave number (k) and all the wave numbers of barotropic kinetic energy is

$$CT(K_M, K_S(k)) = \frac{-P_o}{gs} \int \left\{ \sum_{\substack{m=-k \\ m\neq 0 \\ m\neq k}} \eta(m-k)\ [U_\psi(m)\ V_\tau(-k) - U_\tau(-k)\ V_\psi(m)] \right.$$

$$\left. + \sum_{\substack{m=-k \\ m\neq 0 \\ m\neq k}}^{k} \eta(-m-k)\ [U_\psi(m)\ V_\tau(k) - V_\psi(m)\ U_\tau(-k)] \right\} ds.$$

Note $\sum_{k=-k}^{k} CT(K_S, K_M(k)) = -\sum_{k=-k}^{k} T(K_M, K_S(k))$.

The nonlinear triad exchanges between the barotropic kinetic energy of wave number k and the other barotropic wave number is

$$C(K_M, K_M(k)) = \frac{P_o}{gs}\int_s \sum_{\substack{m=k \\ m\neq 0}}^{k} \Big\{ \xi(m)\,[V_\psi(-k)\,U_\psi(k-m) - V_\psi(k-m)\,U_\psi(-k)]$$

$$+ \xi(m)\,[V_\psi(-k)\,U_\psi(-k-m) - V_\psi(-k-m)\,U_\psi(-k)]$$

$$+ \xi(k)\,[V_\psi(-m)\,U_\psi(m-k) - V_\psi(m-k)\,U_\tau(-m)]$$

$$+ \xi(k)\,[V_\psi(m)\,U_\psi(-k-m) - V_\psi(-k-m)\,U_\psi(m)] \Big\}\, ds.$$

The nonlinear triad exchanges between the baroclinic kinetic energy of wave number k and the other baroclinic wave numbers is

$$C(K_S, K_S(k)) = \frac{P_o}{gs}\int_s \sum_{\substack{m=-k \\ m\neq 0}}^{k} \Big\{ \eta(m)\,[V_\tau(-k)\,U_\tau(k-m) - V_\tau(k-m)\,U_\tau(-k)]$$

$$+ \eta(m)\,[V_\tau(k)\,U_\tau(-k-m) - V_\tau(-k-m)\,U_\tau(k)]$$

$$- \eta(k)\,[V_\tau(-m)\,U_\tau(m-k) - V_\tau(m-k)\,U_\tau(-m)]$$

$$- \eta(k)\,[V_\tau(m)\,U_\tau(-k-m) - V_\tau(-k-m)\,U_\tau(m)] \Big\}\, ds.$$

The exchange between the barotropic kinetic energy of wave number k and the zonal barotropic kinetic energy is

$$C(K_M(0), K_M(-k)) = \frac{P_o}{gs}\int \left\{ \frac{\partial U_\psi(0)}{\partial y}\,[V_\psi(-k)\,U_\psi(k) + V_\psi(k)\,U_\psi(-k)] \right\} ds.$$

The exchange between the baroclinic kinetic energy of the wave number k and the zonal baroclinic kinetic energy is

$$C(K_S(0), K_S(k)) = \frac{P_o}{gs}\int \left\{ \frac{\partial U_\tau(0)}{\partial y}\,[U_\psi(k)\,V_\tau(-k) + U_\psi(-k)\,V_\tau(k)] \right\} ds.$$

The dissipation of barotropic and baroclinic kinetic energy of wave number k are, respectively,

$$DK_M(k) = \frac{P_o}{gs} \int_s [F_m(k)\psi(-k) + F_m(-k)\psi(k)]ds \qquad \text{and}$$

$$DK_S(k) = \frac{P_o}{gs} \int_s [F_o(k)\tau(-k) + F_o(-k)\tau(k)]ds.$$

The conversion between available potential energy of wave number k and baroclinic kinetic energy of wave number k is

$$C(A(k), K_S(k)) = \frac{P_o f_o^2}{gs\Delta P} \int_s [\omega(k)\tau(-k) + \omega(-k)\tau(k)]ds.$$

The rate of change of the available potential energy of wave number k is

$$\frac{dA(k)}{dt} = \frac{P_o R^2}{sg} \int_s \left(\tau(-k) \frac{\partial\tau(k)}{\partial t} + \tau(k) \frac{\partial\tau(-k)}{\partial t}\right)ds.$$

The nonlinear triad exchange of available potential energy of a wave number k and the other APE wave numbers is

$$\begin{aligned} C(A, A(k)) = \frac{P_o}{sg} \int_s \tfrac{1}{2} \sum_{\substack{m=k \\ m\neq 0}}^{k} \Big\{ & \tau(m)\,[V_\tau(-k)\,U_\psi(k-m) + V_\tau(k)\,U_\psi(-k-m)] \\ & + \tau(m)\,[V_\psi(k-m)\,U_\tau(-k) + V_\psi(-k-m)\,U_\tau(k)] \\ & - V_\tau(m)\,[U_\psi(k-m)\tau(-k) + U_\psi(-k-m)\tau(k)] \\ & + U_\tau(m)\,[V_\psi(k-m)\tau(-k) + V_\psi(-k-m)\tau(k)] \Big\} ds. \end{aligned}$$

The conversion between the available potential energy of the wave number k and the zonal available potential energy is

$$C(A(0),\ A(k)) \quad = \frac{2R^2P}{sg} \int \frac{\partial \tau(0)}{\partial y} \left[V_\psi(k)\tau(-k) + V_\psi(-k)\tau(k)\right] ds.$$

The "generation" of available potential energy of wave number k is

$$GA(k) = \frac{P_o}{sg} \int \left[H(k)\tau(-k) + H(-k)\tau(k)\right] ds.$$

The rate of change of barotropic enstrophy of wave number k is

$$\frac{dE_M(k)}{dt} (1 + \delta(k,0)) = \frac{1}{s} \int_s \tfrac{1}{2} \left(\frac{\partial \xi(k)}{\partial t} \xi(-k) + \xi(k) \frac{\partial \xi(-k)}{\partial t}\right) ds.$$

The baroclinic potential enstrophy of wave number k is

$$\frac{dE_S(k)}{dt} (1 + \delta(k,0)) = \frac{1}{s} \int_s \tfrac{1}{2} \left(\frac{\partial q_S(k)}{\partial t} q_S(-k) + q_S(k) \frac{\partial q_S(-k)}{\partial t}\right) ds.$$

The nonlinear triad conversion between the barotropic enstrophy of wave number k and the other barotropic wave numbers is

$$C\left(E_M,\ E_M(k)\right) = \frac{1}{s} \int \tfrac{1}{2} \sum_{\substack{m=-k \\ m=0}}^{k} \Big\{ \xi(m) \left[- ikU_\psi(k-m)\xi(-k) + ikU_\psi(-k-m)\xi(k)\right]$$

$$+ \xi(m) \left[V_\psi(k-m) \frac{\partial \xi(-k)}{\partial y} + V_\psi(-k-m) \frac{\partial \xi(k)}{\partial y}\right]$$

$$- \frac{\partial \xi(m)}{\partial y} \left[V_\psi(k-m)\xi(-k) + V_\psi(-k-m)\ \xi(k)\right] \Big\}$$

$$- \tfrac{1}{2} \sum_{\substack{m=-k \\ m\neq 0 \\ k\neq m}}^{k} - im\xi(m)\ U_{\psi}(k-m)\xi(-k)$$

$$\left. - \tfrac{1}{2} \sum_{\substack{m=-k \\ m\neq 0 \\ k\neq m}}^{k} - im\xi(m)\ U_{\psi}(-k-m)\xi(k) \right\} ds.$$

The nonlinear triad exchange between baroclinic potential enstrophy of wave number k and the other wave number is

$$C\ (E_S,\ E_S(k)) = \frac{1}{s} \int_s \left\{ \tfrac{1}{2} \sum_{\substack{m=-k \\ m\neq 0}}^{k} imq_S(m)\ [q_S(-k)\ U_{\psi}(k-m) + q_S(k)\ U_{\psi}(-k-m)] \right.$$

$$- q_S(m)\ [-ikU_{\psi}(k-m)\ q_S(-k) + ikU_{\psi}(-k-m)\ q_S(k)]$$

$$+ \frac{\partial q_S(m)}{\partial y}\ [q_S(-k)V_{\psi}(k-m) + q_S(k)_{\psi}V\ (-k-m)]$$

$$- q_S(m)\ \left[V_{\psi}(k-m)\ \frac{\partial q_S(-k)}{\partial y} + V_{\psi}(-k-m)\ \frac{\partial q_S(k)}{\partial y}\right]$$

$$- R^2\ \xi(m)\ [V_{\tau}(-k)\ U_{\tau}(k-m) + V_{\tau}(k)\ U_{\tau}(-k-m)]$$

$$+ \tfrac{1}{2} \sum_{\substack{m=-k \\ m\neq 0 \\ m\neq k}}^{k} R^2\ \xi(m)\ U_{\psi}(-k)\ V_{\tau}(k-m)$$

$$\left. + \tfrac{1}{2} \sum_{\substack{m=-k \\ m\neq 0 \\ m\neq k}}^{k} R^2\ \xi(m)\ U_{\tau}(k)\ V_{\tau}(-k-m) \right\} ds.$$

The nonlinear triad exchange between the barotropic enstrophy of wave number k and all the wave numbers of baroclinic potential enstrophy is

$$C(E_S, E_M(k)) = \frac{1}{s}\int_s \sum_{m=-k}^{k} \Big\{ \eta(m)\ [V_\tau(k-m)\ \frac{\partial \xi(-k)}{\partial y} + V_\tau(-k-m)\ \frac{\partial \xi(k)}{\partial y}]$$

$$+ \eta(m)\ [-\ ikU_\tau(k-m)\ \xi(-k) + ikU_\tau(-k-m)\cdot \xi(k)] \Big\}\ ds.$$

The nonlinear triad exchange between the baroclinic potential enstrophy of wave number k and all the wave numbers of barotropic enstrophy is

$$C(E_M, E_S(k)) = \frac{1}{s}\int \sum_{m=-k}^{k} \Big\{ -\frac{\partial \xi(m)}{\partial y}\ [\eta(-k)\ V_\tau(k-m) + \eta(k)\ V_\tau(-k-m)]$$

$$- im\xi(m)\ [\eta(-k)\ U_\tau(k-m) + \eta(k)\ U_\tau(-k-m)] \Big\}\ ds.$$

Note $+\sum_{m=k}^{-k} C(E_M, E_S(k)) = -\sum_{m=k}^{-k} C(E_S, E_M(k))$.

The exchange between the barotropic enstrophy of wave number k and the zonal barotropic enstrophy is

$$C(E_M(0), E_M(k)) = -\frac{1}{s}\int \frac{\partial \xi(0)}{\partial y}\ [V_\psi(k)\xi(-k) + V_\psi(-k)\xi(k)]ds.$$

The exchange between the barotropic enstrophy of wave number k and the zonal baroclinic potential enstrophy is

$$C(E_S(0), E_M(k)) = -\frac{1}{s}\int \Big\{ \frac{\partial \eta(0)}{\partial y}\ [V_\tau(k)\xi(-k) + V_\tau(-k)\xi(k)]$$

$$- R^2\ \frac{\partial \tau(0)}{\partial y}\ [V_\tau(k)\xi(-k) + V_\tau(-k)\xi(k)] \Big\}\ ds.$$

The exchange between the baroclinic potential enstrophy of wave number k and the zonal baroclinic potential enstrophy is

$$C\,(E_S(0),\ E_S(k)) = -\frac{1}{s}\int \frac{\partial q_S(0)}{\partial y}\,[q_S(-k)\ V(k) + q_S(k)\ V_\tau(-k)]\ ds.$$

The exchange between the baroclinic potential enstrophy of wave number k and the zonal barotropic enstrophy is

$$C\,(E_M(0),\ E_S(k)) = \frac{1}{s}\int \frac{\partial \xi(0)}{\partial y}\,[\eta(-k)\ V_\tau(k) + \eta(k)\ V_\tau(-k)]$$

$$- U_\tau(0)\ [ik\eta(-k)\xi(k) - ik\eta(k)\xi(-k)]\ ds.$$

The dissipations of barotropic and baroclinic potential enstrophy of wave number k due to friction are, respectively,

$$DE_M(k) = -\frac{1}{s}\int [F_M(k)\xi(-k) + F_M(-k)\xi(k)]ds, \quad \text{and}$$

$$DE_S(k) = -\frac{1}{s}\int [F_S(k)\ q_S(-k) + F_S(-k)\ q_S(k)]ds.$$

The generation of baroclinic potential enstrophy of wave number k is

$$GE_S(k) = \frac{1}{s}\int [H(k)\ q_S(-k) + H(-k)\ q_S(k)]ds.$$

IV. THE CASCADING AND CONVERSION OF BAROTROPHIC AND BAROCLINIC ENERGY AND POTENTIAL ENSTROPHY

A. The Experiments

Six experiments, including the control run described in Chapter II, Section C, were performed for the purpose of investigation of the barotropic-baroclinic nature of the model. In each experiment, the model was allowed to spin up for 60 days and establish a flow independent of the initial conditions. The next 30 days, at 24-hour intervals, were used for analysis.

The model parameters for these six experiments are given in Table 4.1. The table only has entries for the control run and parameters different than the control run in the other experiments. The definitions of the parameters are found in Chapter II. Briefly, the parameters in the table are: γ is the Newtonian heating coefficient, υ is the eddy viscosity coefficient, k is the linear drag coefficient, R^2 is the square of the Rossby deformation wave number, and U_S is symbolic of the zonal vertical shear forced on the model, at any latitude point, by the Newtonian heating.[1]

Each of the experiments are performed with a defined purpose. The control run parameters were found by tuning the model until a reasonable

---

[1] U_S is set by adjusting the equilibrium temperature profile of the Newtonian heating.

Table 4.1. Model experiment parameters

Control Run	γ(1/sec)	υ (m^2/sec)	k(1/sec)	R^2($1/m^2$)	U_s
Control run	$.6 \times 10^{-6}$	$.05 \times 10^{+6}$	1.8×10^{-6}	3.5×10^{-12}	U_s
Experiment One	$.9 \times 10^{-6}$	---	---	---	--
Experiment Two	---	---	---	4.38×10^{-12}	--
Experiment Three	---	---	---	---	$1.25U_s$
Experiment Four	---	---	1.4×10^{-6}	---	--
Experiment Five	1.2×10^{-6}	$1.3 \times 10^{+6}$	1.2×10^{-6}	---	--

energy cycle, jet structure, and spectrum (considering the limitations of the model) were found as compared to observed midlatitudes (see Chapter II, Section C). The control run parameters are comparable to other studies (e.g., Barros and Wiin-Nielsen, 1974) except for the eddy viscosity coefficient which is smaller by an order of magnitude.

Experiment One (E1) examines the effect of increasing the Newtonian heating coefficient (inverse radiative time constant). Finite amplitude waves created and maintained by the baroclinic instability must extract energy from the zonal flow. The energy of the zonal flow is depleted by this process. The diabatic heating maintains the zonal vertical shear; therefore, the diabatic heating can limit the amplitudes reached by the waves by controlling how quickly the zonal shear flow is replenished. In the absence of eddies, the Newtonian heating coefficient of the control run has an e-folding time of 19 days for restoring the equilibrium temperature (and zonal vertical shear). Experiment One has an e-folding time of 9.6 days. In summary, E1 is used to access the role of diabatic heating in the nonlinear model and the related effects resulting from the zonal shear flow maintenance.

Experiments Two (E2) and Three (E3) increase the Rossby deformation radius and the vertical shear of the zonal wind, respectively. That these two parameter variations are related, to some extent, can be seen from examining the baroclinic instability of the inviscid two-layer model with the simplification of a zonal vertical shear independent of latitude. The neutral curve for infinitesimal amplitudes is

$$2\alpha^2 = 1 + \sqrt{1 - \alpha},$$

where the nondimensional parameters α and α are $\frac{k^2}{R^2}$ and $\frac{\beta}{R^2 U_S{}^2}$, respectively (e.g., Pedlosky, 1979). Thus, an increase in U_S only enhances the instability of all wave numbers but does not change the wave number that is unstable for the least amount of vertical shear. Since the growth rate for all unstable modes is a linear function of U_S, the same can be said of the most unstable mode.

An increase in the Rossby deformation wave number shifts the wave number of maximum instability toward higher wave numbers. The change in R and U_S in E2 and E3 are designed such that the nondimensional parameter α changes by an equal amount for both experiments. This results in the same amount of supercritical shear in both of these experiments, but with different wave number minima of U_S. (In as far as the linear instability without latitude variation of U_S is applicable.)[2]

The variation of the Rossby deformation radius has been shown to have implications for the nonlinear transfer of energy and potential enstrophy. This has been shown analytically for triads with member components near to the Rossby deformation radius (Marshall and Chen, 1982). Experiment Three allows examination of these effects when many triad exchanges are occurring simultaneously.

---

[2]The effect of a latitude variation of the vertical zonal shear is not known in general. For a latitude variation of the zonal vertical shear, which has no vorticity maxima, the critical vertical shear of baroclinic instability is unchanged but the wave number of the most unstable mode is shifted towards shorter wave lengths and the long wave lengths stabilized (Pedlosky, 1964). In general, both barotropic and baroclinic instability play a role.

Experiment Four (E4) analyzes the effect of increased surface friction. The parameterization of surface friction is less dependent on wave number than that of diffusion; however, large wave numbers are damped more heavily than small ones. Linear baroclinic instability theory (with a constant in latitude U_S basic state) suggests that the long waves are stabilized by surface friction and the short wave cut off is unaffected (e.g., Barcilon, 1964; Pedlosky, 1979). The supercritical shear is unaffected but this is only applicable for infinitesimal amplitude. Thus, a narrower half-width of the wave numbers of baroclinic instability is expected.

Experiment Four can be compared to Experiment Five (E5). Increasing the coefficient of diffusion in the model was found, when large enough, to drastically decrease the power laws of the high wave numbers of kinetic and available potential energy. The increased diffusion, however, damps the flow so heavily that comparison of conversion and nonlinear transfer with other model runs were hampered by the inability to distinguish between the small amplitude related effects and the effects of the steeper power law. To partially alleviate this situation, the model parameters for E5 are adjusted so that a reasonable energy cycle is found but the steeper spectra of energy is retained. Experiments Four and Five offer the chance to examine the effects of increased friction with different scale dependence, even though some of the parameter changes of Experiment Five make this comparison less than absolute. Also, the cascades of energy and potential enstrophy are undoubtedly changed for different power laws if inertial range theory has any applicability to cascading in the two-layer model.

B. Barotropic and Baroclinic Character of the Model Experiments

The barotropic and baroclinic zonal and eddy energetics and potential enstrophy are shown in Figures 4.1 and 4.2, respectively. The equations for the eddy and zonal geostrophic baroclinic and barotropic energetics, as derived and discussed in Chapter III, are different especially in the conversion and interaction between the kinetic energies than in previously derived equations (e.g., Wiin-Nielsen and Drake, 1965; Chen and Tribbia, 1981). Direct comparison of some quantities with observation which has used the primitive equation formulations is, therefore, not possible. The details are discussed in Chapter III.

The control run was compared to observation with the classical Lorenz energy cycle in Section C of Chapter II and is not repeated here. The discussion of Figure 4.1 will proceed starting from A_Z at the upper left hand corner. The greatest generation of available potential energy is found in Experiment Three. Note also this experiment has the greatest amount of barotropic eddy energy. In contrast, Experiment Five has the least generation of available potential energy and the least amount of barotropic kinetic energy (K_M). This behavior can be explained by noting that the generation of available potential energy responds to (i.e., stronger eddy K_M) tend to disturb it more. The increased (K_M), found in some experiments, appears to be more effective in increasing the generation of zonal available potential energy than doubling the Newtonian heating relaxation time.

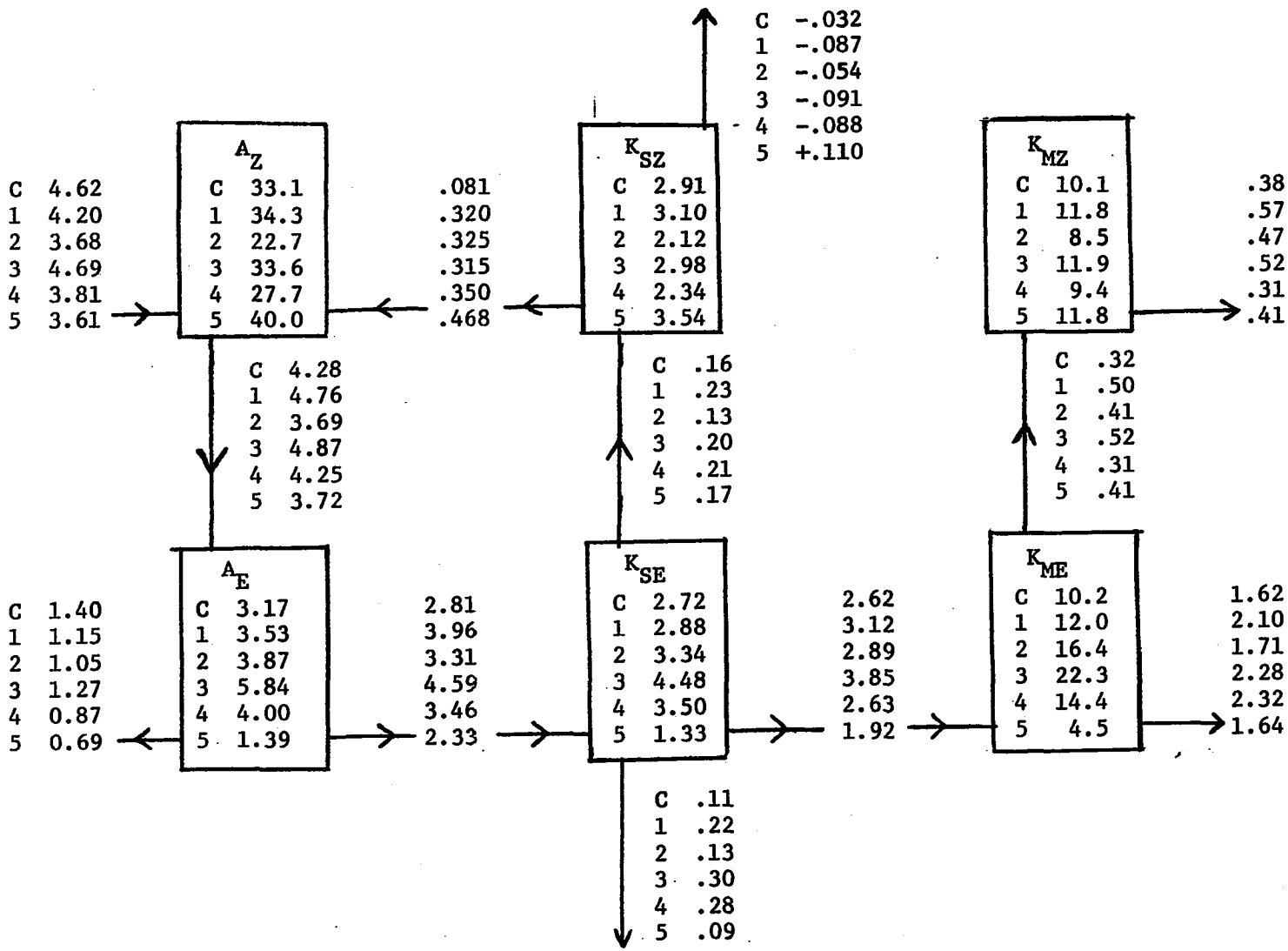

Figure 4.1. Energy diagram based on Figure 3.1 (C = control run and 1-5 = experiment number)

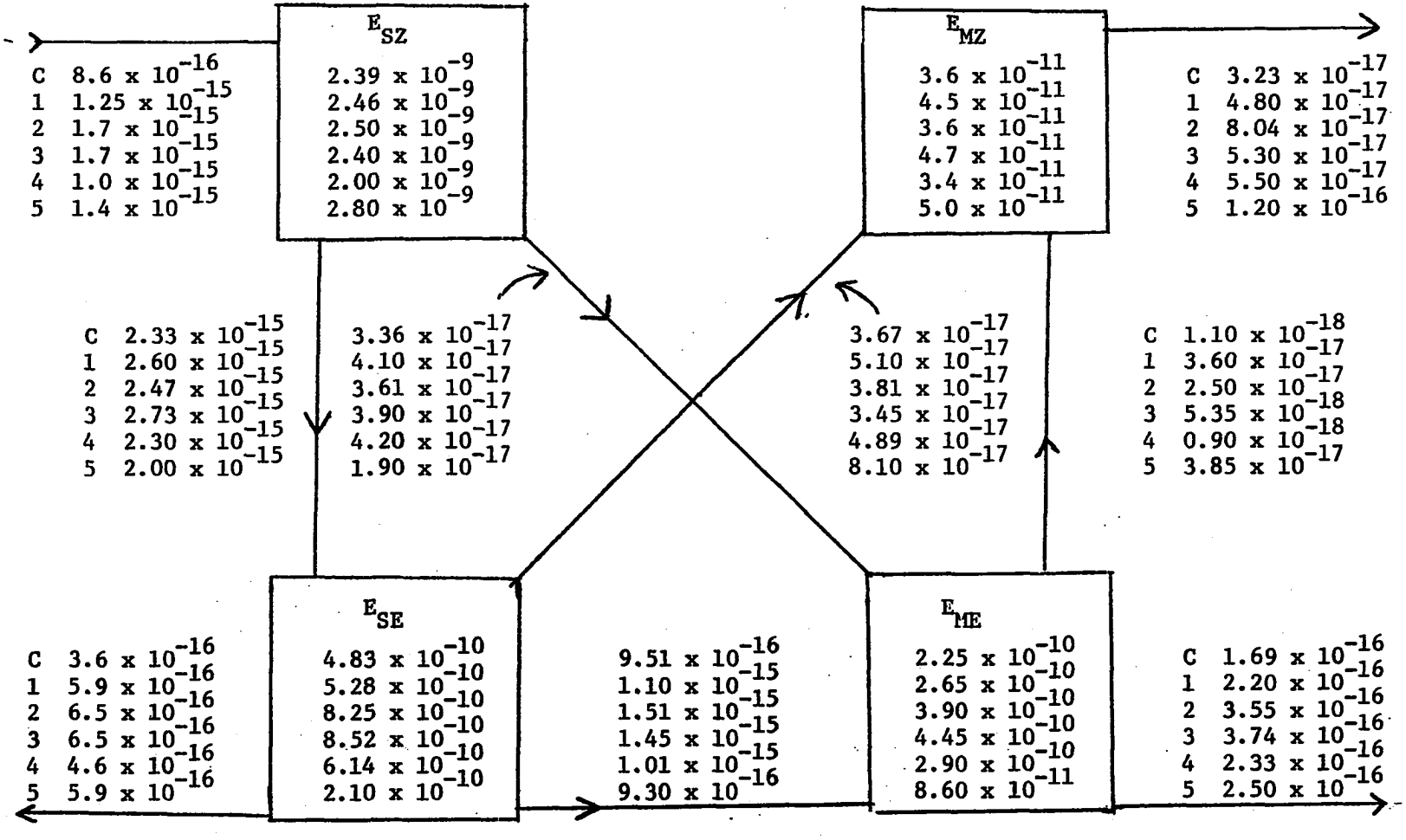

Figure 4.2. Potential enstrophy diagram based on Chen and Tribbia (1981) (C = control run and 1-5 = experiment number)

The conversion of zonal available potential energy (A_Z) to eddy available potential energy (A_E) seems to be dependent upon two factors--the amount of (A_E) and the amount of barotropic eddy kinetic energy. Combining these two factors nicely explains the variation shown by the experiments for this conversion. The implied explanation is that stronger eddies convert more A_Z to A_E but are limited by the amount available.

Eddy available potential energy (A_E) varies in a similar manner as barotropic kinetic energy (K_M). Experiment Four makes a slight exception to this latter conclusion. This relation between A_E and K_M is purely from the dynamics of the flow field whereas the relation between K_S and A is expected from their formulation in the two-layer model (i.e., both are completely specified by the temperature field).

The barotropic and baroclinic kinetic energy diagram can be compared with the one of Wiin-Nielsen and Drake's (1966) computed for the annual mean 1963 northern hemisphere. The vertical shear kinetic energy (as applied to observation) by Wiin-Nielsen's definition is not completely due to thermal wind relationship as is found in the two-layer model formulation (see Chapter III). However, one would expect the thermal wind to dominate the observational shear kinetic energy. Regretfully, a multi-layer atmosphere formulation of vertical mean kinetic energy is not distinct from the thermal wind. The control run is comparable to the observed zonal baroclinic (shear) kinetic energy. The highest zonal baroclinic kinetic energy is found for E5. The heavy damping of the eddies in E5 causes less eddy barotropic kinetic energy, which, in turn, results in a

decrease of the zonal temperature gradient at a slower rate. Note that K_{SZ} is simply related to A_Z; and is a measure of the linear baroclinic instability of the flow. From the study of Stone (1978) on the observed supercritical vertical shear of the earth's troposphere, one could expect that K_{SZ} would be similar in the model control run and real atmosphere.

The control run has less energy than real observation for the baroclinic (shear) eddy kinetic energy (K_{SE}). Since K_{SE} and the available potential eddy energy are directly related (for this two-layer model) by the thermal wind relationship, the same situation is true for A_E. The absence of strong planetary wave contributions to these quantities, to be discussed later in this section, account for the lesser amounts of A_E and K_{SE} than found in observation.

The conversion $C(K_{SE}, K_{SZ})$ only maintains the shear zonal kinetic energy. This is fundamentally different from the conversion as derived by Wiin-Nielsen and Drake (1966) and Chen and Tribbia (1981). Therefore, direct comparison with observation is not possible.

The conversion $C(K_{SE}, K_{ME})$ is also of a different formulation than Wiin-Nielsen and Drake (1965) and Chen and Tribbia (1981). However, by summing up terms that are of a similar form (assuming the wind is basically geostrophic) and placing them as though they converted energy as does the quasi-geostrophic two-layer model, one finds an observed $C(K_{SE}, K_{ME})$ of 2.7 W m^{-2} which is comparable to the control run. This conversion is largest for E3 which has the largest barotropic kinetic energy.

However, the second largest conversion, which occurs in E1, does not have the second largest K_{ME}.

Unlike the primitive equation energetics of Wiin-Nielsen and Drake (1966) and Chen and Tribbia (1981), the zonal barotropic kinetic energy is only supported by the conversion from K_{ME}. The greatest K_{MZ} is found when this conversion, $C(K_{ME}, K_{MZ})$, is largest and the least K_{MZ} is found when this conversion is least for the experiments. The dissipation of K_{MZ} is dependent only on the magnitude and the y variation of the zonal barotropic flow. If the dissipation was only dependent on the former, the relation between K_{MZ} and the conversion, $C(K_{ME}, K_{MZ})$, would be absolute. This is still the dominant factor.

In Table 4.2 is a comparison of the ratios between the baroclinic kinetic energy and the barotropic kinetic energy and the ratio between total baroclinic energy and barotropic energy. For the eddies, these ratios are somewhat constant compared to the variations of these quantities separately. The comparison ratio of A_E and K_{SE} is not shown since any differences in these ratios is simply a manifestation of the differences in zonal and meridional wave number spectra of temperature. The spectra of these quantities will be addressed later.

Figure 4.2, for the model control run can be compared to the observed results of Chen and Tribbia (1983). The generation and dissipation terms are not calculated for observation. The observed conversion of E_{SZ} and E_{SE} is considerably greater by 40%. However, the conversion of E_{SE} to E_{ME} are comparable to those observed by Chen and Tribbia. The conversion from E_{SE} to E_{ME} is 50% greater than observation.

Table 4.2. Ratios of barotropic and baroclinic energies

Experiment Number	K_{SE}/K_{ME}	K_{SZ}/K_{MZ}	$A_E + K_{SE}/K_{ME}$
Control	.27	.29	.58
1	.24	.38	.53
2	.20	.25	.44
3	.20	.25	.46
4	.24	.25	.52
5	.30	.30	.60

The spectra of energies and potential enstrophies for the control experiment, in the zonal wave number, are shown in Figures 4.3 and 4.4. The main differences between these diagrams and those observed in the actual atmosphere (Chen and Tribbia, 1983) is the lack of long wave energies and enstrophies of all types. This difference probably results from the exclusion of longitudinal diabatic heating anomalies (land-sea contrast) and orography in the model. The large standing component found in Chen and Tribbia (1983) for the long waves supports this conclusion.

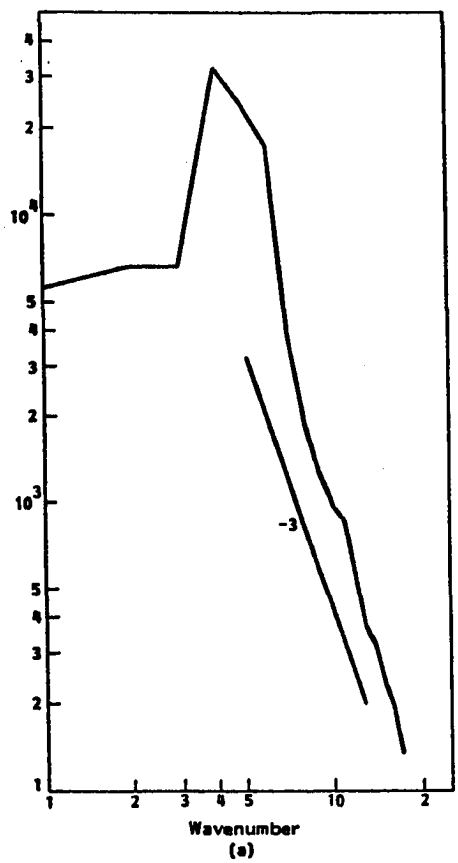

Figure 4.3a. The spectrum of barotropic kinetic energy in the zonal wave number index, Units: Jm^{-2}

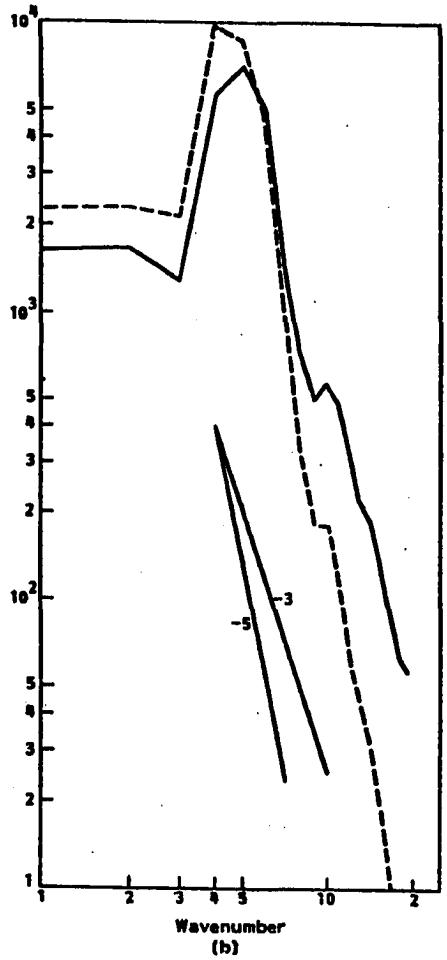

Figure 4.3b. The spectrum of baroclinic kinetic energy (solid line) and available potential energy (dashed line), Units: Jm^{-2}

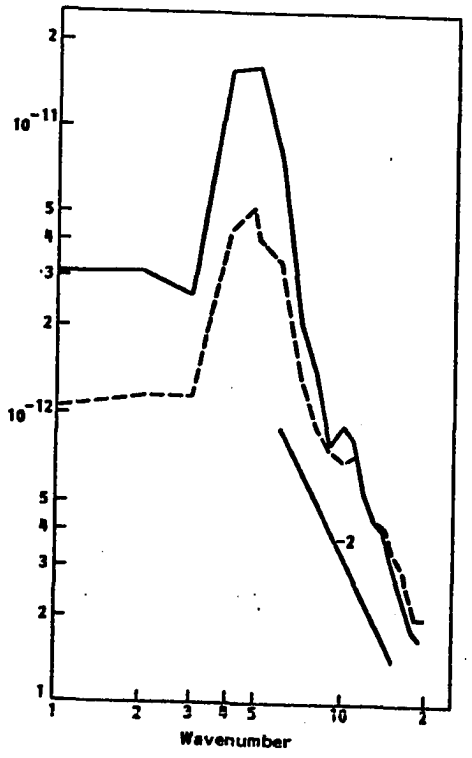

Figure 4.4. The spectrum of barotropic (solid line) and baroclinic enstrophy (dashed line), Units: $m^{-2}s^{-2}$

A weak peak at wave number 6 is found in the observed spectra of the vertical shear and mean kinetic energies. In the control run, a strong peak is found at wave number 4 for the barotropic kinetic energy and a peak at wave number 5 for the baroclinic kinetic energy. The power law in the wave numbers 8-19 for the vertical mean and shear observed kinetic energies are -3.8 and -2.2, respectively. The power laws for the model experiments are shown in Table 4.3 for the one-dimensional zonal wave number index. Charney's (1971) theory of geostrophic turbulence[3] predicts a power law of -3 for both the available potential energy and total kinetic energy spectra. Merilees and Warn (1972) have shown that the vertical resolution of the two-layer model results in a -5 power law for the available potential energy. This has been confirmed numerically by Barros and Wiin-Nielsen (1974). However, strict analysis of the arguments of Merilees and Warn show that what is actually required is that the power law for available potential energy be a factor of -2 less than that of total kinetic energy. The assumption of kinetic energy having a -3 power law is a separate one. For the model experiment, a mean value of -1.7 is found rather than -2 with a smallest value of -1.4 for E1. The theory of Charney (1971) ignores diabatic heating. Merilees and Warn's analysis is based on this theory; therefore, the discrepancy noted, especially for E1, may be due to diabatic heating.

---

[3]This result is for a three-dimensional wave number and the slopes shown here are for the one-dimensional zonal wave number. The similarity of power laws for different indices has been shown by Merilees (1979). Results to be shown later tend to confirm this.

Table 4.3. Power laws for wave numbers 8-19 for various energies

Experiment	A	K_M	K_S	E_M	E_S
Control run	-4.8	-3.5	-3.3	-1.9	-2.4
1	-5.6	-3.9	-3.3	-2.2	-2.5
2	-4.81	-3.5	-3.1	-1.9	-2.3
3	-5.14	-3.5	-3.0	-2.0	-2.3
4	-5.7	-4.0	-3.73	-2.2	-2.7
5	-7.5	-5.9	-5.8	-3.5	-3.6

The baroclinic kinetic energy is by their formulation found to be proportional to the minus second power of the two-dimensional wave number multiplied by the available potential energy. The average power law difference between these two energies in the zonal wave number index is 1.89. The small difference between this and two is probably due to anisotropy between zonal and meridional wave number spectra. The formulation of the barotropic and baroclinic potential enstrophy shows that they are proportional by the second power of two-dimensional wave number multiplied by the respective kinetic energy. The mean power law difference between the enstrophies and kinetic energies is 1.8 for the barotropic and 1.1 for the baroclinic in the model's zonal wave number index. The difference of this latter power law difference from a value of two indicates more anisotropy between meridional and zonal wave number spectra of baroclinic than of barotropic quantities.

Thus far, the gross properties of the different experiments have been examined. It is of interest to display the experiments in a concise

but revealing manner. The one-dimensional zonal wave number index makes good use of the model's symmetry as well as the geometry of baroclinic instability and the directions of Rossby waves propagation. The two-dimensional wave number index (meridional and zonal wave numbers) is not without some flaws. The width of the channel is somewhat arbitrary as are the choice boundary conditions on the north and south walls. These two factors affect the wave number distribution in the meridional index (for a channel model). However, because of the relations between various energy quantities in the two-dimensional wave number index (e.g., $A \times k^2 \propto K_S$, Barotropic Enstrophy $\times k^{-2} \propto K_M$, etc.) the spectra of all energies and enstrophies can be deduced from the spectra of barotropic and baroclinic kinetic energies. The comparison of experiments in terms of energy and enstrophy spectra becomes much more simplified and concise. The conversions and cascades of energy and enstrophy do not have such simple relations between each other.

Figure 4.5 shows the barotropic (solid line) and baroclinic (dashed line) kinetic energies for each of the experiments. The logarithm of energy has been taken so all scales can be shown simultaneously and comparison can be made with Figures 4.3 and 4.4.

Each of the figures can be thought of as subdividing the kinetic energy of the channel in a three-dimensional index. The two vertical normal modes of the linearized two-layer model (see Chapter II, Section A.2) make the vertical subdivision much simpler than that of the Earth's atmosphere (e.g., Baer, 1981). The meridional wave number and zonal wave number make up the rest of the three-dimensional index.

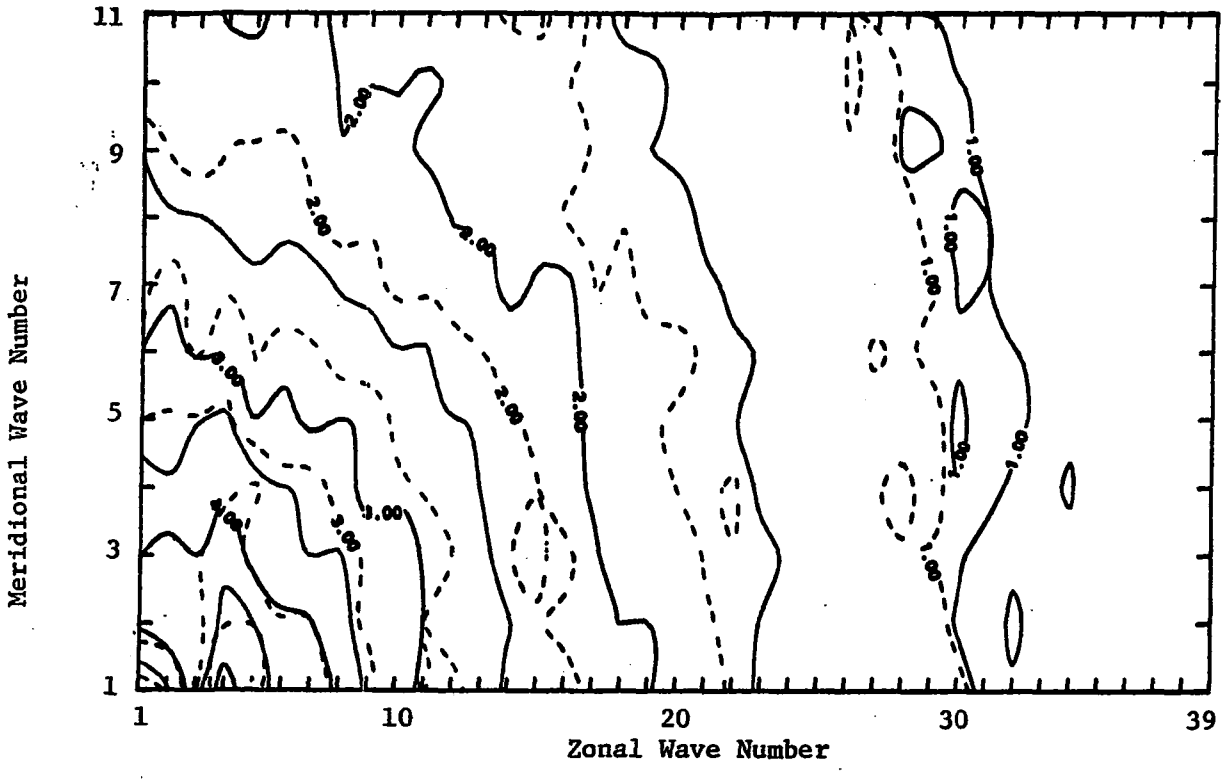

Figure 4.5a. The control run logarithm of barotropic (solid line) and baroclinic (dashed line) kinetic energy: (a) control run, (b) Experiment One, (c) Experiment Two, (d) Experiment Three, (e) Experiment Four, and (f) Experiment Five

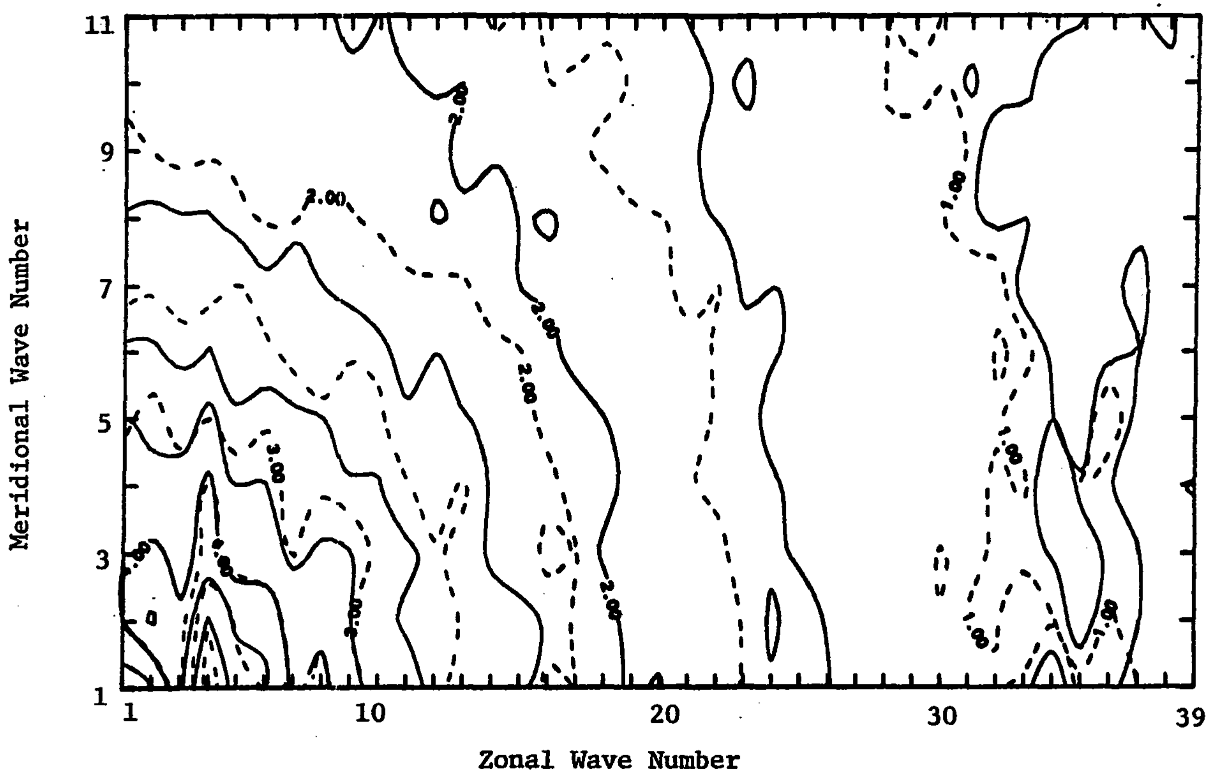

Figure 4.5b. Experiment One

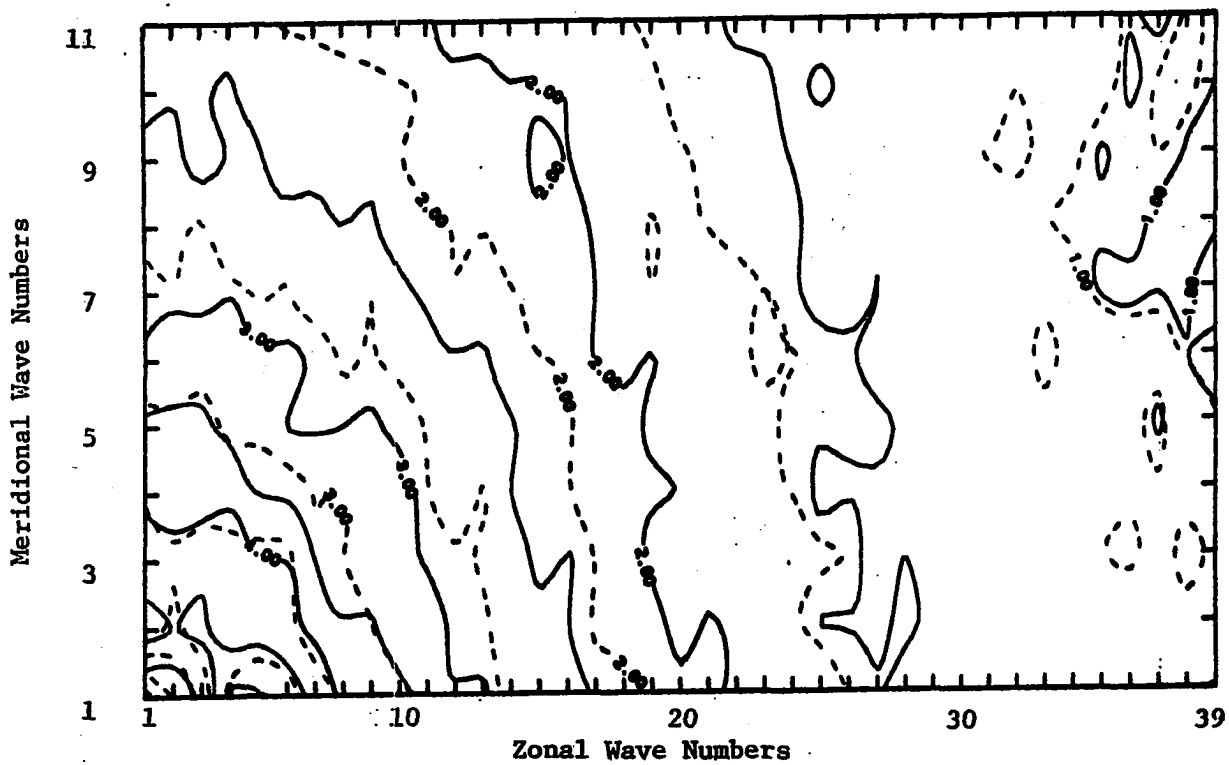

Figure 4.5c. Experiment Two

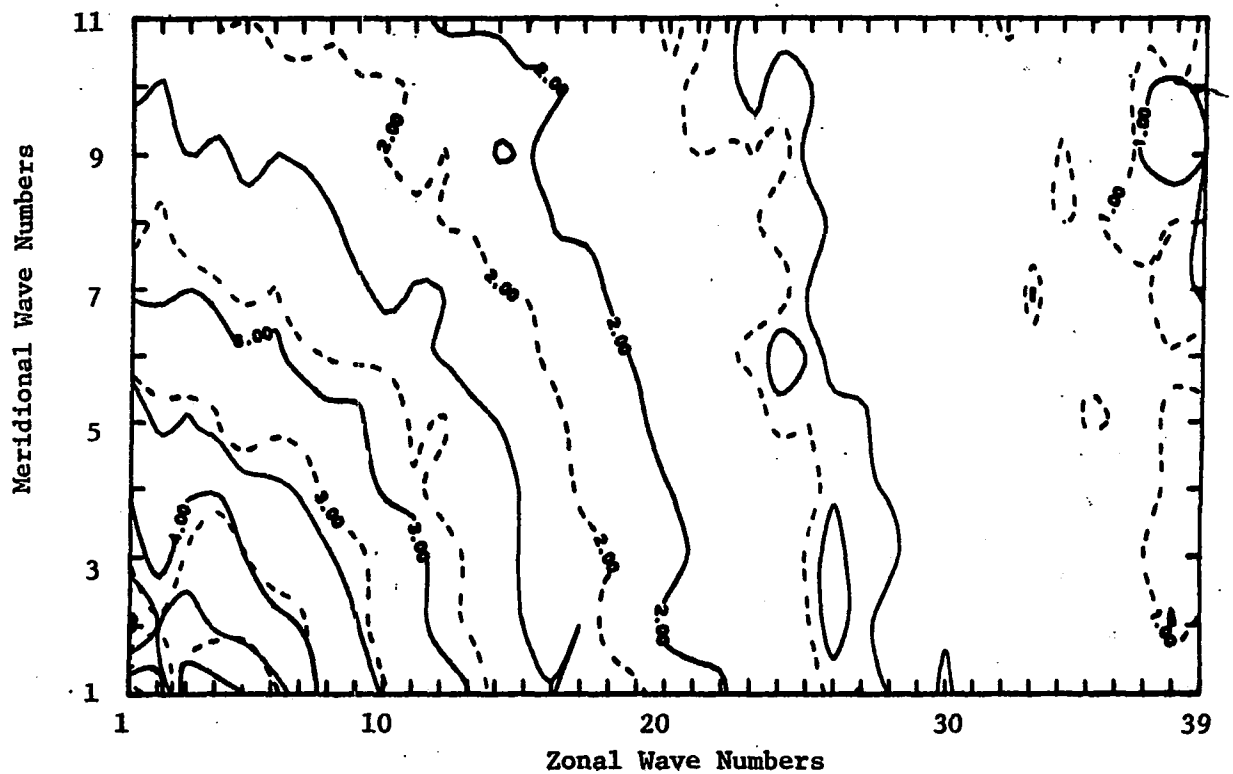

Figure 4.5d. Experiment Three

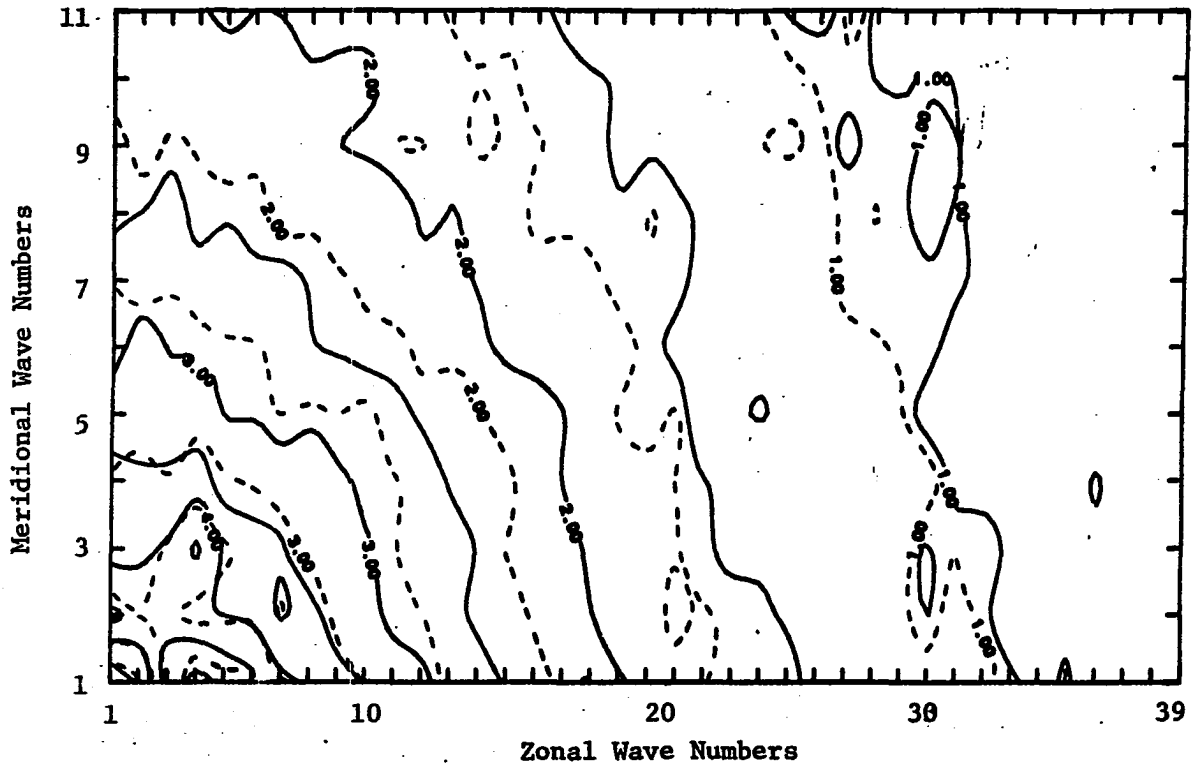

Figure 4.5e. Experiment Four

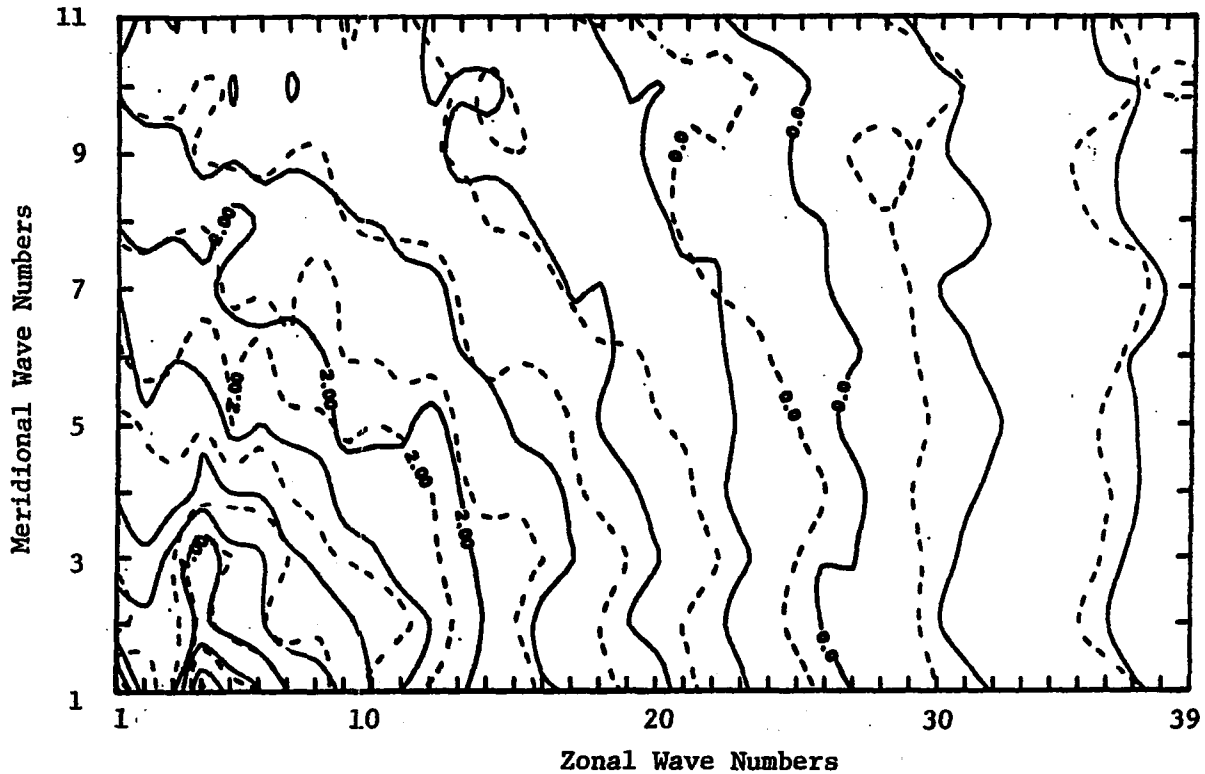

Figure 4.5f. Experiment Five

The barotropic kinetic energy of the control run generally, but not monotonically, decreases away from zonal wave number 4 and meridional wave number 1.[4] The contours of energy for all but the smallest wave numbers roughly form one quadrant of a family of ellipses with foci, near to small zonal wave numbers, on the line with merdional wave number equal to two. (The circular appearance of the contours in Figure 4.5 is due to the stretching of meridional wave number.) The baroclinic kinetic energy of the control run has a similar appearance, only the decrease of energy with higher wave number is slightly less steep. The most energetic wave numbers have baroclinic kinetic energy an order of magnitude less than the barotropic kinetic energy. The smallest scales (largest wave numbers) are almost equal in both types of energy.

In Experiment One, the barotropic kinetic energy (K_M) has more energy in the largest scales than in the control run but has a similar distribution. This larger amount of energy is expected from the stronger maintenance of the supercritical shear of the flow by the shorter radiative time constant. The wave numbers in the domain of 8-21 zonal wave numbers and of 4-10 meridional wave numbers have K_M comparable to the control run. Wave numbers greater than this domain have barotropic energies greater than the control run. The baroclinic energy (K_S) is also greater

---

[4]The severest truncation of spectral components is the meridional wave number. By no coincidence, this is the most expensive truncation of the two computationally (see Chapter II for further details).

in the largest wave numbers than in the control run and is slightly shifted to higher zonal wave numbers. Wave numbers of K_S in the domain of 8-13 zonal wave number and of 2-8 meridional wave number are of comparable K_S to those of the control run. Wave numbers larger than these have less K_S than in the control run.

K_M of Experiment Two has more energy in the largest scales and a somewhat different distribution of K_M in these scales. There are some extra "islands" of large K_M in the lower zonal wave numbers. The larger amount of energy is expected from arguments previously mentioned based on the linear baroclinic instability; however, the upscale shift of K_M (and K_S) compared to the control run is contrary to the downscale shift that linear baroclinic instability gives for a decreased Rossby deformation radius. This problem will be discussed again in the next section. Wave numbers in the domain of 7-9 zonal wave numbers and 3-5 meridional wave numbers are comparable in K_M to that of the control run. Larger wave numbers have less K_M than the control run. K_S is comparable to the control run for the domain of 8-3 zonal wave numbers and 4-8 meridional wave numbers. K_M and K_S become comparable and sporadic at about zonal wave number 31.

In E3, the small wave number peak of K_M spreads out in zonal wave number, shifts slightly to smaller zonal wave numbers compared to the control run and has larger magnitude. The larger magnitude is expected from the larger amount of supercritical shear in this experiment. The overall K_M in midscales (5-8) is comparable to E2. K_S is broader in the smaller zonal wave number peak than the control run but more peaked at

zonal wave number 4 than E2. K_S and K_M become comparable at about zonal wave number 32.

K_M of E4 is similar to the control run except there is more K_M in zonal wave number 4 and less K_M in the domain of 6-8 zonal wave number and 3-4 meridional wave number. As mentioned in the previous section, the linear baroclinic instability analysis with surface frictions suggests a narrower half width of baroclinic instability zonal wave number than found here. K_S and K_M become comparable at about zonal wave number 27.

Experiment Five has greater K_M and K_S than the control run for zonal wave number 4 and quickly drops off with increasing wave number. By zonal wave number 28, K_M is two orders of magnitude less than the control run. K_S and K_M become comparable at zonal wave number 38.

These results provide a reference for comparison of the model data, used here for analysis, and for future studies. Some of the features of these spectra seem to transcend parameter changes in the model. The way energy is partitioned between meridional and zonal wave numbers away from the baroclinically unstable wave numbers manifests a similar pattern in all experiments. Even the largest scales retain some similarities in all of the experiments. A drastic change in the forcing method of the model may change the latter similarities found in the experiments but probably not the former similarities.

C. Cascading and Conversion in the Spectral Domain

The purpose of this section is fourfold. The first deals with evaluating the diagram of Salmon (1978) (based on Rhines (1977)) for the two-layer model (Figure 1.5) by direct calculation in the zonal wave number index. The second purpose is the comparison of the control run with the observational study of Chen and Tribbia (1983). Third, the extension of the spectral two-layer study of Barros and Wiin-Nielsen (1974) to barotropic and baroclinic components is made. Fourth, the experiments are used to examine the dynamics of the two-layer model.

The total baroclinic energy is subdivided into available potential energy and baroclinic kinetic energy as was done in Chapter IV. For the two-layer quasi-geostrophic model K_S and A are related by the thermal wind relation such that both quantities can be completely specified by the temperature field. This is probably the reason why Salmon combined K_S and A into the total baroclinic energy. This simple relation between K_S and A does not extend to multi-layer or ageostrophic effects; hence, the concept of total baroclinic energy is not directly applicable to the actual atmosphere. K_S and A are still related, in part, for a multi-level atmosphere to the degree the atmosphere is hydrostatic and geostrophic.

This section of Chapter IV is divided into two parts. First, the discussion of conversion and cascading begins with the left side of the energy diagram in Figure 4.1. Conversion and cascading of available potential energy is discussed first. The discussion then progresses to the right of the diagram. Second, potential enstrophy conversion and cascading is discussed beginning with the right side of Figure 4.2.

The generation of available potential energy is shown in Figure 4.6 for the model experiments. The vertical bars in this figure give the control run results. Note that the "generation" is a loss of energy for all wave numbers except the zonal component (see Figure 4.1). Comparison with observation by Saltzman (1970) shows that the loss of long wave A is too small (except wave number 4) in the model. This is expected because of the aforementioned lesser amount of A_E in the largest scales of the model. The mid-scales and smaller scales are comparable to observation with the exception that the model does not have the minor observed peak at wave number 10.

The model's diabatic heating depends on two factors--the deviation of temperature from the zonal equilibrium temperature and the radiative time constant. It is observed from the different experiments that the loss of A_E is highly affected by the dynamics of the flow. Those experiments with the larger amplitude temperature waves have the greatest loss of A_E. Experiment One, which has a reduced radiative time constant (compared to the control run), has much less generation of A_E than the control run but less, on the average, than the wave numbers of E3 and similar magnitude as E2. The existence of the temperature wave is due to the advection pattern of the barotropic waves on the zonal temperature gradient. If the eddy barotropic kinetic energy is an indicator of the intensity of these waves, then a 25% increase in K_{ME} seems to be roughly equivalent to doubling the radiative time constant of Newtonian heating. The generation of zonal available potential energy has a similar trend, maybe even more so (see Figure 4.1).

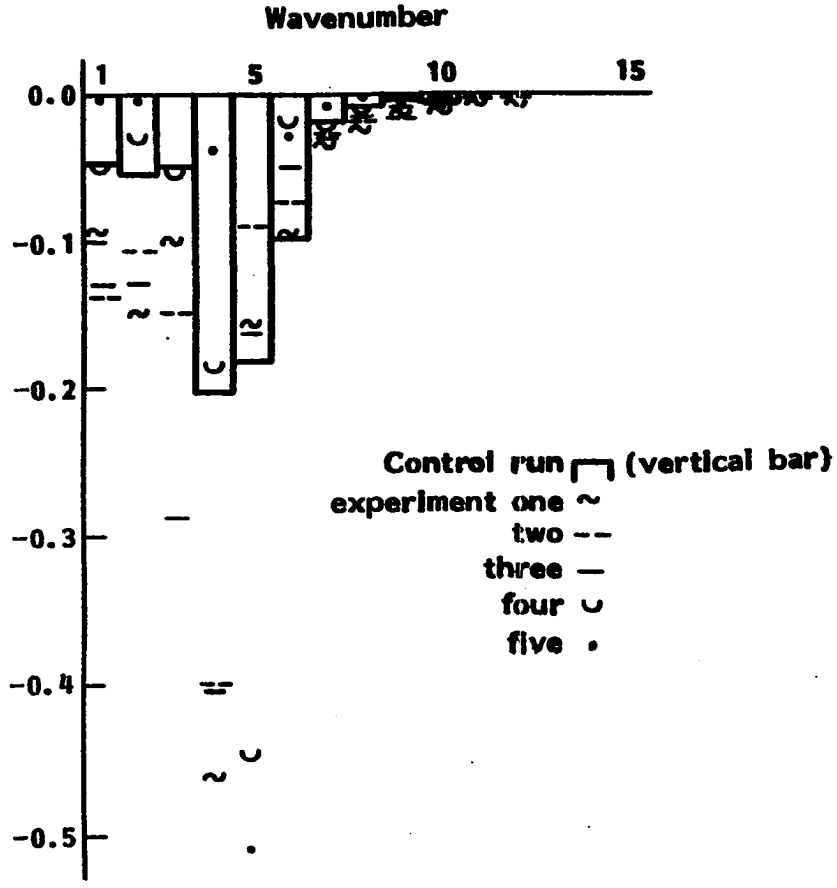

Figure 4.6. Generation of available potential energy in zonal wave number index, Units: Watt m^{-2}

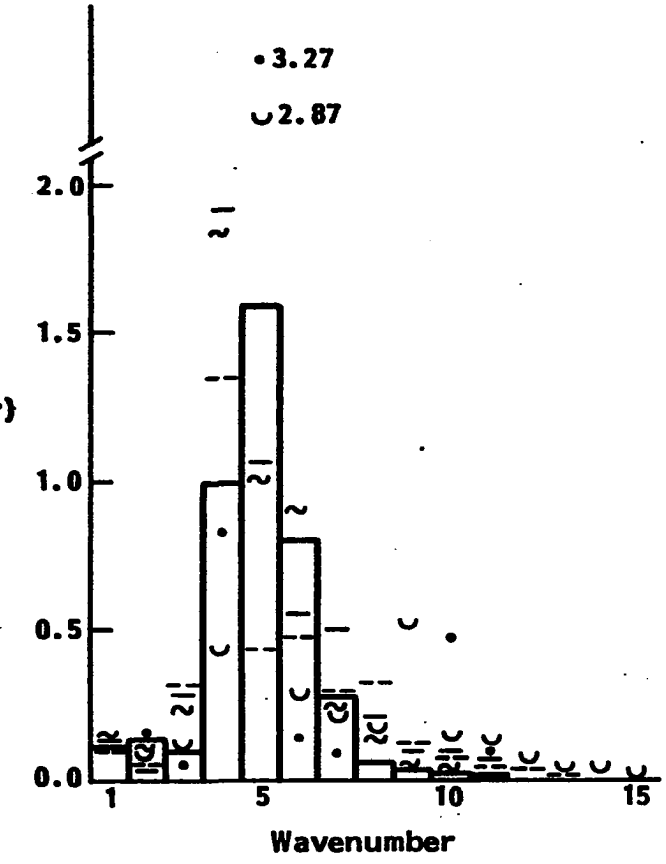

Figure 4.7. Conversion of zonal to eddy available potential energy, Units: Watt m^{-2}

The conversion from zonal to eddy available potential energy is shown in Figure 4.7. For wave numbers greater than 3, the model control run conversion is slightly larger and of similar trend as observation (e.g., Saltzman, 1970; Tomatsu, 1979). The longer wave observational conversions of this quantity are mainly due to standing waves (e.g., Chen, 1982). Thus, as mentioned previously, the absence of longitudinal diabatic heating dependence and orography that produce large standing waves (e.g., Kasahara, 1966) account for the smaller conversions of the long waves in the model.

The friction increase in E4 and E5 have the largest peaks with the smallest half-widths for the A_Z to A_{ZE} conversion. These two experiments have this similar trend in many of their conversions. Experiments One, Two and Three (E1, E2, E3) are shifted upscale by a wave number compared to the control run.

The nonlinear scale exchanges of available potential energy (A) are shown in Figure 4.8. The general appearance of this figure is different from observations (Saltzman, 1970). However, the principal function of this redistribution of energy is the same. Those scales with the largest A in both observation and in the model lose A to other scales. In the model, waves 4 and 5 have the largest A and in the earth's atmosphere the largest scale has the most A. Therefore, the upscale cascading of A in the model is not surprising, even though such a process is not observed in our atmosphere. From these results, one can speculate that for an atmosphere with similar parameters as that of the earth but with a smooth lower boundary and no longitudinal diabatic heating dependence,

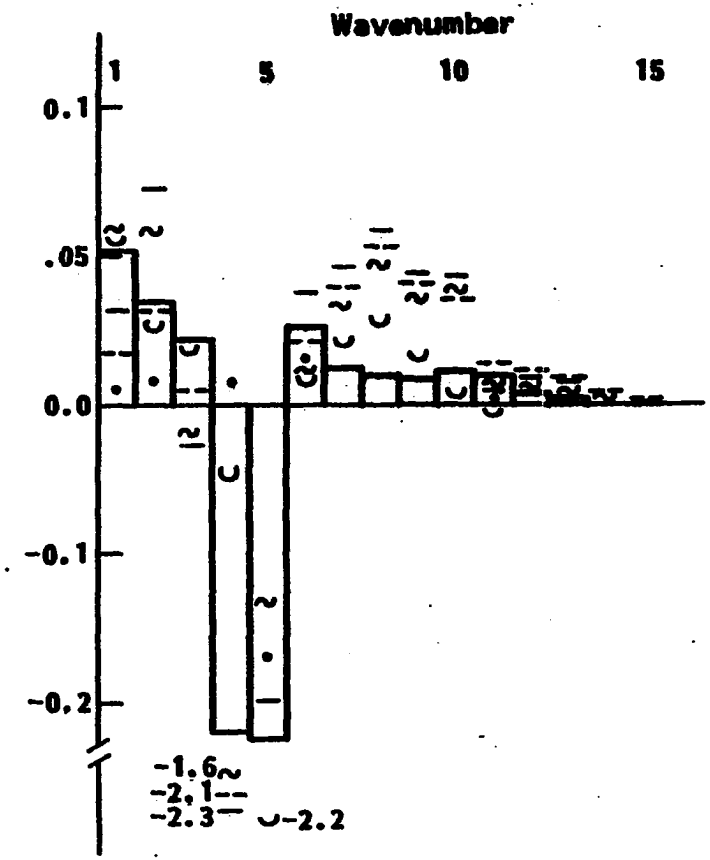

Figure 4.8. Nonlinear triad redistribution of available potential energy in wave numbers. Symbols are displayed in Figure 4.6, Units: Watt m-2

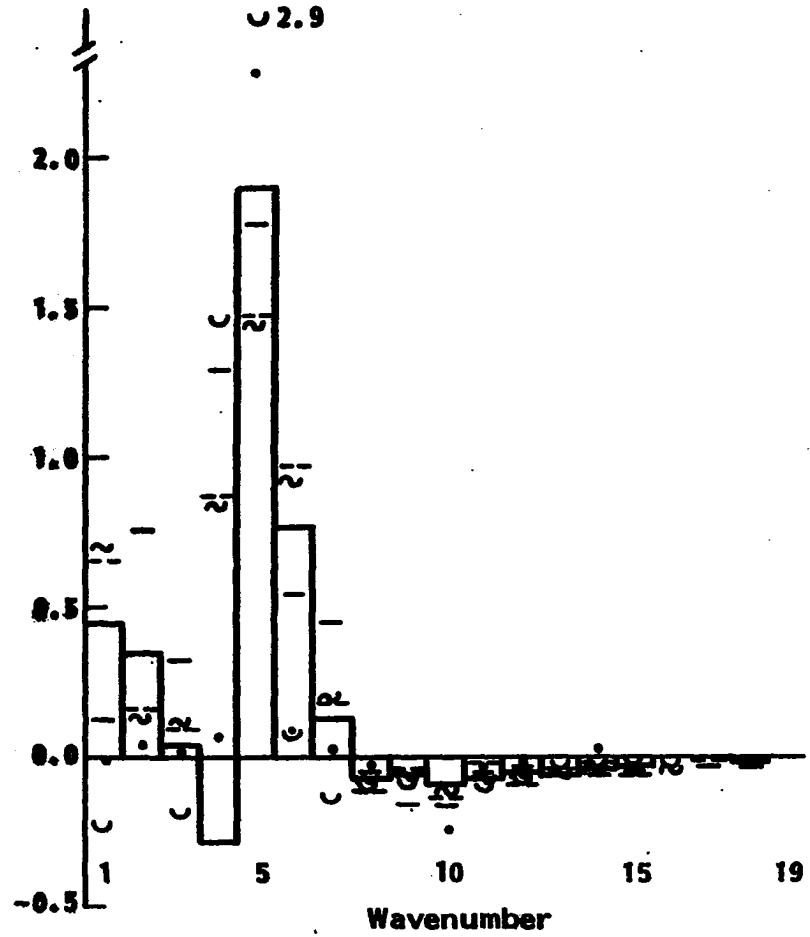

Figure 4.9. Conversion of available potential energy into baroclinic kinetic energy, Units: Watt m^{-2}

the upscale cascading of A may be found. Also, it may be speculated that the ocean may have upscale cascading of A from the scale of the deformation radius. Since A is only part of the total baroclinic energy, the discussion of the related part of Salmon's diagram will follow the discussion of baroclinic kinetic energy.

Experiment Five has less cascading of A than other experiments. This may be due to the heavier damping of higher wave numbers in this experiment. Experiment 2 and Experiment 3 have the greatest cascading of A. This may result from the greater number of wave numbers forced by baroclinic instability as well as the greater forcing.

Figure 4.9 displays the conversion of A to K_S in the zonal wave number.[5] From this conversion and the conversion from zonal to eddy available potential energy, one has an indication of how the finite amplitude baroclinic instability of the model is performing. The control run has the largest conversion of A to K at wave number 5 where the two-layer model of Barros and Wiin-Nielsen (1974) has a smaller maximum at wave number 4. Also, Barros and Wiin-Nielsen's model does not have anything like the negative conversion at wave number 4. Observation of this conversion is usually, but not always, positive and has more conversion by the long waves. Also, the spectrum usually peaks at wave number 6 for observation.

---

[5] Computation of this conversion requires omega (ω). The omega equation is cast in the form of a Helmholtz equation, transformed by the natural eigenfunctions (which are the model basis functions as a result of the same boundary conditions) and solved spectrally. The diabatic heating is used in computing ω.

Experiments Two, Three and Four are shifted slightly upscale (down wave number) for the conversion of A into K as compared to the control run.[6] This is also true of E2 and E3 for the conversion of A_Z to A_E. According to the linear baroclinic instability theory, one expects a shift in these conversions toward larger wave number for E2 as compared to the control run (this was discussed in Chapter IV, Section A). Therefore, even though the general picture given by linear baroclinic instability is correct, the specifics are not. The a priori ruling out of the cascades of energy in the linear baroclinic instability and the dependence of the triads on the wave number R are suspect. Salmon (1981) has speculated that the correlation between ω and temperature of a wave may be "scrambled" by the existence of other finite waves. Another explanation is the competition between waves for the energy of the zonal flow. Any of these four ideas or their combination could possibly explain these discrepancies.

Large, narrow peaks with a maximum of wave number 5 are found in Figures 4.8 and 4.9 for E4 and E5. This result was expected from linear baroclinic instability with surface friction for E4 as compared to the control run. The explanation, though, may be sought in simpler terms. One would expect marginal unstable waves to become damped with increasing friction. Thus, increasing friction would stabilize wave numbers nearest to the long wave and the short wave cutoffs leaving a few waves with little competition for the energy of the zonal flow.

---

[6] The same shifts are noted for the kinetic energy spectra in the previous section.

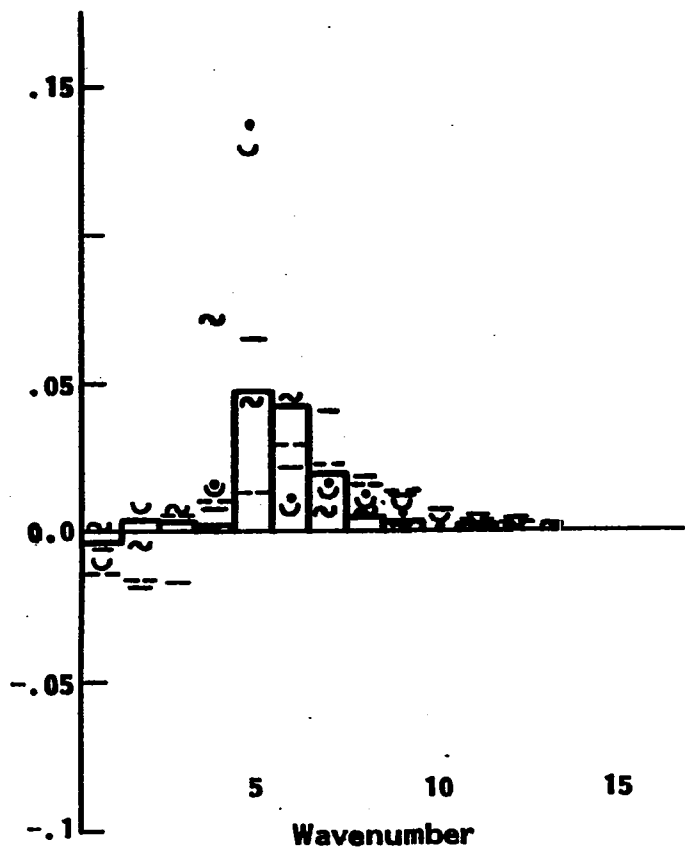

Figure 4.10. Conversion of eddy to zonal baroclinic kinetic energy. Symbols are defined in Figure 4.6, Units: Watt m^{-2}

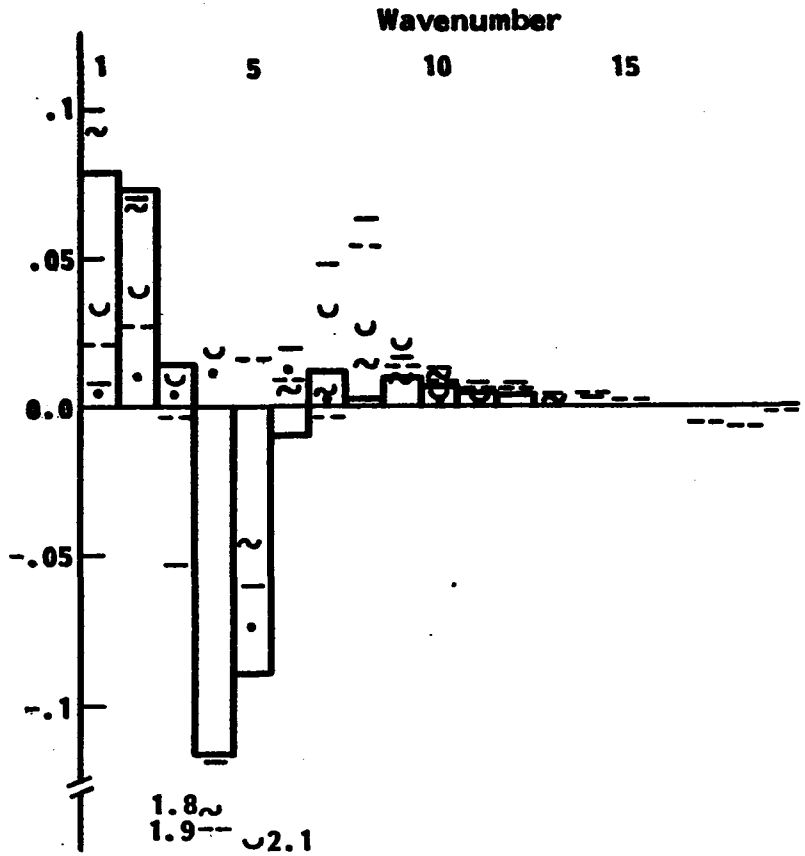

Figure 4.11. Nonlinear triad redistribution of baroclinic kinetic energy among zonal wave numbers, Units: Watt m^{-2}

The conversion from baroclinic eddy to zonal baroclinic kinetic energy is given in Figure 4.10. This conversion cannot be compared to any other study since this is the first time it has been calculated in this form. In Chapter III, the relation between this conversion and other formulations (e.g., Wiin-Nielsen and Drake, 1966; Chen and Tribbia, 1981) is explained. For the purpose here, note the main function of this conversion is the maintenance of K_{SZ}. From Figure 4.10, this is seen to be accomplished mainly by the most energetic wave numbers and the next higher wave numbers. In E4 and E5, this conversion is dominated by wave number 5.

Figure 4.11 shows the redistribution of baroclinic kinetic energy among wave numbers by the nonlinear triad exchanges. Even though this figure involves losses and gains of K_S[7] only, the barotropic kinetic energy is involved in the redistribution process. This can be seen by examining the triads of this redistribution process (e.g., Marshall and Chen, 1982). Wave numbers 4 and 5 are seen to lose energy to both smaller and larger scales. These results are only slightly comparable to the results of Chen and Tribbia's (1983) observational study which has large K_S losses from wave numbers 2, 4, 10, and 12 and peak gains for wave numbers 1, 3 and 6. The magnitudes for these transfers of energy are slightly larger than those found in the model. The previously mentioned long wave physics may explain the long wave differences but the medium scale differences are left unexplained.

---

[7] The same can be stated of the total baroclinic energy or A.

The sum of Figures 4.8 and 4.11 gives the cascading of total baroclinic energy. Both A and K_S have comparable contributions. Note that the trends of the respective experiments are similar in both figures. These results confirm the direction of the cascading in wave numbers higher than the Rossby deformation wave number in Salmon's diagram (1978, 1980). However, these results contradict the low wave number direction of cascading of total baroclinic energy in Salmon's diagram for all the experiments. The direction of cascading for the baroclinic low wave numbers of Rhines (1977) is the same as Salmon. Rhines inferred this direction of cascading for low wave numbers from an inviscid initialization experiment where a spot of energy is introduced into the low wave numbers only and the fields allowed to evolve. The baroclinic energies cascaded downscale. The cascading of the model baroclinic energy in equilibrium seems to be quite different than these initialization experiments. The theory of Rhines is inferred from the flow field and Salmon's is based on closure modeling and triad[8] properties. This is a direct calculation; hence, it is concluded that this part of Salmon's diagram should be modified for the two-layer model.

The conversion from baroclinic to barotropic kinetic energy is displayed in Figures 4.12, 4.13 and 4.14. Figure 4.12 is the linear part of the conversion of baroclinic to barotropic kinetic energy which is like other classical conversions in that no scale changes of energy occur

---

[8]Marshall and Chen (1982) showed the triads near to the deformation scale can cascade in either direction.

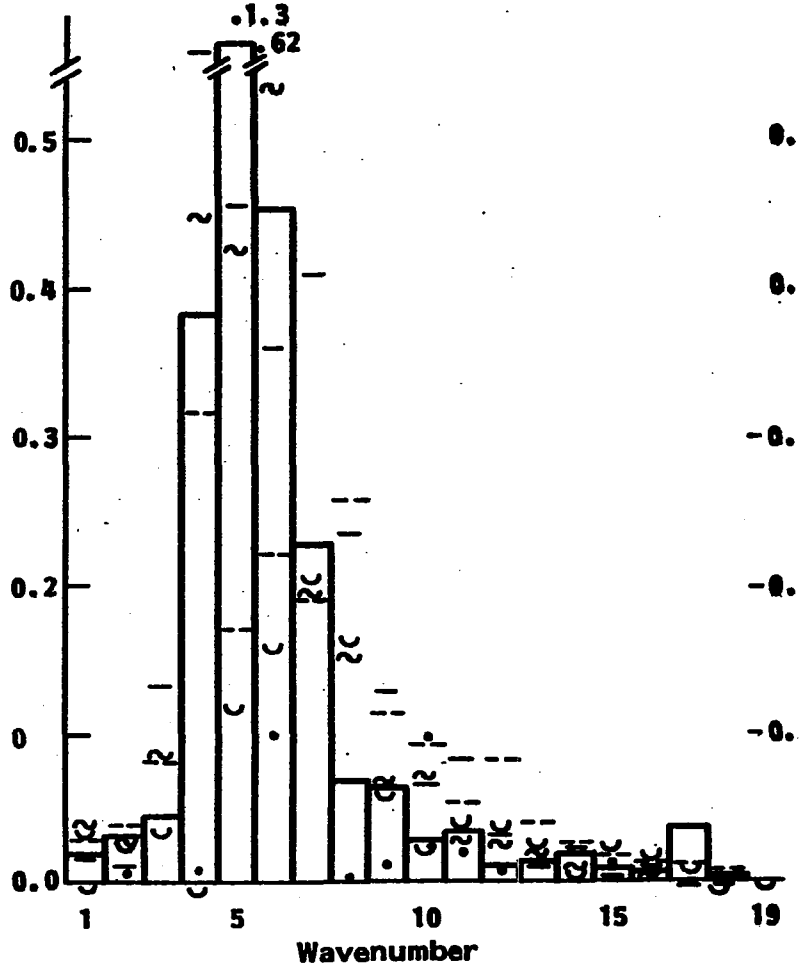

Figure 4.12. Linear baroclinic to barotropic conversion of energy. Symbols are displayed in Figure 4.6, Units: Watt m^{-2}

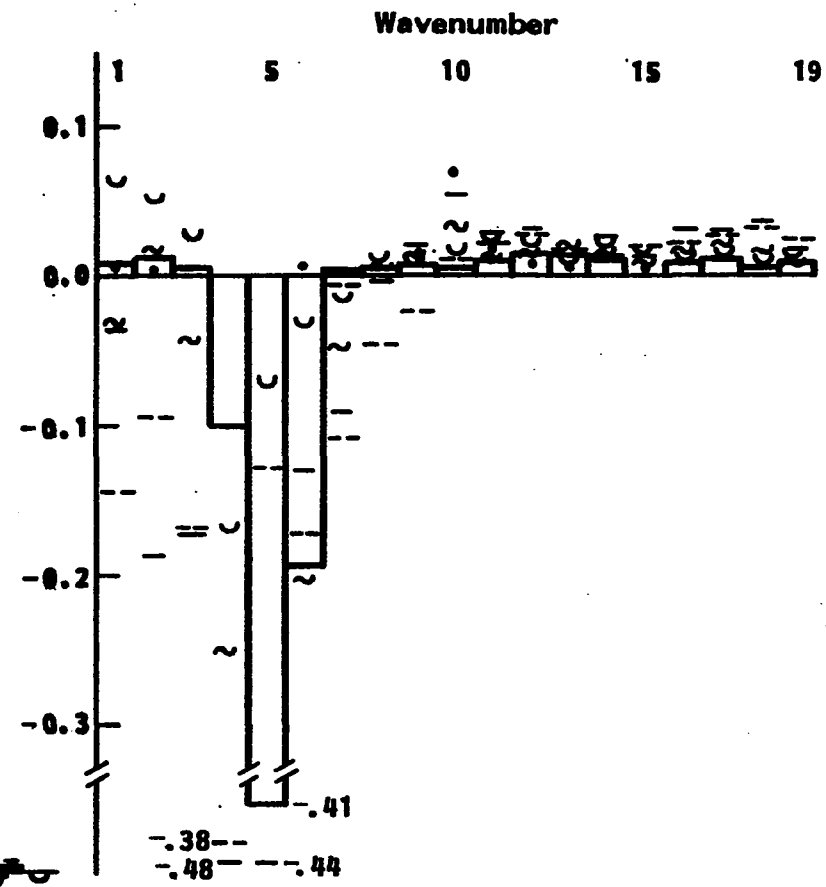

Figure 4.13. Nonlinear triad exchange of baroclinic kinetic energy of wave number k with all the wave numbers of barotropic kinetic energy, Units: Watt m^{-2}

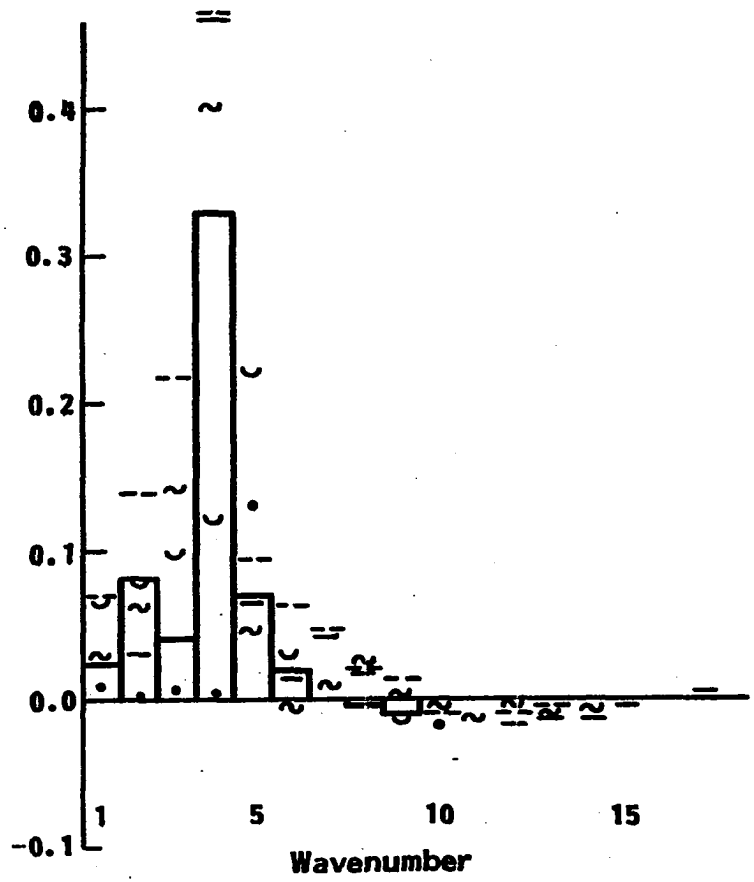

Figure 4.14. Nonlinear triad exchange of the barotropic kinetic energy of wave number k with all the wave numbers of baroclinic kinetic energy, Units: Watt m^{-2}

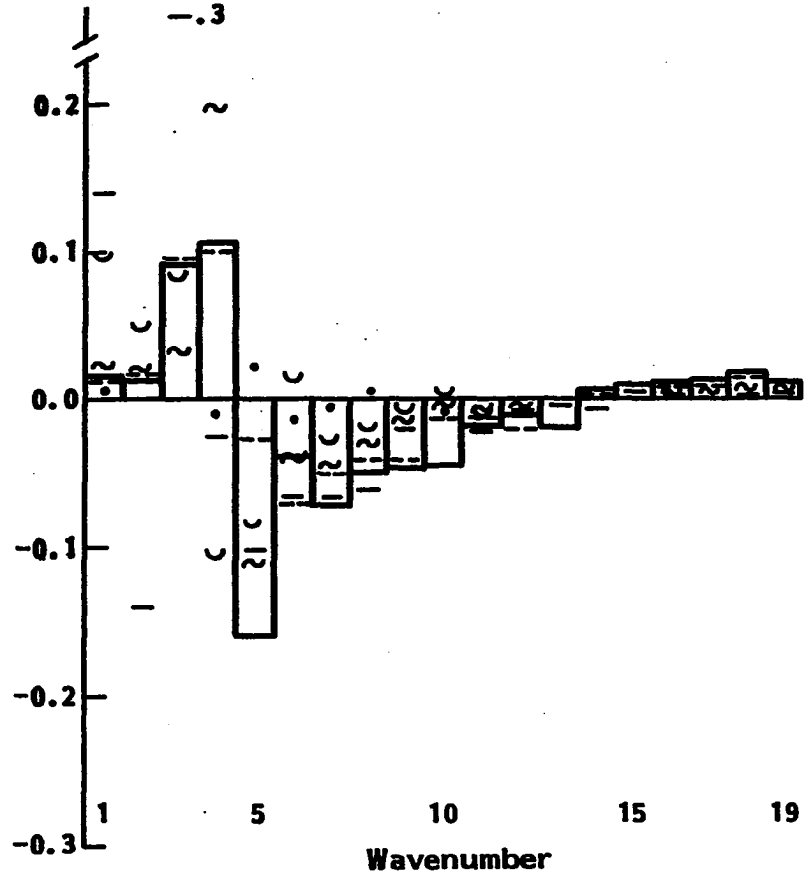

Figure 4.15. Nonlinear triad redistribution of barotropic energy among wave numbers. Symbols are defined in Figure 4.6, Units: Watt m^{-2}

with this conversion. The example of Wiin-Nielsen (1962) discussed in Chapter I for a single wave and zonal flow is germane to this part of the K_S to K_M conversion. From the arguments presented in Chapter I, this conversion should be broadened toward smaller scales as compared to the conversion of A to K_S. This is indeed the situation when Figures 4.9 and 4.12 are compared for all experiments with the possible exception of Experiment 5.

Figure 4.13 shows the spectrum of energy gained by the barotropic wave numbers due to the triad part of the conversion from baroclinic to barotropic kinetic energy. Figure 4.14 displays the spectrum of energy gained by the baroclinic wave numbers due to the triad part of the baroclinic to barotropic conversion of kinetic energy. When the conversion wave numbers are summed over the spectrum, the values from both of these figures are the same but of opposite sign. Thus, one can physically see the result of Chapter III--energy can change scale as it converts from baroclinic to barotropic kinetic energy. This same conclusion can be reached by examining the triad relations within the context of conservation of energy and potential enstrophy.

The main effect of this scale exchange is found to be upscale cascading. Comparisons of the linear and triad parts of the K_S to K_M conversion show that they are comparable magnitude. The single wave argument of Wiin-Nielsen (1962) is not applicable to the triad part of this conversion. However, by examining the triad relations with conservation of energy and potential enstrophy, one can find that the largest scales (those greater than the deformation scale) are restricted

severely in the rate of change of barotropic energy due to the triad process (Salmon, 1980).

The results here are in agreement with Salmon's diagram; however, the vertical arrow representing the conversion from total baroclinic energy to barotropic energy should not connect the same wave numbers but should be still around the Rossby deformation wave number. This same correction may also be applicable to the related diagram of Rhines (1977) for the ocean.

Since the Rossby deformation wave number is increased in E3, it is of interest to note any changes in the baroclinic to barotropic conversion. Experiment Three, as well as E2 and E1, convert more energy at about wave number 4 compared to wave number 5 than in the control run.

The comparison of this conversion with the observational study of Chen and Tribbia (1983) is complicated by the differences in formulation. Their conversion has the largest magnitudes at the largest scales (wave numbers 1-3) with a secondary maximum wave numbers 13-15. Wave number 4 converts a large amount of energy toward shear kinetic energy. Wave numbers 8-10 and 15-18 convert a small amount of energy to vertical shear kinetic energy. These results suggest the observed cascade spectra are more complicated than the two-layer results computed in this study and deduced in the studies of Salmon (1980) and Rhines (1977).

Herring (1980) has investigated the quasi-geostrophic turbulence based on the idea of Charney (1971) that atmospheric flow tends toward isotropy in the three-dimensional index (where the vertical coordinate is stretched by the static stability divided by the rotation rate). The width of the

channel would obstruct this tendency as well as the existence of only two vertical modes. The effect of this latter constraint has already been seen to affect the power laws of the baroclinic quantities. The more vertical degrees of freedom[9] for the actual atmosphere may be in part responsible for the complexities of the observational baroclinic to barotropic kinetic energy conversion.

The triad redistribution of barotropic kinetic energy among wave numbers is displayed in Figure 4.15. Wave numbers 5-10 for the control run give up energy to higher and lower wave numbers. This confirms another part of Salmon's diagram (1980). Experiment Three has erratic sign changes for this quantity in low wave numbers. Experiment Five has little cascading of barotropic kinetic energy.

The steep power law of E5 kinetic energies appears to be caused by two related effects: the strong dissipation and smaller cascading of energies. Examination of the formulation of the cascades shows that the amplitude of the smaller scales affect the amount of energy they receive by cascading. This is particularly pronounced when two components of a triad are in the smaller scales.

Observation of the nonlinear transfer of vertical mean kinetic energy among wave numbers (Chen and Tribbia, 1983) shows a large gain of K_M by wave number 1 and smaller gains by wave numbers 7, 12-14, and 17-18. All other wave numbers give up energy to this process with large contributions from wave numbers 2 and 9. If one sums over groups of wave numbers,

---

[9] The term vertical degrees of freedom is used because there are no higher vertical normal modes than the barotropic one for the earth's atmosphere (e.g., Pedlosky, 1979).

say 1-4, 5-11, and 12-18, the overall observational picture of this nonlinear transfer is similar to the model's control run. However, on an individual wave number basis, the results are quite different.

Adding individual wave numbers from Figures 4.11, 4.13, 4.14, and 4.15 gives the nonlinear transfer (the cascades) for total kinetic energy in zonal wave numbers. Adding Figure 4.8 to the previously mentioned figures gives the cascading of total energy in the zonal wave number index. When these calculations of all the cascades are summed over wave number, all of the nonlinear transfers of energy sum to zero except Figure 4.13 and 4.14 which sum over wave number to become equal magnitude but opposite sign. The total cascading of kinetic energy can be compared to the classical spectral energetics observed in the atmosphere. In both the model control run and in observations (Saltzman, 1970), scales on the order of the Rossby deformation radius cascade energy to both smaller and larger scales by the triad processes. Observations, however, also has a large loss of energy from wave number 2 to other scales which is not found in the model. Chen's results (1982) show that a large part of this observed wave number 2 behavior is due to the standing contribution. This suggests the previously mentioned physics not included in the model are responsible (e.g., Smagorinsky, 1953; Kasahara, 1966) for the wave number 2 behavior.

Figure 4.16 displays the conversion of eddy to zonal barotropic kinetic energy. Wave numbers 5 and 6 support K_M except for Experiments Two and Four. Experiment Five does most of the K_M maintenance by wave number 5. The form of this conversion for a quasi-geostrophic formulation makes it difficult to compare with the study of Chen and Tribbia (1983). Their

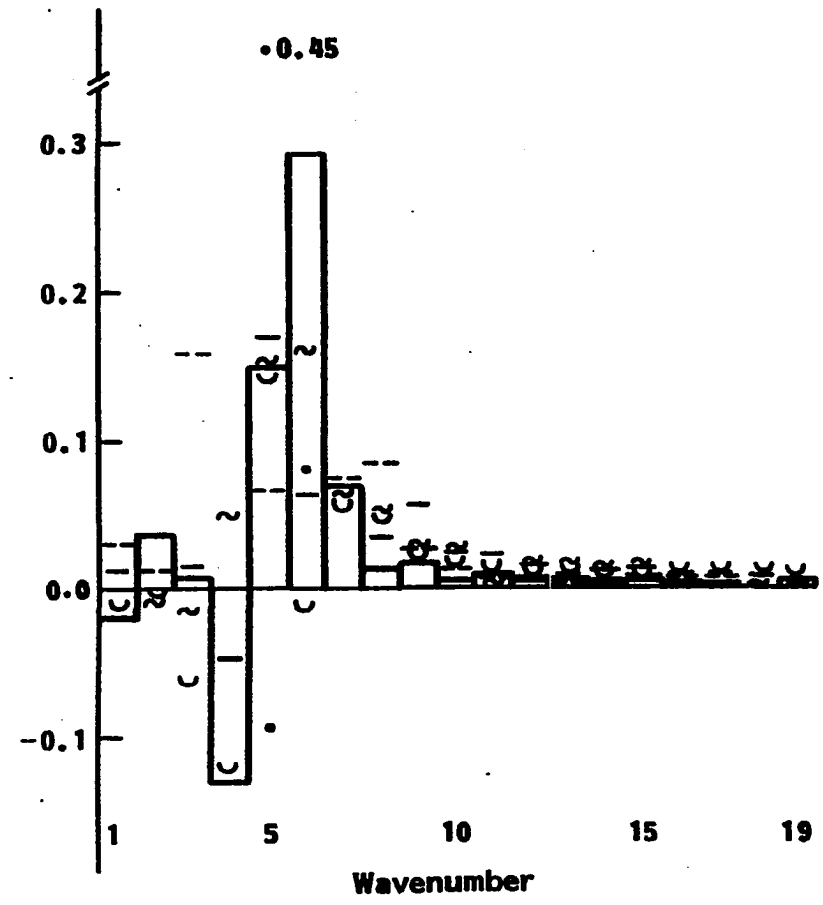

Figure 4.16. Conversion of eddy to zonal barotropic kinetic energy. Symbols are defined Figure 4.6, Units: Watt m^{-2}

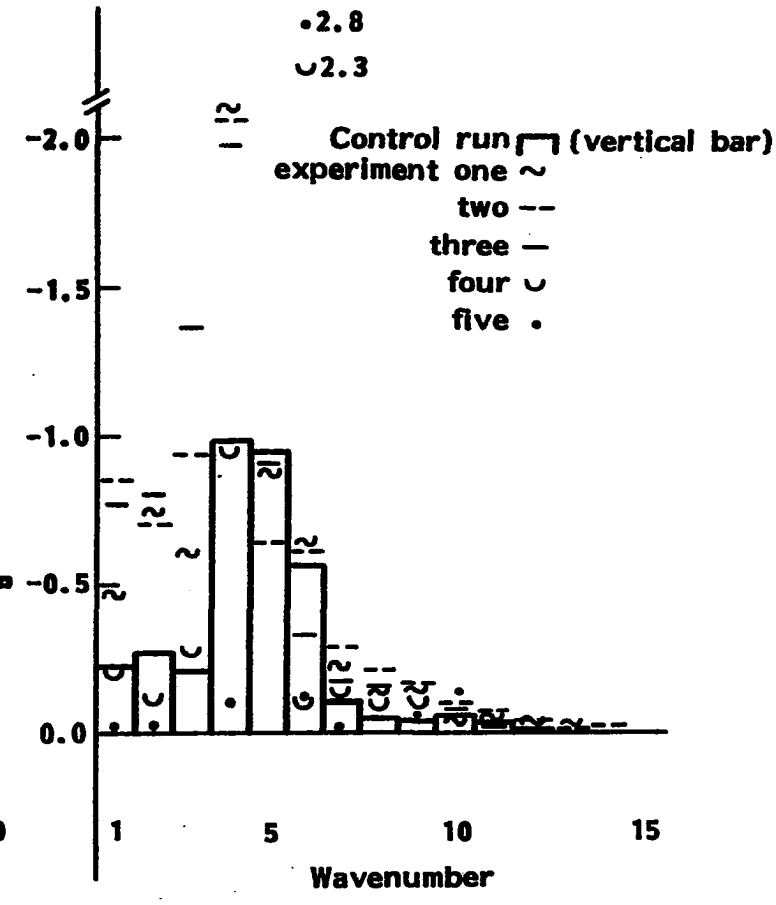

Figure 4.17. Generation of baroclinic potential enstrophy in the zonal wave number index Units: 10^{-16} s^{-2}

primitive equation formulation gives a zonal vertical mean energy that is supported by conversion not only from the eddy vertical mean energy but from the eddy vertical shear energy as well. Chapter III discusses the details.

Next, the enstrophy part of Salmon's diagram (1978) is investigated. Most of the potential enstrophy enters by the generation of zonal baroclinic enstrophy (E_{SZ}) (Figure 4.17). The same diabatic heating process (and some friction) contribute to the loss of eddy baroclinic potential enstrophy (E_{SE}). This is displayed in Figure 4.2. The larger the amplitude of E_{SE} for a wave number, the larger the loss of E_{SE} for the experiments. Since E_S is completely specified by the temperature field, this result is not surprising in light of how the Newtonian heating works. There is no observational study to compare with this figure because of the difficulty of obtaining accurate radiation and friction data.

The conversion from zonal to eddy baroclinic potential enstrophy is shown in Figure 4.18. The maximum conversion occurs at wave number 6 except for E1, E2, and E3, in which it occurs at wave number 5. The higher wave number dependence of potential enstrophy, as compared to energy, shows up only slightly in this conversion. The general distribution is very similar to that of baroclinic eddy to zonal energy conversion, with the same wave number maximums for the respective experiments.
The observational study of this conversion (Chen and Tribbia, 1983) has the largest conversions from zonal to eddy K_S in wave numbers 1, 2, and 3 with wave number 2 being the maximum. Wave numbers 4-9 show a decrease in magnitude from the large scales with an abrupt decline between wave number 3 and 4. Overall magnitudes are similar to this study.

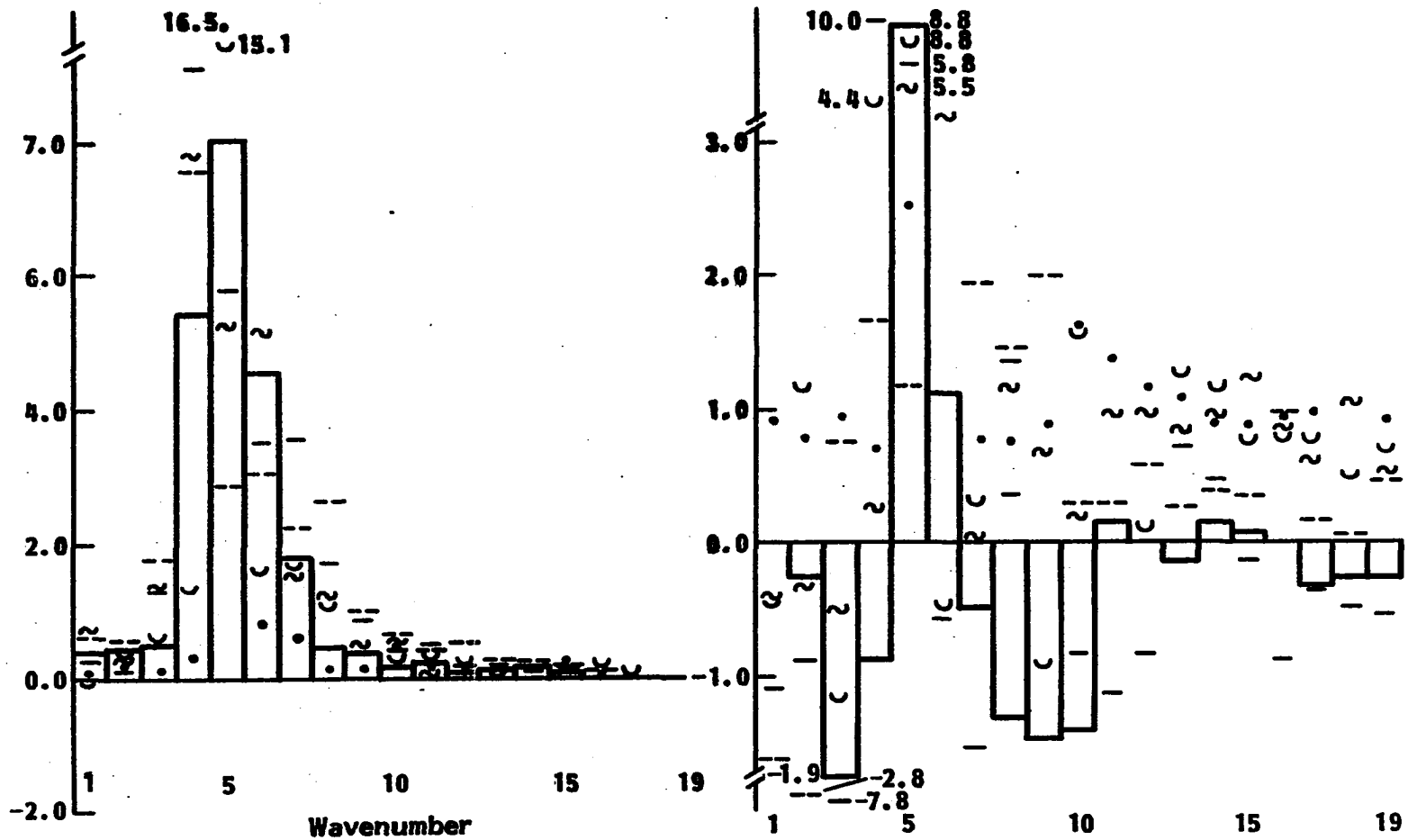

Figure 4.18. Conversion of zonal to eddy baroclinic potential enstrophy. Symbols are defined in Figure 4.17, Units: $10^{-16} s^{-2}$

Figure 4.19. The nonlinear triad redistribution between wave numbers of baroclinic potential enstrophy. Symbols defined in Figure 4.17, Units: 10^{-16} s^{-2}

The nonlinear triad redistribution of baroclinic potential enstrophy among wave numbers is shown in Figure 4.19. The experiments exhibit a large amount of variation in this quantity. The only consistent pattern for these cascades for all experiments is the gain of potential enstrophy by either wave number 4 or 5. Like the triad redistribution of baroclinic energy, this process involves the barotropic enstrophy as well. For this reason, inertial range theory is not invoked. Also, the constant flux of baroclinic enstrophy is not found.

For the same quantity Chen and Tribbia (1983) have wave numbers 1-7 losing baroclinic enstrophy to smaller scales. This is quite different from the results here. Their magnitudes are smaller also.

Experiment Three is the most similar to the control run. Experiments Two, Three, Four, and Five all have a relative large positive value in her higher wave numbers. The reason for this is unclear.

Figure 4.19 displays the conversion of baroclinic potential enstrophy of zonal wave number k with all the barotropic wave numbers. Figure 4.21 is the conversion of barotropic enstrophy of wave number k with all the baroclinic wave numbers. Like the barotropic-baroclinic energy conversion, scale exchanges can occur as energy converts between these two types of enstrophy. The scale exchanges tend to be downscale. There is a large amount of variation between experiments, but the general trend seems to be very similar and confirms a part of Salmon's diagram but with higher k. Experiment Two exhibits a relatively large amount of conversion in the higher wave numbers.

Experiments Four and Five have a large gain of baroclinic potential enstrophy at wave number 10 in Figure 4.20. This anomalous wave number

10 behavior can also be seen in Figures 4.9, 4.12, 4.13, 4.14, and 4.17 for E5. Since E5 has a large conversion and amplitude at wave number 5 and wave number 10 is a higher harmonic, one may expect a connection. The trend for a certain asymmetry in a wave number 5 pattern, such as the tilting of the wave so that momentum is transported to the jet, may be picked up by the Fourier analysis as wave number 10.

The trend of this conversion (small low wave number conversions and higher wave number conversions) can be motivated by a simple extension of Wiin-Nielsen's (1962) zonal flow and one wave example (see Chapter III, Section D). The result, when compared to the barotropic-baroclinic energy conversion, shows the higher wave number dependence. Higher wave numbers do tend to convert more compared to their smaller magnitudes of baroclinic enstrophy storage. Experiment Two, in particular, does this.

Observation of the barotropic-baroclinic conversion of potential enstrophy (Chen and Tribbia, 1983) has maximum conversion at wave numbers 3, 5, 7, and 8. Conversion rates are slightly smaller and the larger wave numbers (11-18) have much less conversion than found in this study.

The nonlinear triad redistribution of barotropic enstrophy among wave numbers is shown in Figure 4.22. Barotropic enstrophy is lost from wave numbers 5-15 to larger and smaller wave numbers. The control run and E1 have large gains in wave number 4 but E3 and E4 have a large gain in wave number 3. Experiment Three has the strongest up- and downscale cascading. The general trend fits Salmon's diagram but, again, the cascading center is shifted a little toward a higher wave number than the wave number of the Rossby deformation radius.

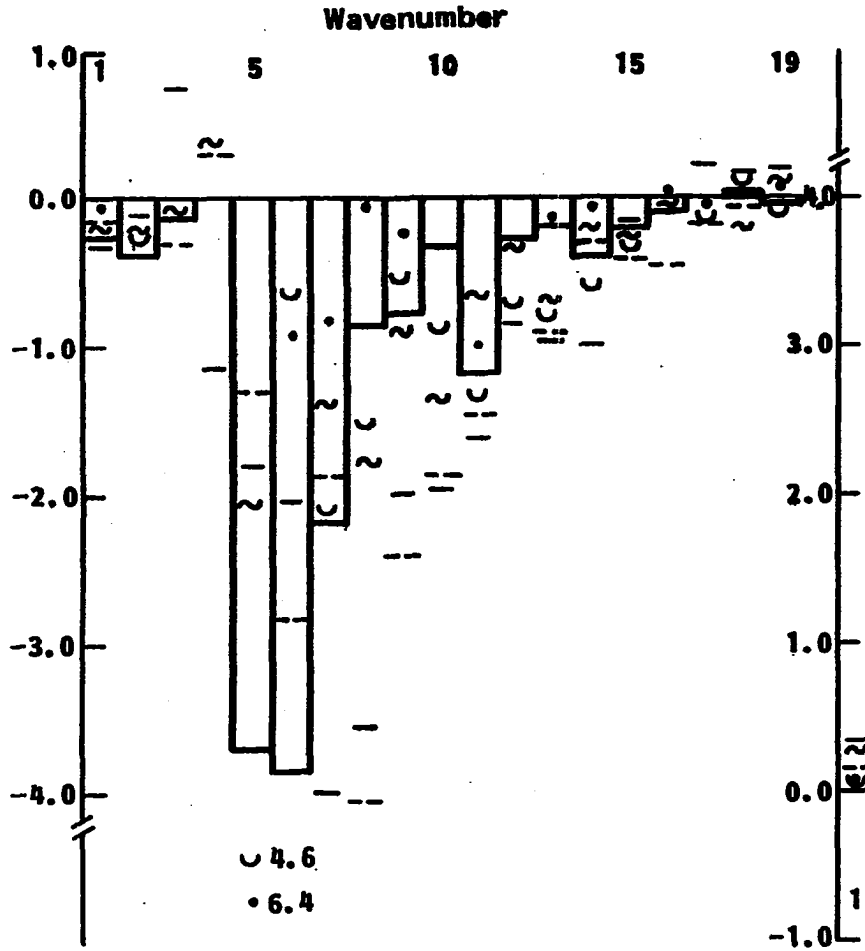

Figure 4.20. The nonlinear triad exchange between the baroclinic potential enstrophy of wave number k and all the wave numbers of barotropic enstrophy, Units: $10^{-16}s^{-2}$

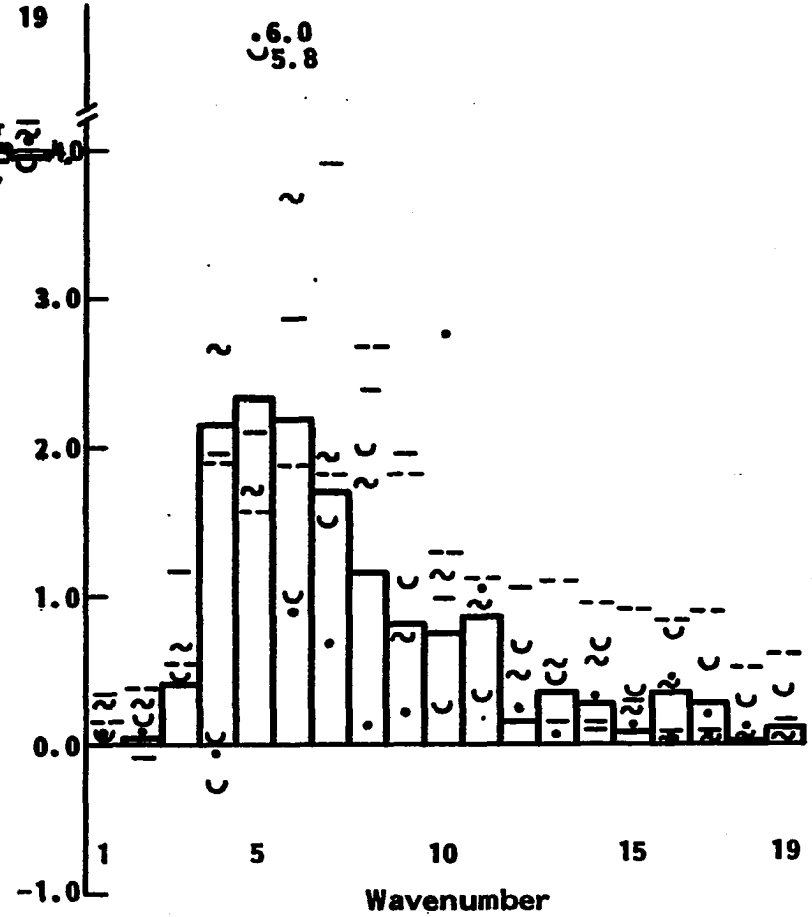

Figure 4.21. The nonlinear triad exchange between the barotropic enstrophy of wave number k and all wave numbers of baroclinic potential enstrophy, Units: $10^{-16}s^{-2}$

Even though the appropriateness of using inertial subrange theory to explain the -3 power law can be questioned (especially in view of the barotropic-baroclinic conversion), the criterion can still be evaluated. These criteria are: source and sinks are far from the subrange, constant flux of enstrophy towards large wave numbers and a vanishing flux of kinetic energy in the -3 power law inertial subrange. Barros and Wiin-Nielsen (1974) have shown that all of these three criteria are not strictly valid for a two-layer model's total kinetic energy cascades. However, the constant flux of enstrophy is reasonably close. Barotropic quantities are used because the form of the barotropic vorticity equation in some cases becomes the two-dimensional vorticity equation; therefore, motivating two-dimensional turbulence. The friction and forcing criteria are violated a priori. From Figure 4.22, the constant flux of barotropic enstrophy can be inferred to be not so. The steep power law for E5 may be related to the small amount of barotropic enstrophy cascading. From Figure 4.15, the kinetic energy is inferred to not have a vanishing flux of kinetic energy (from a subjective integration) in the wave numbers of the -3 power law. However, the flux looks small.

Observation of the nonlinear scale exchanges of vertical mean enstrophy (Chen and Tribbia, 1983) show a maximum loss from wave numbers 6 and 7 with large gains by wave numbers 1 and 14-17.

The exchanges between the eddy and zonal barotropic enstrophy are given in Figure 4.23. Wave numbers greater than 5 support the zonal barotropic enstrophy. All experiments have some eddy barotropic enstrophy gain from the zonal component in wave number group 3-5. This

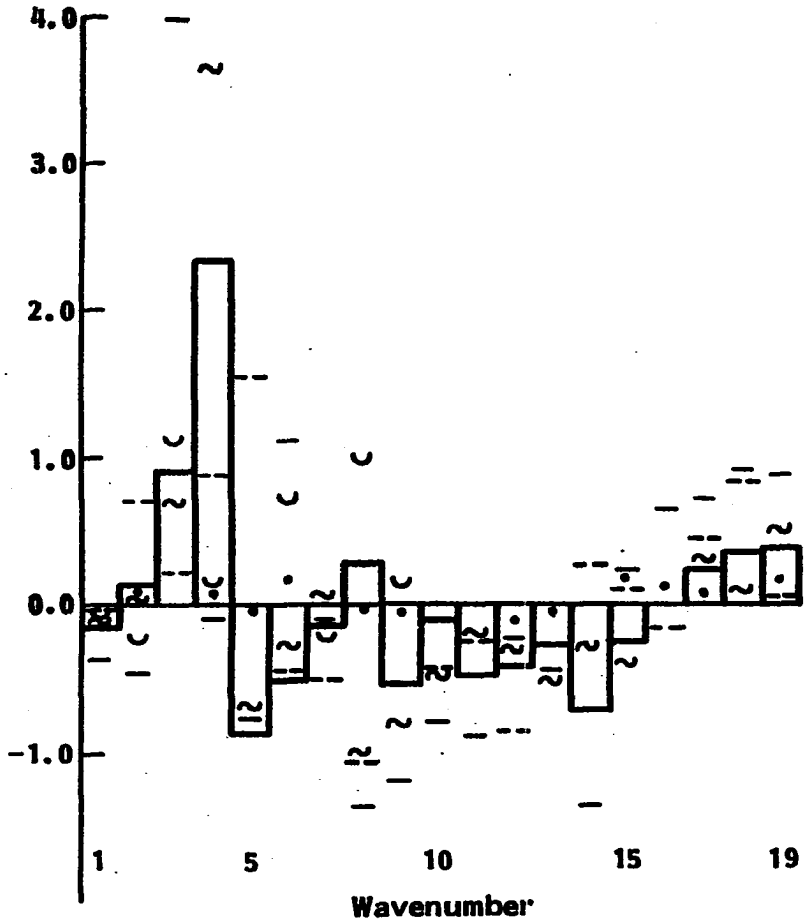

Figure 4.22. The nonlinear triad redistribution of barotropic enstrophy between wave numbers. Symbols are defined in Figure 4.17, Units: 10^{-16} s^{-2}

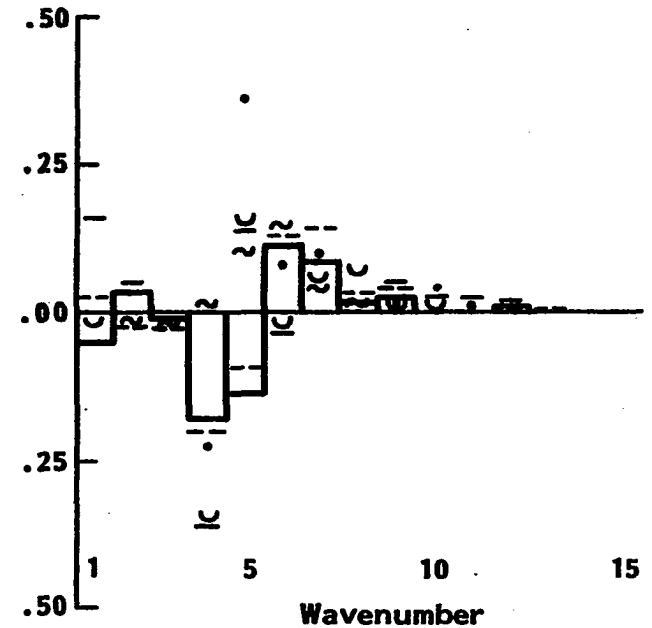

Figure 4.23. The exchange between eddy and zonal barotropic enstrophy. Symbols are defined in Figure 4.17, Units: 10^{-16} s^{-2}

cancellation between medium and small wave numbers accounts for the small overall conversion. Observation (Chen and Tribbia, 1983) is much smaller in magnitude than the model calculation with a large gain by wave number 3 from the zonal component. The largest support of the zonal barotropic enstrophy comes from wave numbers 2 and 3 in observation.

V. CONCLUDING REMARKS

The purpose of this study is to examine the atmospheric cascades and conversions with the simplest baroclinic nonlinear model. The complex nature of this nonlinear phenomenon mandates such a study. The main difference between this and previous studies is direct calculations of the model cascades are made rather than inferred. The future gain of such studies is basic understanding of the nonlinear atmosphere which relates to such diverse topics as predictability and subscale parameterization.

The quasi-geostrophic two-layer equations are integrated in a channel domain by the spectral transform method and the N-cycle scheme. Newtonian heating, surface drag and a small diffusion are used. The model is initialized with a temperature field and related vertical shear similar to the one found in the winter mid-latitude atmosphere. The model is allowed to evolve until the overshoot of eddy energies has passed. Day 50 through day 80 are used for analysis at one day intervals. The analysis is done with the barotropic and baroclinic spectral energetics and potential enstrophy equations in quasi-geostrophic form.

The simple vertical structure of the two-layer quasi-geostrophic model produces a useful degeneracy. The vertical mean and deviation (shear) of Wiin-Nielsen (1962) are coincident with the two vertical normal modes (barotropic and baroclinic) of the linear form of this model. For this reason, the modal stream functions are used in all the derivations. Also,

the relation between thermal wind and the baroclinic stream function is such that this stream function could be called the thermal stream function.

The derivation of the barotropic and baroclinic spectral energetics shows large differences in form with the vertical shear and mean energetics of Wiin-Nielsen and Drake (1965) and Chen and Tribbia (1981). These differences are most pronounced in the conversions of baroclinic eddy kinetic energy to baroclinic zonal kinetic energy, baroclinic zonal kinetic energy to barotropic eddy kinetic energy and baroclinic eddy energy to barotropic zonal energy. The latter two conversions do not exist in the quasi-geostrophic formulation. This quasi-geostrophic formulation is shown to account for the computed behavior of the primitive equation energetics. The potential enstrophy equations have all the same conversions as Chen and Tribbia (1983). However, differences exist in the form of the conversions due to the approximations inherent to the two-layer quasi-geostrophic model.

The main purposes of the analysis method used are as follows. The first is direct calculation and evaluation of the diagram of Salmon (1978) (based on Rhines (1977)) for the two-layer model. The second is the comparison of the control run with the observational study with Chen and Tribbia (1983). Also, analysis of different experiments are used to examine the finite amplitude dynamics of the model.

Five experiments and a control run were made for investigating the model flow fields with the barotropic and baroclinic formulation. Experiment One (E1) increases the Newtonian heating coefficient compared to

the control run. Experiment Two (E2) increased the Rossby deformation wave number. Experiment Three (E3) increased the zonal vertical shear. Experiment Four (E4) increased the surface friction. Experiment 5 (E5) mainly increased the diffusion coefficient to the control run. These experiments were characterized by displaying the barotropic and baroclinic energies in different wave number indices.

The diabatic heating of the model is found to be more sensitive to an increase of barotropic energy than to an equivalent increase in the Newtonian heating relaxation time. Increasing the Rossby deformation wave number results in the maximum of zonal wave number shifting towards lower wave number (as compared to the control run). This contradicts the results expected from linear inviscid baroclinic instability theory. This same result is found in the conversions from eddy available potential energy to baroclinic kinetic energy and baroclinic energy to barotropic energy. Increases in the zonal vertical shear and Rossby deformation wave number result, as expected from linear instability theory, in greater energy in Experiments Three and Two, respectively. Increases in friction narrow the spectrum of baroclinically unstable waves in both linear baroclinic instability theory and in the model finite waves. The effects of increased diffusion are most dramatic in the model, resulting in a narrow spectrum and steep high wave number power laws.

A number of differences exists between the results of this study and those of Chen and Tribbia's (1983) observational study. The major difference is in the largest scales. These are believed to result from

the absence of the physics for orography and longitudinal dependence of diabatic heating.

The cascading and conversion results are summarized by redrawing the schematic diagram of Salmon (1980).

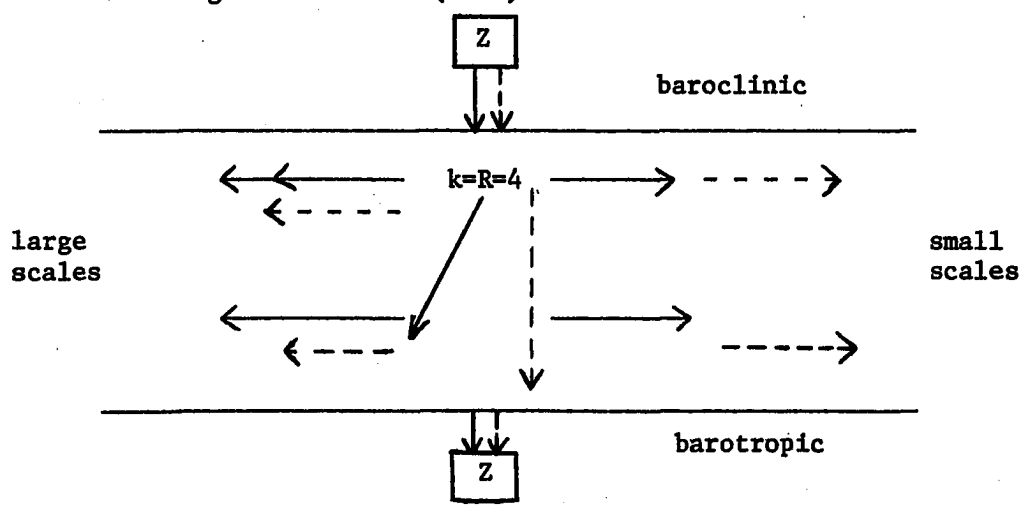

Figure 5.1. Proposed cascading diagram. Arrows: Solid - energy, dashed - enstrophy

The placement of the zonal flow (Z) as distinguishable from other wave numbers is done noting the zonal flows different role in the formulation given in Chapter III. Also, interactions between the zonal flow and waves do not satisfy the relation of three separate components.

The upscale cascading of baroclinic energy (the sum of available potential and baroclinic kinetic energy) is in contradiction with both Rhines (1977) and Salmon (1980) in direction. In Rhines' initialization experiment, a "spot" of energy is introduced into only the high baroclinic wave numbers of a two-layer model and found to cascade downward toward the Rossby deformation radius. This is a very different situation compared to the forcing of scales near to the Rossby deformation radius by

baroclinic instability. For all experiments, energy is cascaded away from the forced scales. The potential enstrophy is cascaded away from the larger wave numbers of the forced wave numbers and wave numbers slightly larger.

The upscale cascading of energy as it is converted from baroclinic to barotropic energy is a modification of Salmon's diagram and could be used to modify a similar diagram of Rhines (1977). Scale exchanges of energy can occur as energy is converted from baroclinic to barotropic energy as can be seen in the triads of the two-layer model (e.g., Marshall and Chen, 1982) and from the formulation of Chapter III. The conversion of baroclinic to barotropic potential enstrophy can also result in scale exchanges as well. The main trend of these conversions is to convert more potential enstrophy at higher wave numbers than the same energy conversion.

The behavior of the barotropic kinetic energy and enstrophy is unchanged from that postulated by Salmon (1980) or Rhines (1977). The behavior of the barotropic kinetic energy and enstrophy are very much in accord with results found in two-dimensional turbulence simulations.

All of the experiments follow the general trend of the diagram shown on the previous page, with the possible exception of Experiment Five. This experiment, which has a large diffusion coefficient compared to other experiments, shows a decrease in cascading of most types. This is thought to be directly related to the steep power laws found in this experiment. It is argued that the large damping of smaller scales in E5 also affects the cascading of energy towards them resulting in a compounded loss of amplitude.

VI. BIBLIOGRAPHY

Baer, F. 1981. Three-dimensional scaling and structure of atmospheric energetics. J. Atmos. Sci. 38:52-68.

Barcilon, V. 1964. Role of Ekman layers in the stability of the symmetric regime in a rotating annulus. J. Atmos. Sci. 21:291-299.

Barros, V. R. and A. Wiin-Nielsen. 1974. On quasi-geostrophic turbulence: a numerical experiment. J. Atmos. Sci. 31:609-621.

Boville, B. A. 1980. Amplitude vacillation of an f-plane. J. Atmos. Sci. 37:1413-1423.

Bradely, J. H. S. and A. Wiin-Nielsen. 1968. On the transient part of the atmospheric planetary waves. Tellus 20:533-544.

Burger, A. 1958. Scale considerations of planetary motions of the atmosphere. Tellus 10:195-205.

Burrows, W. R. 1976. A diagnostic study of atmospheric spectral kinetic energetics. J. Atmos. Sci. 31:2308-2321.

Charney, J. G. 1948. On the scale of atmospheric motions. Geophysiske Publikasjoner 17:3-17.

Charney, J. G. 1971. Geostrophic turbulence. J. Atmos. Sci. 28:1087-1095.

Charney, J. G. and A. Eliassen. 1949. A numerical method for predicting the perturbations on the middle-latitude westerlies. Tellus 1:38-54.

Chen, T.-C. 1982. A further study of the spectral energetics of the winter atmosphere. Mon. Wea. Rev. 110:947-961.

Chen, T.-C. and H. G. Marshall. 1983. Time variation of atmospheric energetics in the FGGE winter. Dept. of Earth Sciences. Submitted to Tellus.

Chen, T.-C. and J. J. Tribbia. 1980. On the nonlinear cascades of enstrophy over the tropics at 200mb during two Northern Hemisphere summers. Mon. Wea. Rev. 106:458-468.

Chen, T.-C. and J. J. Tribbia. 1981. Formulation of an observational study for nonlinear cascades of barotropic and baroclinic flows in the atmosphere. Technical Report. Dept. of Earth Sciences, Iowa State University.

Chen, T.-C. and J. J. Tribbia. 1983. On the nonlinear cascading of the baroclinic and barotropic flows in the atmosphere. Dept. of Earth Science, Iowa State University.

Colucci, S. J., A. Z. Loesch and L. F. Bosart. 1981. Spectral evolution of a blocking episode and comparison with wave interaction theory. J. Atmos. Sci. 38:2092-2111.

Derome, J. 1979. Forced waves in a middle latitude beta plane model. p. 243-265. In Dynamical Meteorology Seminar 1979. European Centre for Medium Range Weather Forecasts, England.

Eliasen, E., B. Machenhauer, and E. Rasmussen. 1970. On a numerical method for integration of the hydrodynamical equations with a spectral representation of the horizontal fields. Rept. No. 2. Institut for Teoretisk Meteorologi, Copenhagen.

Fjortoft, R. 1953. On the exchanges in the spectral distribution of kinetic energy for the two-dimensional, nondivergent flow. Tellus 5:225-230.

Fjortoft, R. 1959. Some results concerning the distribution and total amount of kinetic energy in the atmosphere as a function of external heat sources and ground friction. p. 194-211. In B. Bolin (ed.) The atmosphere and the sea in motion. The Rockefeller Institute Press, New York.

Gall, R. L., R. Blakeslee, and R. C. J. Somerville. 1979. Baroclinic instability and the selection of the zonal scale of the transient eddies of middle latitudes. J. Atmos. Sci. 37:767-784.

Herring, J. R. 1980. Statistical theory of quasi-geostrophic turbulence. J. Atmos. Sci. 37:969-977.

Holmström, I. 1963. On a method for parametric representation of the state of the atmosphere. Tellus 15:127-149.

Holmström, I. 1964. On the vertical structure of the atmosphere. Tellus 16:288-308.

Horn, L. H. and R. A. Bryson. 1963. An analysis of the geostrophic kinetic energy spectrum of large-scale atmospheric turbulence. J. Geophys. Res. 68:1059-1064.

Kasahara, A. 1966. The dynamical influence of orography on the large-scale motion of the atmosphere. J. Atmos. Sci. 23:259-271.

Kasahara, A. and K. Puri. 1981. Spectral representation of three-dimensional global data by expansion in normal mode functions. Mon. Wea. Rev. 109:37-51.

Kraichnan, R. H. 1967. Inertial subranges in two-dimensional turbulence. Phys. Fluids 10:1417-1423.

Leith, C. E. 1968. Diffusion approximation for two-dimensional turbulence. Phys. Fluids 11:671-673.

Lilly, L. K. 1969. Numerical simulation of two-dimensional turbulence. The Physics of Fluids Supplement 2:240-249.

Lorenz, E. N. 1955. Available potential energy and the maintenance of the general circulation. Tellus 7:157-167.

Lorenz, E. N. 1960. Maximum simplification of the dynamical equations. Tellus 12:243-254.

Lorenz, E. N. 1967. The nature and theory of the general circulation of the atmosphere. WMO No. 218.

Lorenz, E. N. 1971. An N-cycle time-differencing scheme for stepwise numerical integration. Mon. Wea. Rev. 99:644-648.

Marshall, H. G. and T.-C. Chen. 1982. Baroclinic nonlinear exchanges of energy and potential enstrophy in the quasi-geostrophic two-layer model. Geophys. Astrophys. Fluid Dynamics 22:71-84.

Merilees, P. E. 1976. Fundamentals of large-scale numerical weather prediction. In Weather forecasting and weather forecasts. NCAR Colloq. Notes 1:2-137.

Merilees, P. E. 1979. On the kinematic properties of the -3 law for kinetic energy. Tellus 21:487-492.

Merilees, P. E. and T. Warn. 1972. The resolution implications of geostrophic turbulence. J. Atmos. Sci. 29:990-991.

Nielsen, E. 1981. A numerical simulation of the atmospheric general circulation with a barotropic model. M.S. thesis. Dept. of Earth Sciences, Iowa State University.

Nielsen, E., T.-C. Chen, and J. J. Tribbia. 1981. A numerical simulation of the atmospheric general circulation with a barotropic model. Tech. Rept. Dept. of Earth Sciences, Iowa State University.

Onsager, L. 1949. Statistical hydrodynamics. Nuovo Cimento Supp. 6:279-287.

Orzag, S. A. 1970. Transform method for the calculation of vector-coupled sums: application to the spectral form of the vorticity equation. J. Atmos. Sci. 27-890-895.

Orzag, S. A. 1971. Numerical simulations of incompressible flows within simple boundaries: Galerkin, spectral representation. Studies in Appl. Math. 50:293-327.

Pedlosky, J. 1964. The stability of currents in the atmosphere and the ocean. part II. J. Atmos. Sci. 21:342-353.

Pedlosky, J. 1970. Finite amplitude baroclinic waves. J. Atmos. Sci. 27:15-30.

Pedlosky, J. 1979. Geophysical fluid dynamics. Springer-Verlag, New York.

Peterson, W. P. 1978. Cray-1 real to complex fast Fourier transform binary radix subroutine. Cray Research, Inc., Minneapolis, Minn.

Phillips, N. A. 1951. A simple three-dimensional model for the study of large-scale extratropical flow patterns. J. Meteorol. 8:381-394.

Phillips, N. A. 1956. The general circulation of the atmosphere: a numerical experiment. Q. J. R. Meteorol. Soc. 82:420-461.

Rhines, P. B. 1975. Waves and turbulence on a beta-plane. J. Fluid Mech. 69:417-431.

Rhines, P. B. 1977. The dynamics of unsteady currents. In The sea. John Wiley and Sons, New York.

Rhines, P. B. 1979. Geostrophic turbulence. Ann. Rev. Fluid Mech. 11:401-441.

Robert, A. J. 1966. The integration of a low order spectral form of the primitive meteorological equations. J. Meteorol. Soc. Japan, Ser. 2, 44:237-245.

Rosen, R. P. and D. H. Salstein. 1982. General circulation statistics on short time scales. Mon. Wea. Rev. 110:683-698.

Salmon, R. 1978. Two-layer quasi-geostrophic turbulence in a simple special case. Geophys. Astrophys. Fluid Dynamics 10:25-52.

Salmon, R. 1980. Baroclinic instability and geostrophic turbulence. Geophys. Astrophys. Fluid Dynamics 15:167-211.

Salmon, R. 1982. Geostrophic turbulence. Topic Ocean Phys. 80:30-78.

Saltzman, B. 1957. Equations governing the energetics of the larger scales of atmospheric turbulence in the domain of wave number. J. Meteorol. 14:513-523.

Saltzman, B. 1970. Large-scale atmospheric energetics in the wave number domain. Rev. Geophys. Space Phys. 8:289-302.

Smagorinsky, J. 1953. The dynamical influence of large-scale heat sources and sinks on the quasi-stationary mean motions of the atmosphere. Q. J. R. Meteorol. Soc. 79.342-366.

Smagorinsky, J. 1963. General circulation experiments with the primitive equations, I- the basic experiments. Mon. Wea. Rev. 91:99-165.

Steinberg, H. L. 1971. On power laws and nonlinear cascades in large-scale atmospheric flow. Tech. Rept. 0026300-4-T. Dept. of Meteorol. and Oceanog., Univ. of Mich., Ann Arbor. 143 pp.

Steinberg, H. L., A. Wiin-Nielsen, and C. H. Yang. 1971. On nonlinear cascades in large-scale atmospheric flow. J. Geophys. Res. 76:8829-8840.

Stone, P. H. 1978. Baroclinic adjustment. J. Atmos. Sci. 35:561-571.

Tomatsu, K. 1979. Spectral energetics of the troposphere and lower stratosphere. Adv. Geophys. 21:289-405.

Wiin-Nielsen, A. 1959a. On barotropic and baroclinic models, with special emphasis on ultra-long waves. Mon. Wea. Rev. 87:171-183.

Wiin-Nielsen, A. 1959b. On certain integral constraints for the time integration of baroclinic models. Tellus 11:45-59.

Wiin-Nielsen, A., 1962. On transformation of kinetic energy between the vertical shear flow and vertical mean flow in the atmosphere. Mon. Wea. Rev. 90:311-323.

Wiin-Nielsen, A. 1967. On the annual variation and spectral distribution of atmospheric energy. Tellus 19:540-559.

Wiin-Nielsen, A. 1970. A theoretical study of the annual variation of atmospheric energy. Tellus 22:1-16.

Wiin-Nielsen, A. 1974. On the motion of various vertical modes of transient, very long waves. Tellus 23:87-98.

Wiin-Nielsen, A. and M. Drake. 1965. On the energy exchange between the baroclinic and barotropic components of atmospheric flow. Mon. Wea. Rev. 93:79-92.

Wiin-Nielsen, A. and M. Drake. 1966. An observational study of kinetic energy conversions in the atmosphere. Mon. Wea. Rev. 94:221-230.

Yang, C. H. 1967. Nonlinear aspects of the large-scale motion in the atmosphere. Tech. Rept. 08759-1-T. Dept. of Meteorol. and Oceanog., Univ. of Mich., Ann Arbor. 173 pp.

VII. ACKNOWLEDGMENTS

I thank Dr. Tsing-Chang Chen for serving as my major professor, suggesting this thesis topic to me, computational and drafting funds, travel funds for computations at the National Center for Atmospheric Research, and his comments on this manuscript.

I thank Dr. J. Tribbia for the core of the numerical model, help in debugging the model, traveling to my orals, some geostrophic turbulence references, computational funds, and his comments.

I thank my committee members Dr. B. Munsun, Dr. R. Shaw, Dr. J. Stanford, and Dr. D. Yarger for their comments and questions.

I thank my wife, Marianne, for unending support and encouragement. I thank my parents, James and Shirley Marshall, for their encouragement.

I thank J. Hoekstra of Iowa State University and R. Valent of the National Center for Atmospheric Research for programming advice.

I thank Mrs. B. Marvick for typing this thesis and drafting, and Richard Beachler for drafting.

This study is supported in part by the National Science Foundation Grants ATM-792458, ATM-7951800, and ATM-8108216.

VIII. APPENDIX: DEFINITIONS OF SYMBOLS, SUBSCRIPTS AND SUPERSCRIPTS USED

Symbol	Definition
ψ	Barotropic modal stream function. Mean of the 250mb and 750 mb streamfunctions.
τ	Baroclinic modal stream function. One half the difference of the 250mb and 750mb stream functions. In the two-level model τ is proportional to temperature (or thickness).
ξ	Barotropic or vertical mean vorticity.
ξ^*	Vorticity at an arbitrary level.
η	Baroclinic or vertical difference vorticity.
q_S	$\eta + R^2\tau$, baroclinic potential vorticity.
σ	Static stability.
R	$\sqrt{2}/L_R$, $\frac{\sqrt{2}f}{\sqrt{\sigma\Delta p}}$.
R*	Ideal gas constant.
L_R	Internal Rossby deformation radius.
$\overline{(\ )}$	Zonal average of a quantity.
U_ψ	$-\frac{\partial\psi}{\partial y}$. Zonal barotropic wind speed.
$U_\tau(k)$	$\frac{1}{2\pi}\int_{-\infty}^{\infty} U_\tau\, C^{ikx} dx$. The kth spectral component of the zonal baroclinic wind speed.
$(\ )'$	Zonal departure of a variable, $(\ ) = \overline{(\ )} + (\ )'$. Also $(\ )_E$.
K_M	Barotropic kinetic energy (or vertical mean kinetic energy).
K_{MZ}	Barotropic zonal kinetic energy.
K_S	Baroclinic kinetic energy (or vertical shear kinetic energy).

K_S	Baroclinic eddy kinetic energy.
A	Available potential energy.
E	Total baroclinic energy (K_S + A).
E_M	Barotropic enstrophy.
E_S	Baroclinic potential enstrophy.
s	Area of the channel model.
F_M	Vertical mean diffusion and scf friction.
F_S	Vertical difference diffusion and scf friction.
H	Diabatic heating.
F_o	F_S + H.
P	Pressure.
β	Ambient gradient of planetary vorticity.
f	$f_o + \beta_y$.
f_o	Average ambient planetary vorticity.
ω	$\frac{dP}{dt}$, omega.
ν	Diffusion coefficient.
γ	Newtonian diabatic heating coefficient.
k	Surface drag coefficient.